Group 5: Solar: EGEE 580
EESiPV: Electrochemical Energy Storage integrated Photovoltaics

Due on Friday, March 4^{th}, 2011

Dr. Grayson and Dr. Elsworth

Rebecca Hott
Mark Labarbera
Jeff Rayl
Kuangyuan Zhang

Executive Summary

A series of Electrochemical Energy Storage integrated PhotoVoltaic (EESiPV) systems have been modeled for the continuous generation of 1 MW minimum of electrical power delivered to the grid in the Buffalo, NY, Raleigh, NC and Phoenix, AZ areas. An energy analysis, economic projections and life cycle assessment of each system design and location have been used to determine the feasibility of the EESiPV system model.

The solar resource and climate in each location are used to model power generation from both cadmium telluride and polycrystalline silica photovoltaic arrays. The photovoltaic systems used in each models are scaled to deliver a minimum of 24 MW hrs delivered to the grid after all conversion and storage inefficiencies during the minimum solar production months. During the course of the year the PV arrays will be providing excess electrical power beyond storage and 1 MW base load demands; this excess can be sold directly to the grid without energy storage inefficiencies.

A vanadium redox flow battery is integrated with the photovoltaic array to store excess electrical energy during sunlight hours and release 1MW of electric power consistently during nights and low solar days. A total of 25 MW hrs of electrical energy storage capacity, 4 MW charging capacity and 1MW discharge capacity system is designed and modeled. The energy storage system utilized in these systems has a 94% charge to discharge power efficiency.

Each EESiPV system modeled here is subject to an economic analysis in which projected carbon credits, cost of electricity, federal, state and local incentives are weighed against the projected 25 year life of the system components. A life cycle assessment of each system component is carried out to determine the aggregate of all environmental impacts resulting from the construction, operation and disposal of the EESiPV system.

Contents

1. Introduction

Production of electric power from the acquisition, processing and combustion of fossil fuels has been shown to adversely affect local and global environments. Utilizing solar energy, specifically photovoltaic systems, to generate electric power can help avert some of these environmental impacts. One of the leading issues facing solar energy is the intermittency of solar radiation. In order to provide stable and sustainable electric power that can continuously meet energy demands, research and development of an integrated photovoltaic power generation and electrochemical energy storage device is required.

Our group has chosen to design and evaluate an Electrochemical Energy Storage integrated Photovoltaic (EESiPV) system for *continuous, stable and sustainable grid-connected power generation*, including a life cycle assessment on economic, policy and environmental impacts. The following pages include our expansive and complete literature review on the above matter.

2. Background

2.1. Solar Energy

2.1.1. The Solar Resource

Insolation:
Insolation, or irradiance, is the amount of solar radiation incident on the Earth's surface at any given time. The solar constant, G_{sc}, represents the amount of solar energy received on a unit surface area normal to the sun per a unit of time. [1] Measurements can be taken outside of the Earth's atmosphere producing extraterrestrial solar radiation data or near the Earth's surface producing terrestrial solar radiation data. [2] Units for irradiance and the solar constant are W/m^2.

Despite being called a constant, the actual value of G_{sc} varies throughout the year. When the sun is closest to the Earth, at perihelion, the solar constant is about 1400 W/m^2. And when the sun is farthest away from the Earth, at aphelion, the solar constant is about 1330 W/m^2. Throughout the rest of the year, the extraterrestrial radiation varies between these limits. [1] The American Society for Testing and Materials (ASTM) adopted an average value of 1366.1 W/m^2 for the solar constant at Air Mass Zero (AM0). Air mass is the average length of atmosphere that solar radiation must travel through before reaching the Earth's surface. AM0 represents extraterrestrial solar radiation outside of the Earth's atmosphere.

ASTM adopted two values for the solar constant at Air Mass 1.5, the terrestrial solar radiation near the Earth's surface when traveling through 1.5 lengths of the atmosphere. This is equivalent to radiation penetrating the atmosphere at a 45° angle. Irradiance can be broken down into several categories. Figure 1 illustrates the atmospheric effects on solar radiation.

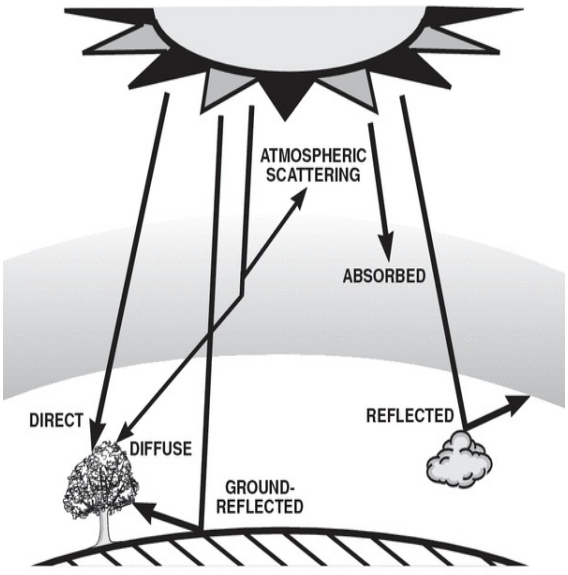

Figure 1: Breakdown of global radiation by the atmosphere into components. [3]

Global radiation is the total available radiation. Direct, or beam, radiation is the unscattered radiation emanating directly from the center of the sun. Direct solar radiation also includes a portion of the circumsolar radiation produced from a 2.5-degree cone around the sun center. Solar radiation that has been changed by scattering in the atmosphere is known as diffuse radiation. [4] An average value of 1000 W/m^2 has been set by ASTM for the solar constant of Global radiation while an average value of 900 W/m^2 has been set for the solar constant of Direct radiation. [2] The difference between the two represents diffuse radiation. Diffuse radiation has been reflected by the atmosphere.

The solar spectrum describes the irradiance per wavelength of radiation. ASTM has also created solar radiation spectra for both AM0 and AM1.5. ASTM E-490 is the standard solar spectrum at AM0 and ASTM G-173-03 is the standard solar spectrum at AM1.5. Spectral irradiance in $W/(m^2nm)$ is plotted against wavelength (nm) to create these spectra as shown in figure 2. The AM1.5 global spectrum was designed for flat plate modules while the AM1.5 direct spectrum was created for solar concentrator purposes. [2] We will use the AM1.5 spectrum for our analysis.

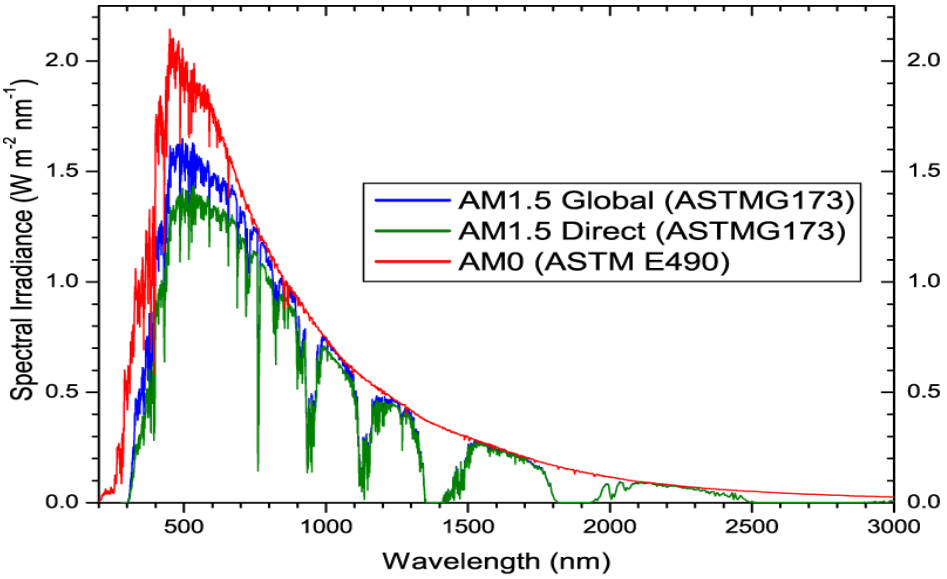

Figure 2: American Society for Testing and Materials standard solar spectrum divided into global and direct components for AM1.5 and global spectra for AM0. [2]

Relationship between wavelength and energy:
Photovoltaic technology responds to wavelengths in the shortwave range below 3000 nm. Short wave radiation accounts for 99% of solar radiation. The shortwave band is further subdivided into infrared (37% of radiation), visible light (44% of radiation) and ultraviolet (7% of radiation). The visible light band is between 350 and 750 nm. Photovoltaic devices can collect the greatest amount of solar radiation in the visible light region, as can be seen in figure 3.

Electromagnetic radiation can be described by either wavelength or energy. In order to convert between the two the relationship given in equation 1 is used. Based on this

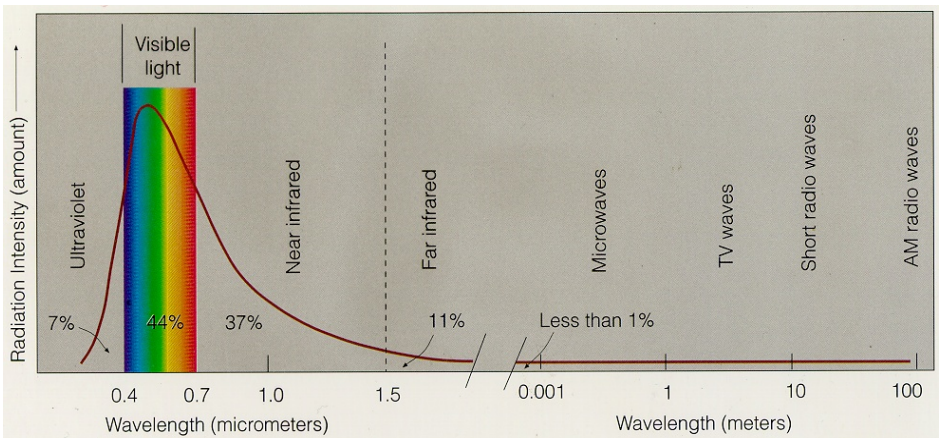

Figure 3: Breakdown of the blackbody radiation curve by wavelength for the sun. [5]

relationship, the main range of photon energies that photovoltaics operate with is from approximately 0.4 eV (3000 nm) to 3.5 eV (350 nm).

$$E(eV) = \frac{hc}{\lambda} = \frac{1239.8}{\lambda(\mu m)} \tag{1}$$

Where h is Planck's constant, c is the speed of light in a vacuum and λ is the wavelength of radiation.

The National Renewable Energy Laboratory created a map of the solar resource in the United States. Daily solar radiation values at the terrestrial level, along with the power-producing capability of a photovoltaic panel, oriented due south at an angle from horizontal equaling the latitude of the collector location, was used to create this map. It is based on the kWh/m^2 of energy that would be produced in a day. Data was taken from various locations throughout the U.S. and extrapolated to obtain a gradient resource map. [6] This map is extremely useful in determining major locations for photovoltaic panel installation. Figure 4 shows the irradiance for the United States.

Critical Issues with the Solar Resource:
While several issues exist when studying the solar resource for energy applications, the main issue with utilizing this resource is intermittency. The solar resource is intermittent on both a daily and seasonal level. Radiation from the sun peaks during the middle of the day and during the summer months creating a continual energy supply problem. Figure 5 shows an example of daily and monthly average irradiance.

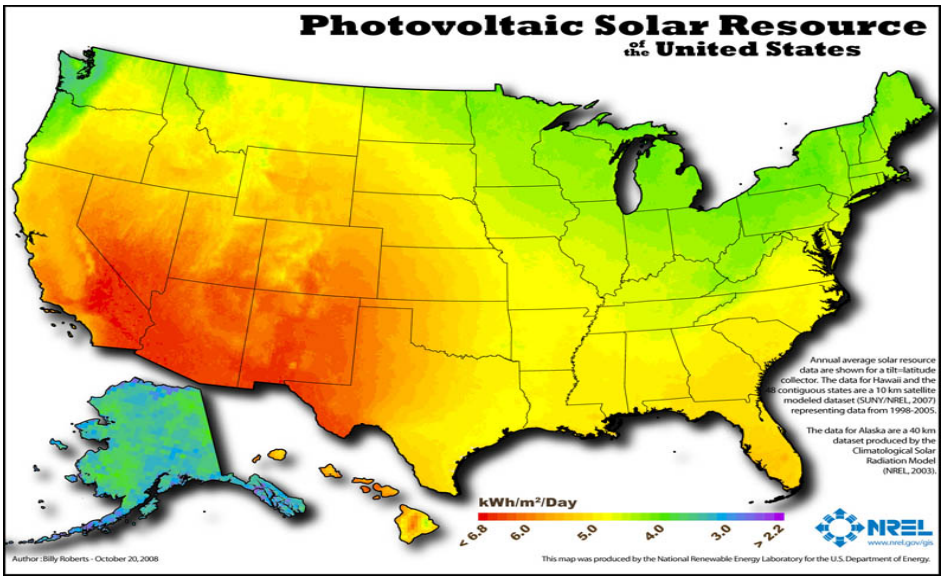

Figure 4: Solar resource map for the United States of America based off of climate data (long term average). [6]

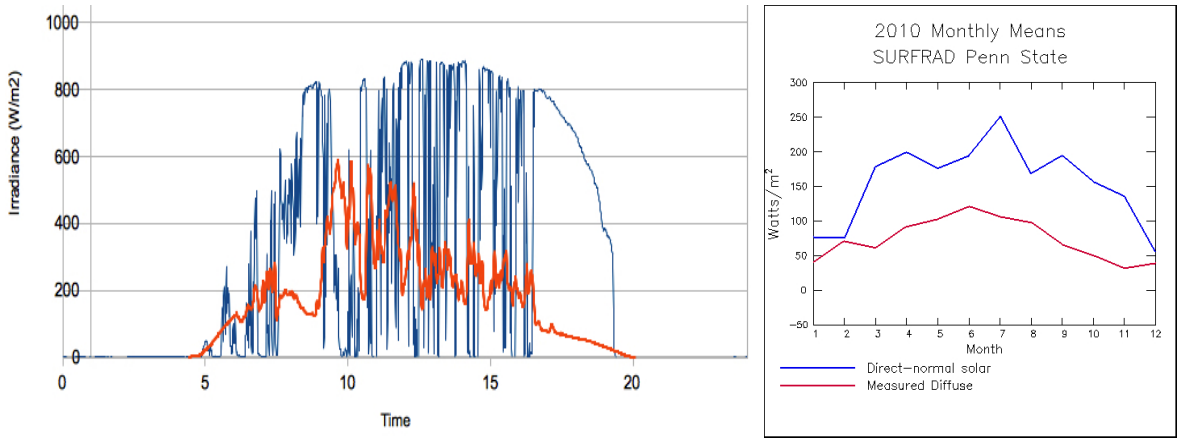

(a) (b)

Figure 5: (a) Daily [where the blue is direct and orange is diffuse] and (b) monthly average (per 24 hours) irradiance for State College, Pennsylvania. [7]

Variability exists with location. As can be seen in the NREL Photovoltaic Solar Resource map in figure 4, the solar resource varies significantly across the United States. In general, the solar resource decreases with increasing latitude away from the equator. Atmospheric conditions including cloud cover, aerosol content and ozone layer thickness affect solar radiation at the Earth's surface. This can been seen in figure 2 where it shows solar radiation being scattered and absorbed into the atmosphere as well as reflected by cloud cover. Many variables affect insolation, which is why solar radiation spectra and resource maps are developed to provide a basis for evaluation of solar radiation and simulator design. [3]

Solar Resource Conclusions:
Three locations have been chosen to design and evaluate an electrochemical energy storage system integrated photovoltaic power system. These locations are Phoenix, Arizona, Raleigh, North Carolina, and Buffalo, New York. They represent a high, medium and low level of solar resource respectively throughout the United States. These three locations represent the diversity of the United States' solar resource. Also, they are the three locations of the American Solar Energy Society conference from 2010, 2011 and 2009, respectively.

2.1.2. Solid-State Physics

Solid-state physics refers to the branch of materials that use bound charge carriers completely confined within the material. Solid-state materials have no mechanically moving parts. In solid-state physics, materials are broken down into three categories; insulators, semiconductors and conductors. The modern method for determining which of these categories a material falls into is the level of conductivity, σ. Conductivity defines how easily charge is transported through a material. Insulators have a conductivity $\sigma > 10^4(\Omega cm)^{-1}$, semiconductors have a conductivity $10^4 > \sigma > 10^-8(\Omega cm)^{-1}$ and conductors have a conductivity $\sigma < 10^-8(\Omega cm)^{-1}$. [8]

The solution to Schrődinger's equation yields a relationship between energy and momentum that defines the allowable energy levels inside a solid at a point. A gap, called the bandgap, represents the energy required for an electron to move to the next orbital in relation to the atomic nuclei. As these allowable energy levels are extrapolated throughout a solid, bands of allowable energy level occur. These bands are represented in band diagrams. These band diagrams illustrate the allowable energy levels and positions of charge carriers inside of a material's crystal structure. As these nuclei and orbitals are arranged in a crystalline geometry, the energy band levels that are illustrated in figure 6 are created.

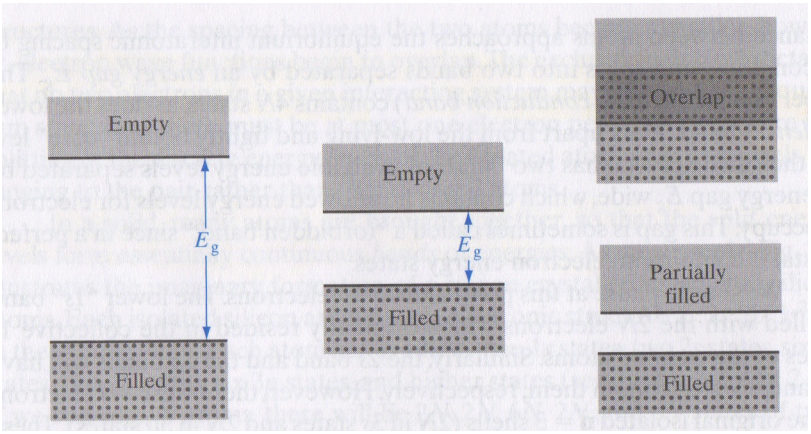

Figure 6: Band diagrams for (a) insulators, (b) semiconductors and (c) conductors illustrating the categorization of materials based on of band gap and conductivity. [9]

The lower band is known as the valence band, the ground state energy level, and the upper band is known as the conduction band, the excited state energy level. In solids, energy

levels are described using the electron-volt (eV). The electron-volt is defined as "the energy given to an electron by accelerating it through 1 volt of electric potential difference." [10]

Historically materials were characterized by their band gaps. Materials with relatively empty valence bands and a few electrons in the conduction band were conductors. Materials with valence bands partially filled and a small gap ($< 3eV$) were semiconductors. Materials with a full valence band and a large band gap ($> 3eV$) were insulators. Materials that have overlapping valence and conduction bands or extremely small bandgaps are conductors. [1] Generally, bandgap is sufficient to determine the type of material; however, it is a function of temperature. This is the reason that conductivity has taken the place of bandgap to determine the type of a material.

In photovoltaics, the main focus is on the light-matter interactions that occur on the atomic level. All solar radiation has an associated energy level corresponding to the wavelength or frequency of the radiation. There are two very different processes that occur when light interacts with matter. The first is the photoelectric effect. In this process high-energy photons (the energy particle associated with light) impact a material imparting enough energy to an electron that it is ejected to vacuum space where it is no longer bound.[9] The second effect is the photovoltaic effect.

2.1.3. The Photovoltaic Effect

The photovoltaic effect consists of four steps: 1) light absorption causing a particle to transition from a ground to excited state, 2) generation of at least a free negative and free positive charge carrier, 3) a differential charge transport mechanism, and 4) charge carrier recombination and return to a ground state. [11] Figure 7 illustrates the stages of the photovoltaic effect.

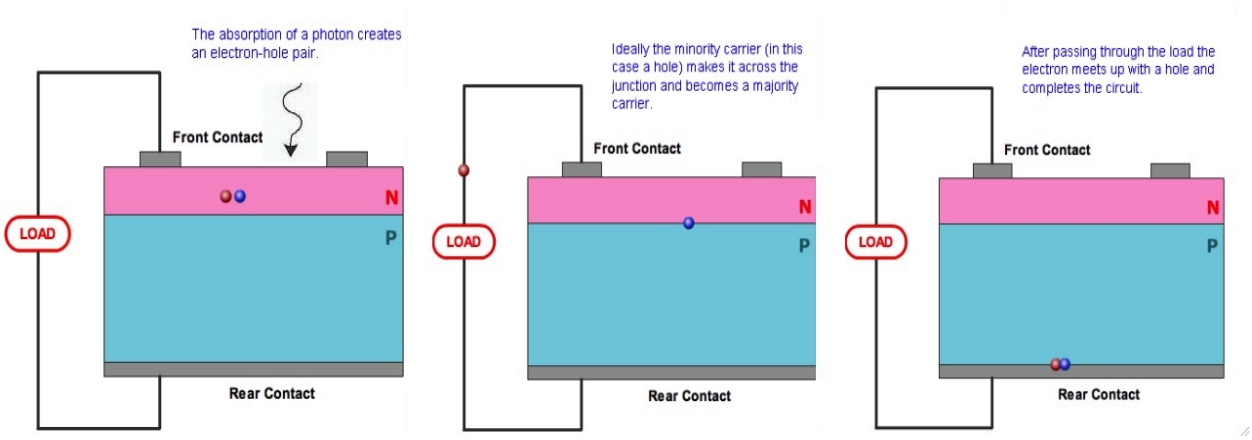

(1-2) (3) (4)

Figure 7: Stages of the photovoltaic process shown on a basic p-n junction photovoltaic device. [12]

1) Light can interact with matter in one of three ways. Light can be absorbed, reflected, or transmitted. The absorption of photons is determined by a material's absorption coefficient

as a function of wavelength, $\alpha(\lambda)$. The absorption coefficient is explained further in the materials section.

2) The absorption of a photon must at least generate a positive and a negative charge carrier. In many cases a third particle, a phonon, will be involved in the light-matter interaction. The phonon is the quantum particle of momentum and its presences is determined by the solution to Schrődinger's equation.

3) The differential charge transport can be caused by either built-in electric fields which are an inherent property of the material and generated by electrostatics (forces between positive and negative charges) and effective forces which are created by the relative band positions of the materials.

4) There are three types of recombination that can occur, band-to-band recombination, Shockley-Read-Hall recombination and Auger recombination. Recombination occurs throughout the bulk of the semiconductor during the photovoltaic process.

2.1.4. Photovoltaic Materials

While the photovoltaic effect was discovered in 1839 by a french scientist Edmund Becquerel [13], it wasn't until 1954 that Bell Laboratories was able to use it to generate significant power. Considered the first modern solar cell, three scientists at Bell Labs created a silicon-based solar cell as an alternative to dry-cell batteries for telephones. This first useful cell had a light conversion efficiency of 4.5%. [14] While numerous photovoltaic materials are used, silicon is currently the main photovoltaic material and has been for many decades. [15] PV materials can be broken down into three categories: monolithic, thin film and advanced materials. Monolithic PV materials are bulk semiconductors that are constructed from the top down, all the fabrication occurs on the same substrate. The main monolithic material is silicon. Thin-film is a broad term for PV materials that are built from the bottom up. Thin film materials include III-V semiconductors like GaAs, CdTe and CIGS. Advanced materials is a category for new materials in thin films that are currently being researched. These materials include dye-sensitized solar cells (DSSC), organic photovoltaics (OPV) and quantum dots. Figure 8 illustrates the potential efficiencies for numerous devices based on the blackbody radiation from AM0 and AM1.5.

Monolithic Silicon:
Silicon is categorized by its internal crystal structure. Single crystal silicon (sc-Si) is highly purified and contains refined silicon that has a uniform crystal structure throughout the entire material. This is called long-range crystalline order. Poly-crystal silicon (pc-Si) has large crystal structures that do not span the entire material. The raw material, SiO_2, is used for pc-Si and sc-Si, but the processing, and hence crystalline structure, is very different. The highly ordered crystal structure of sc-Si allows much higher charge carrier mobilities (μ_n and μ_p) and hence better current transportation. Poly-crystal silicon does not have a uniform crystal structure. This causes grain boundaries, or the place where different crystal structures meet, to impede the free flow of charge carriers. If the crystal structure is non-uniform on the nanometer scale the material is then called nano-crystal silicon (nc-Si).

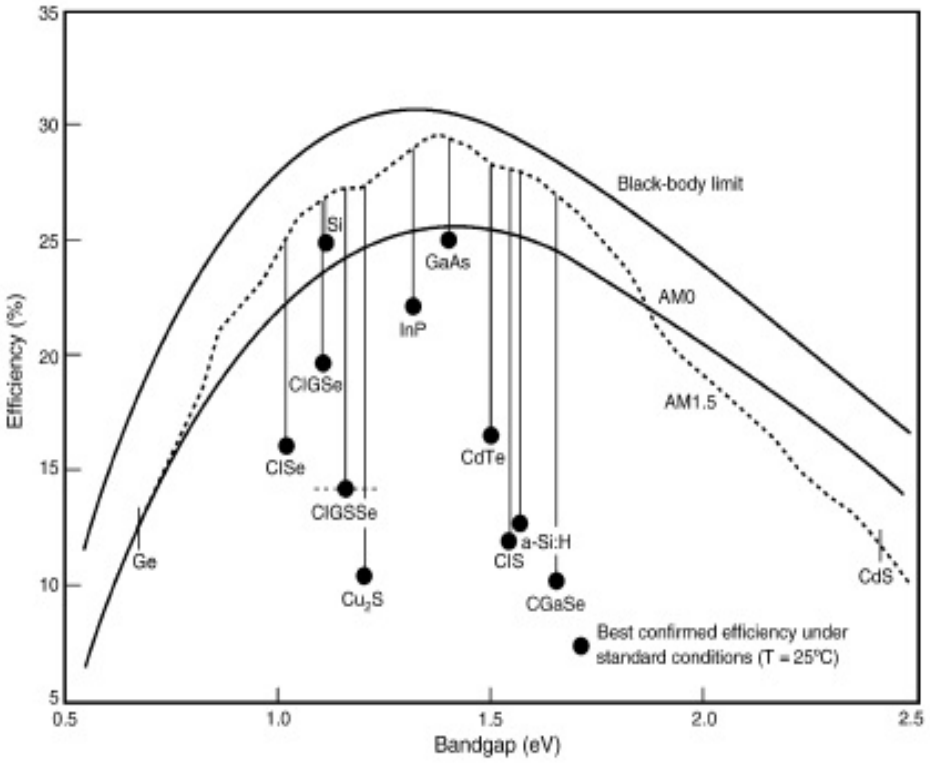

Figure 8: Performance gaps between best device efficiencies in the laboratory and attainable efficiencies for several solar cell technologies. The dotted curve shows the maximum theoretical efficiencies. [16]

Silicon is an indirect bandgap semiconductor; the maximum energy state in the valence band and the minimum energy state in the conduction band have different momentum values. In order to reach an excited state, electrons must absorb a phonon as well as a photon of significant momentum and energy (greater than silicon's bandgap of 1.12eV). This also requires photons to travel a greater distance into the material before they can be absorbed. This requires the silicon cell to have thicknesses of a few hundred micrometers, and is described by the absorption coefficient α. Figure 9 shows the spectral absorption coefficients for several semiconductor materials.

Despite the large amount of raw material required in the manufacture of silicon solar cells, they compose over 80% of the global solar cell production as of 2009. [15] Poly-crystal silicon cells have achieved efficiencies of approximately 20% and module efficiencies of 13-16%. Single crystal silicon cells have achieved efficiencies of almost 25% with module efficiencies between 15-20%. [17] Silicon modules have little room to improve much beyond current technology due to a physical efficiency limit of 29%. One of the largest drawbacks of crystalline silicon PV is that, due to the large amount of raw silicon required for manufacturing, the cost is very closely tied to the market value of silicon rather than purely the manufacturability of the devices.

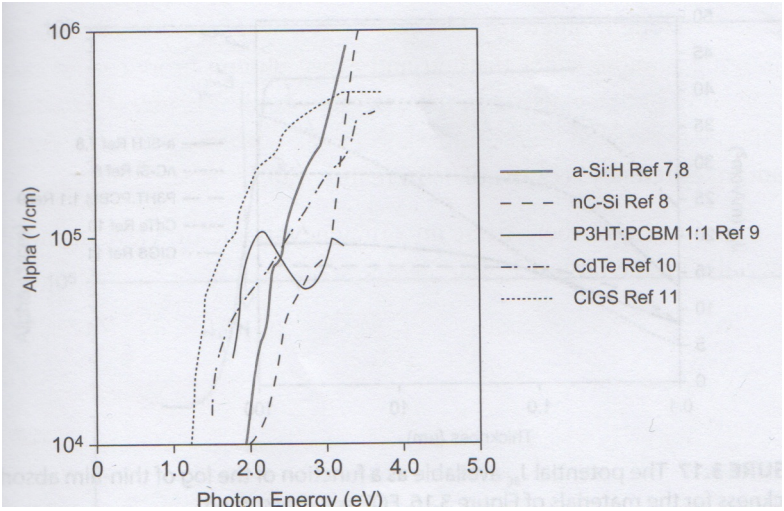

Figure 9: Absorption coefficients as a function of photon energy for various photovoltaic materials. [11]

Thin-Films:
Thin-film materials are built from the bottom up unlike monolithic photovoltaics. All thin films are composed of one or more heterojunctions, or junctions created by two different materials. The thin film refers to the absorber layer, the active photovoltaic material. Thin films is a very broad term for PV materials and describes numerous different materials. Silicon can even be used as a thin film through a different manufacturing method.

Amorphous Silicon:
Rather than attempting to generate a uniform crystal structure, in silicon the crystal size can be decreased to utilize different material benefits. Once the crystal size in silicon is reduced below the nanometer scale the material becomes amorphous. Amorphous silicon (a-Si) has no long-range crystal structure and is composed primarily of grain boundaries. Since there is no long range crystal structure the conservation of momentum principle that causes limits in the absorption coefficient of crystalline silicon no longer applies essentially making amorphous silicon a direct bandgap semiconductor. This allows extremely thin layers ($\approx 0.3\mu m$) of a-Si to be used in cell fabrication. Since such a thin layer of absorber is required a-Si is called a thin film photovoltaic material. Amorphous silicon also has a larger bandgap (1.7eV) than crystal silicon. Efficiencies of a-Si are around 5-7% with a high of 12%. [17] One of the large issues that faces a-Si is the large quantity of dangling bonds that occur from the lack of crystal structure. These dangling bonds are defects that can trap charge carriers. In order to overcome this, silane (SiH_4) is used as the base material for deposition. The hydrogen bonds to the dangling bonds in the a-Si rendering them electrically neutral and allows better charge transport. Great amounts of hydrogen are used on the material; the the actual PV material is a-Si:H. [8]

III-V Semiconductors:
III-V Semiconductors are heterojunctions composed of materials from the third (IIIA) and fifth (VA) columns on the periodic table. These are p-type, positively charged, and n-type, negatively charged, materials used to create a pn junction in a solar cell. The first example

of III-V PV cells is gallium arsenide (GaAs). A considerable amount of research has gone into the development of GaAs solar cells. GaAs is a direct bandgap semiconductor; the maximum energy state in the valence band and the minimum energy state in the conduction band have the same momentum values. The excitation of electrons in GaAs does not require the interaction of phonons. Because of this, GaAs cells have a very high absorption coefficient and have achieved very high efficiencies and have the highest potential efficiency of any photovoltaic material.[18] This highest achieved efficiency for a single heterojunction GaAs solar cell is 28% under 1000x concentration. [16]

III-V semiconductors, as well as other thin-films, can be deposited on top of each other to create tandem cells. Tandem cells are stacks of photovoltaic materials with different bandgaps to achieve better broadband absorption. Tandem cells have achieved the highest efficiencies of any photovoltaic materials because of the broadband absorption. These cells work by having each section optimized for a specific section of the solar spectrum. Each successive cell absorbs a different portion of the spectrum to have the entire tandem cell absorb as much broadband radiation as possible. Their complex design, and hence manufacturability, makes these cells extremely expensive with costs as high as $10,000 per square meter. Due to the very high costs, tandem cells are used solely in concentration PV and for extraterrestrial applications. Concentration photovoltaics (CPV) utilize highly reflective surfaces to increase the amount of radiation incident on the PV cell. Concentrators can increase the amount of radiation by as little as 2 or 3 times to as much as several hundred and even several thousand times. The PV material used in CPV is very small (a few cm^2) while the reflective surface takes up a majority of the incident surface. [19] For extraterrestrial applications, the cost per weight of delivery is the driving factor allowing for the expensive cells to be cost effective. The highest achieved efficiency of any solar cell is a GaAs-based tandem heterojunction type with an efficiency of 42.3% under an illumination of 406 suns or 406 times concentration. The cell is composed of three different III-V semiconductors, InGaAs, GaAs and InGaP. [20] Other thin-film materials include cadmium telluride (CdTe) and CIS or CIGS (copper indium [gallium] [di]selenide).

CdTe:
Cadmium telluride cells are composed of a heterojunction between the absorber CdTe and the transport medium or window CdS. CdTe is a direct bandgap absorber with a bandgap of 1.45eV. While just under 17% efficienct is the highest reported efficiency for CdTE, the maximum theoretical efficiency is 29%. [21] The highest efficiency CdTe cells are actually made from polycrystal material rather than single crystal material. Thin films display higher efficiencies in poly rather than single crystal form due to the increase in grain boundaries aiding in minority carrier transport. [22] Unlike monolithic PV, CdTe photovoltaics can also be deposited on a flexible substrate, allowing much easier manufacturing via a process called roll-to-roll. There is a slight decrease in performance while using a flexible substrate but this allows CdTe to be manufactured at a much lower cost than most other PV technologies. [21] The largest manufacturer of photovoltaics in the United States, First Solar, manufactures CdTe solar cells and are almost single-handedly responsible for the scale of thin-film PV production. First Solar is the first PV manufacturer to reach the $1.50 per watt level of production. Also, despite cadmium being toxic to humans, CdTe cells can be relatively easy to recycle into raw components.

[23] Figure 10 shows typical device configurations for CdTe and CIGS.

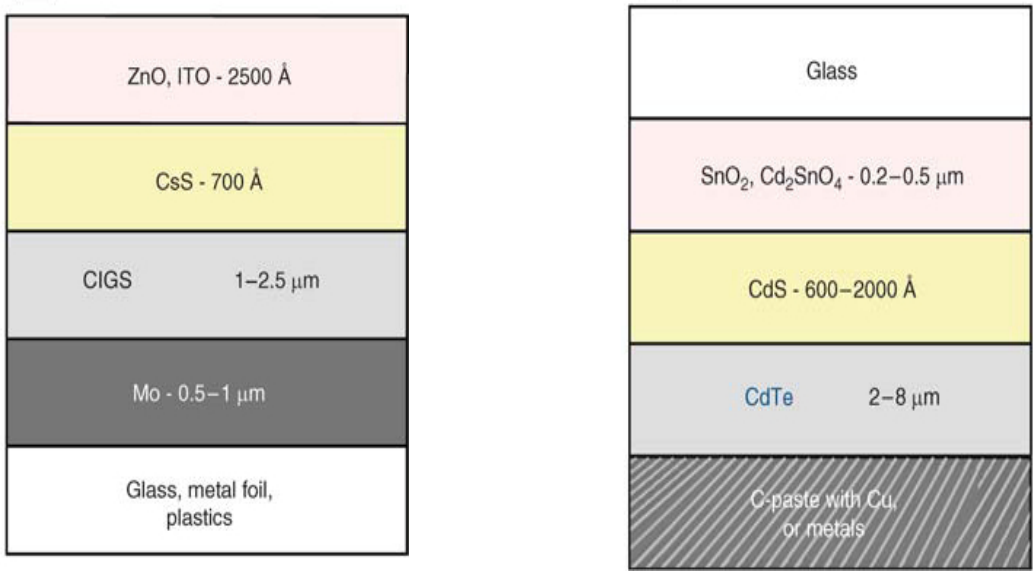

(a) (b)

Figure 10: PV cell structure for (a) CIGS and (b) CdTe showing the layer thicknesses. [24]

CIGS:
Prior to CIGS, CIS was used as a photovoltaic material. Due to the rarity of indium for manufacturing, gallium was added into the alloy to produce CIGS. CIGS has a bandgap that can be tailored by altering the concentrations of materials in the alloy. The most common bandgap created is 1.15eV which is very close to the ideal bandgap for a solar cell of 1.1eV. [11] Efficiencies for CIGS range from 7-12% for modules with the highest laboratory efficiency of 19.5%. [16] CIGS has the potential to increase performance by almost 50% before reaching the maximum physical limit. CIGS has become a very popular material in recent years with the creation of Solyndra, cylindrical CIGS-based photovoltaic modules. [25] Several issues facing CIGS include a strong temperature dependence and large defect concentrations. [24] Despite reducing the amount of indium used, the scarcity of indium is still a drawback to CIGS.

Advanced Materials:
In order to combat the scarcity of some PV materials there are several new advanced concepts that have great potential. There are numerous areas of current research and development in advanced photovoltaic materials. Areas of focus are on dye-sensitized solar cells (DSSC), organic photovoltaics (OPV) and quantum dots. Both dyes and OPV utilize conductive organic polymers or small organic molecules.

Dyes are molecules with absorption-caused excitation. They are called dyes simply because they interact with the visible light portion of the EM spectrum and hence show color. Rather than generating free electrons and holes when absorbing photons, dye cells generate excitons. An exciton is an excited electron and hole pair that is loosely bound by remaining coulombic attraction. These excitons must then be dissociated before they can

travel through the cell. DSSCs differ from traditional PV cells in that the dye serves no purpose in transport of electrons and only acts as an absorber. Dyes are generally deposited on a semiconductor surface where the semiconductor acts as the charge transport medium. Hence DSSCs are actually composed of dye-semiconductor solar cells or organic/inorganic hybrid cells. The best-performing cells are TiO_2-electrolytes, used in conjunction with ruthenium-based dyes and fluorine-based dyes. [26] The dyes are deposited on the semiconductor substrate, sensitizing the substrate to the wavelength associated with the color of the dye. While many dyes have great efficiency for the portion of the spectrum that they absorb, most dyes have large bandgaps which limit the available energy. The TiO_2-electrolyte cell is commonly called the Gratzel cell after Michael Gratzel who created the first TiO_2 DSSC in 1991. [27] Gratzel's original cell achieved efficiencies ranging from 7.1-7.9% using a ruthenium dye (Ru(2,2'bipyridine-4,4'-dicarboxylic acid)$_2$ (μ-(CN)RU(CN)(2,2'-biphyridine)$_2$)$_2$). Further modifications have yielded performances above 10%. [28]

Organic solar cells have several potential advantages compared with conventional inorganic solar cells, including lightweight modules, flexibility, and the potential for low-cost fabrication using continuous roll-to-roll printing techniques. LPPPT (a ladder poly (para-phenylene thienylene) polymer), MEH-PPV (Poly (2-methoxy-5-(2-ethyl-hexyloxy) -1,4-phenylene vinylene)) and P3HT:PCBM (poly(3-hexythiophene): C_{61}-butyric acid methyl ester) are a few examples of organic PV materials. [29] Of these, P3HT:PCBM has the greatest potential as a photovoltaic material. Similar to DSSCs, organics have a separate absorber and transport medium. For P3HT:PCBM, P3HT is the absorber material and PCBM is the transport medium. Rather than a single junction, organic cells are composed of a bulk heterojunction where the donor and acceptor layers are blended together increasing the junction surface area. The large surface area allows for better exciton dissociation across the junction. Each absorber layer is as thin as 100nm making the absorber material requirements very low. [30] Another benefit of OPV is an embodied energy of under half that of crystalline silicon. [31] Despite numerous advantages there are still many obstacles for organic PV to overcome. The highest reported efficiency for P3HT:PCBM is just over 6%. While there are numerous current advancements in R&D, like the addition of carbon nanotubes to increase conductivity [32] and altering the spectral absorption with various concentration ratios [33], efficiencies must still be further increased in order to make OPV competitive with inorganic PV.

Both DSSC and OPV share a common drawback; they suffer severe degradation under long-term illumination. Most cells are only able to perform for less than 2000 hours and suffer from rapid efficiency loss before completely failing. One study by Kawano et al. found a half-life (time for a 50% reduction in efficiency) of as low as 3 hours for an unencapsulated OPV materials. [30] In order for DSSC and OPV to be commercially competitive "long-term stability and protection against environmental influences are significant challenges." [8]

Quantum dots are an attempt at creating inorganic molecules. Once a semiconductor is made small enough quantum confinement occurs, a potential well is created and the quantum dot begins to act in a manner between bulk semiconductors and molecules.

Ideally, quantum dots would function by multiple exciton generation (MEG). MEG is a cascading effect of one photon generating one exciton which in turn generates another exciton. It has been shown in the laboratory that MEG can generate up to 7 excitons for PbSe. [34] One of the greatest challenges in creating tangible quantum dot photovoltaic cells is the extremely short lifetime of excitons. After the excitons have been generated they only exist for a few picoseconds ($1x10^{-12}$s). It is difficult to dissociate excitons into a free electron-hole pair in that time since excitons have a short diffusion length. [35] While this has been proven in the laboratory it has yet to be produced as a commercial product. [36]

Material Conclusions:
While many of the advanced photovoltaic materials show great promise, currently none are cost effective for large scale power generation. Both monolithic and thin film photovoltaics have been proven to be reliable sources of energy for significant power production. For our system designs we will focus on the two least expensive (in $/W) materials in each of the two categories. Polycrystalline silicon and cadmium telluride will be used as our photovoltaic materials.

For each of the three locations we will perform a performance analysis using both materials to determine the costs and benefits for power generation and the overall system costs. Not all locations will necessarily yield the same material as the optimum choice.

2.1.5. Device Modeling

The voltage of a device is directly related to the band structure of the materials and the work functions of the contacts. The voltage can be obtained for any device by the relationship given in equation 2.

$$V_{oc} = \int_L^R \xi(x) - \xi_o(x)\, dx \qquad [11] \qquad (2)$$

Where $\xi(x)$ is the electric field at the operating point and $\xi_o(x)$ is the electric field at thermodynamic equilibrium. The limits of integration, L and R, refer to the left and right contacts. This integral is over the width of the material. The electric and effective fields of the design arise from the device and the materials used.

The current for any device can be determined by the following relationships for electron current density, J_n, and hole current density, J_p.

$$J_n = e\mu_n n\xi + e\mu_n \xi_n' + eD_n \frac{dn}{dx} + eD_n^\tau \frac{dT_n}{dx} \qquad [11] \qquad (3)$$

$$J_p = e\mu_p p\xi + e\mu_p \xi_p' + eD_p \frac{dp}{dx} + eD_p^\tau \frac{dT_p}{dx} \qquad [11] \qquad (4)$$

These equations ultimately state that there are four factors that affect the current density of photovoltaic materials as the four terms of the equations. From left to right the factors are an electric field, effective fields (changes in affinity or band density of states), diffusion (gradients of charge carriers), and temperature gradients. These terms describe a manner

of breaking the symmetry of the charges in the device to generate current flow in one direction over the other. For detailed modeling of PV materials the above equations are the absolute relationships. Figure 11 shows a typical current-voltage (I-V) curve for a photovoltaic device.

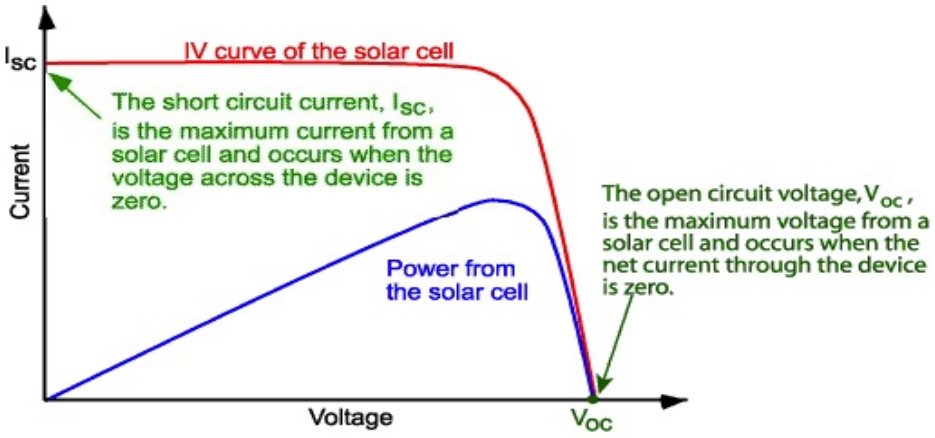

Figure 11: Current-voltage relationship for a PV device illustrating the maximum power point. [12]

The point on figure 11 that intersects the y-axis is the short-circuit current, I_{sc}, and the x-intersect is the open-circuit voltage, V_{oc}. The point at the knee of the power curve is called the maximum power point. Modern PV systems have sophisticated maximum power point tracking (MPPT) systems that will optimize the power generated by controlling the operating point of the device. I-V curves are generated for a specific level of irradiance. Standard Testing Conditions (STC) for photovoltaic devices are an irradiance of $1000W/m^2$, an air mass of 1.5 and a cell temperature of 25°C. [37] The spectrum used in STC is shown in figure 2.

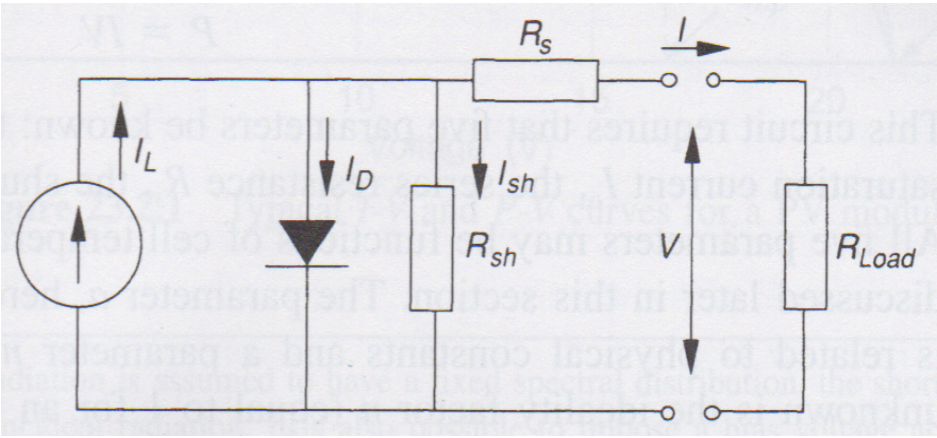

Figure 12: Equivalent circuit model for a basic photovoltaic device. [4]

The single-diode model, or five-parameter model, is the most frequently used model. The model consists of a current source, I_L, a diode, series, R_s, and shunt, R_{sh}, resistance and a

characteristic load, R_L. This model is ultimately a light dependent one way current source. The equivalent circuit model for the five-parameter model is shown in figure 12. The expression used to model the current is a function of voltage. Rather than using equations 3 and 4 which are beneficial for evaluating detailed device performance, equation 5 is more useful for modeling device performance in complex simulations.

$$I = I_L - I_o[e^{\frac{q}{nkT_c}(V+IR_s)} - 1] - \frac{V + IR_s}{R_{sh}}[4] \tag{5}$$

Where I_L is the light current, I_o is dark current or reverse saturation current, k is the Boltzmann constant, T_c is the cell temperature, V is the voltage produced by the cell and n is an ideality factor for the diode. This equation can be solved by hand through an iterative process, or through complex computer algorithms that can model temporal performance of photovoltaic devices. The parameters from equation 5 are determined by the materials and design of the photovoltaic device.

In order to accurately model the performance of simulations, numerous different approaches have been created. Table 1 shows several historical models for photovoltaic performance.

Table 1: Historical PV performance models (based on previous work by Klise and Stein).[38]

Model	Array Performance Model	Target Systems	Year(s) Developed
PVSS	One-diode equivalent circuit	PV	1976-77
SOLCEL	One-diode equivalent circuit	PV, CPV	1976-85
Evans et al.	Power-temperature coefficient	PV, CPV	1970-80
SOLSTOR	SOLCEL model (One-diode)	Hybrid, PV, CPV	1972-82
PVForm	Modified Temp. Coefficient	Hybrid, PV, CPV	1985
PVWATTS Version 1	Indentical to PVForm	PV	2008 (Current)
PVSIM	Two-diode equivalent circuit	Hybrid, PV,CPV	1996
Sandia PV Array (PV-efficients MOD)	Empirically derived I-V co	PV(w/ thin film), CPV	1991-2004

2.1.6. Ground Placing Layout

Besides the solar resource and materials used in solar cells, the ground-placing layout is another important aspect of producing energy with photovoltaics. This layout usually involves the panel arrangement and determining the mounting structures to incorporate into the design.

System Layout:
Photovoltaic power plants are subdivided into basic arrays, and then array units to comprise the final system. The first step in configuring the layout of photovoltaic panels involves determining the basic array. This depends on the rated maximum power, in

Watts, of the photovoltaic panel chosen. Ito, et al. completed a study on a 100 MW size photovoltaic power system using four types of modules. Multi-crystalline silicon was used as their base case with 30 modules making up the basic array. The next step is to determine the array unit. Ito, et al. used 4200 modules or 140 basic arrays to construct a 500 kW array unit. Each array unit was approximated to be 100 m in length and width. Finally, the system was created with 200 sets of the 500 kW array units. Their final system size was approximated to be 1.1 km in length by 2.1 km in width with 840,000 modules. Figure 13 shows Ito, et al's basic array, array unit and final system. [39]

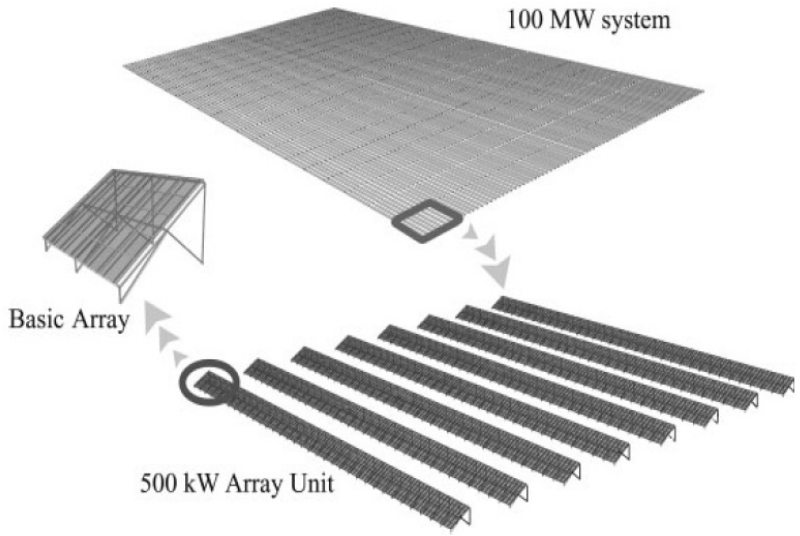

Figure 13: Array configuration of a 100MW fixed tilt very large scale PV plant. [39]

Moore and Post compiled a report on the Tucson Electric Power Company's 4.6 MW dc utility-scale grid-connected photovoltaic system. The Springerville Generating Station Solar System is composed of 135-kW dc array units. Array strings are composed of two rows of nine modules. Within each array there are 450 crystalline silicon modules measuring 91 m by 43 m. Figure 14 shows the Springerville PV generating plant. [40] A similar design to Tucson's PV system will be utilized for our electrochemical energy storage integrated photovoltaic system due to similar system sizes.

Tracking the Solar Resource:
Tracking mechanisms are employed to allow solar collectors to follow the path of the sun during the period of a day. By following the path of the sun, greater amounts of insolation are collected by the solar cells and more energy can be produced. [1] Mechanical tracking structures have typically been regarded as unreliable, power consuming and expensive. They were seldom used in commercial PV systems. Over the years, however, manufacturers have decreased their production costs and increased their reliability making them acceptable to use and now an essential part of photovoltaic power systems. [41] Figure 15 depicts the gradual increase in tracking system use with large-scale photovoltaic power plants from 2006 to 2008 as well as the total capacity of large-scale photovoltaic power plants.

Figure 14: Tucson Electric Power Company's 4.6 MW dc photovoltaic power plant. [41]

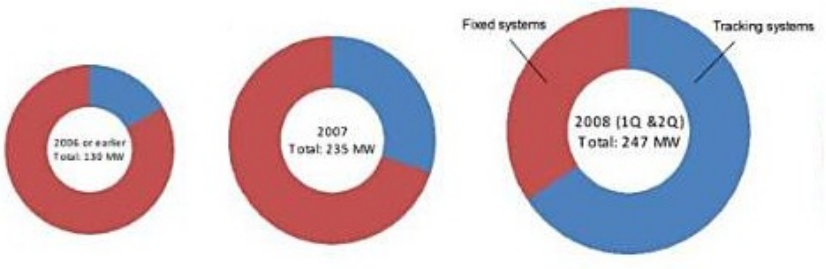

Figure 15: Breakdown of large-scale PV plants between fixed axis and tracking systems. [41]

Operation:
Tracking structures mainly operate in one of two approaches. The first approach utilizes the astronomical calendar by following time and geographical coordinates. This is the most common approach where the sun is tracked according to its position in the sky throughout the day at a specific latitude and longitude. The second approach is based on light sensors. Photosensitive devices are employed in this approach and include photoresistors, photodiodes and phototransistors. Depending on the light intensity and direction these devices continuously track the sun during the day. Figure 16 illustrates the differences between the tracking approaches and the sun's true position on an east-west and north-south axis. [42] The light-sensor approach almost exactly follows the path of the sun on a north-south axis.

Both approaches have positive and negative aspects about them. W. S. Energia composed a list of these aspects. The light sensor is extremely accurate on tracking the sun with little influence from installation misalignments. It is, however, not dependable on a cloudy day and is still a fairly new technology. Sources of error and installation misalignments negatively affect the use of the astronomical tracking approach. The accuracy, however, does not depend on the weather and would be more reliable during incremental conditions. This approach has been widely used and has been established as the main approach. [42]

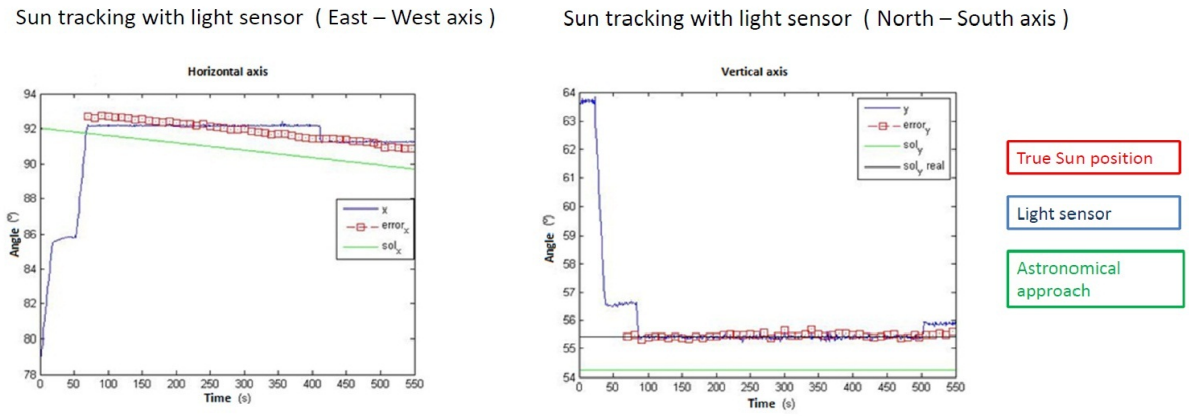

Figure 16: The true sun position, light-sensor position and astronomical positions with respect to time. [42]

Tracking Structures:
Multiple different configurations, many of which utilize tracking devices, are available for employment in photovoltaic power systems. Tracking devices are classified by their motion about an axis system, typically one or two. Single-axis tracking devices have one axis of rotational freedom while double-axis tracking devices have two degrees of rotational freedom. [41] Figure 17 displays different configurations for tracking systems.

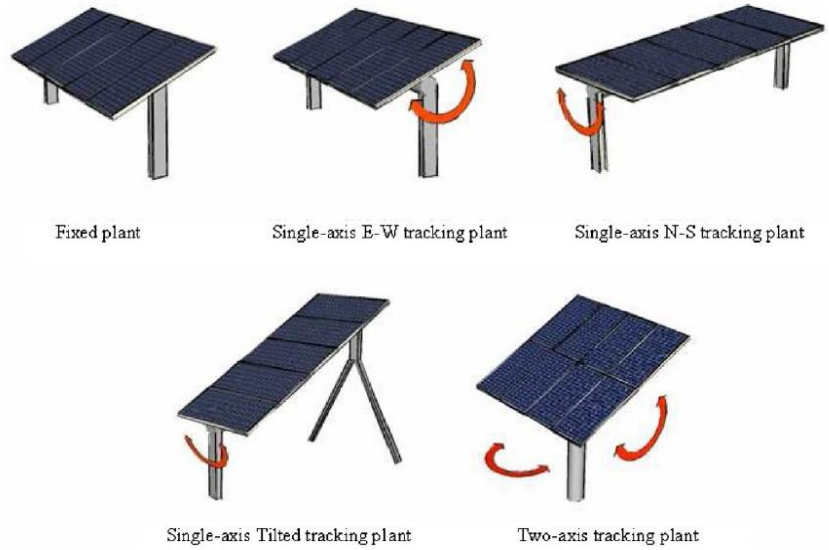

Figure 17: Various tracking methods used for photovoltaic arrays. [43]

A mounting structure can be can completely fixed in a horizontal manner as in the top left image. Both inclination and orientation are fixed in this configuration. Photovoltaic panels are typically oriented to the south and inclined approximately 30 degrees depending on the latitude. NREL created their PV Solar Resource map based on flat plate collectors with this orientation. In the case of a single-axis tracking structure, four different configurations

could be utilized. A horizontal single-axis can be parallel to the east-west direction or north-south direction, shown in the above image on the top, middle and right, respectively. A horizontal single-axis structure could be oriented parallel to the earth's axis. [43] This image is not shown above, but movement occurs about the polar axis. [1] The last configuration for a single-axis tracking structure is shown on the bottom left of the above image. These tracking structures move in a north-south direction and are optimally tilted. Two-axis tracking structures, as shown on the bottom right, are capable of tracking the sun both in a north-south and east-west direction. [43]

Aste and Pero [43] completed an analysis on a large-scale ground-mounted PV plant for three cities in Italy. They looked at various factors affecting photovoltaic performance in Milan, Rome and Palermo. Power production from fixed, single- and double-axis tracking devices was analyzed in each city. Figure 18 displays their results.

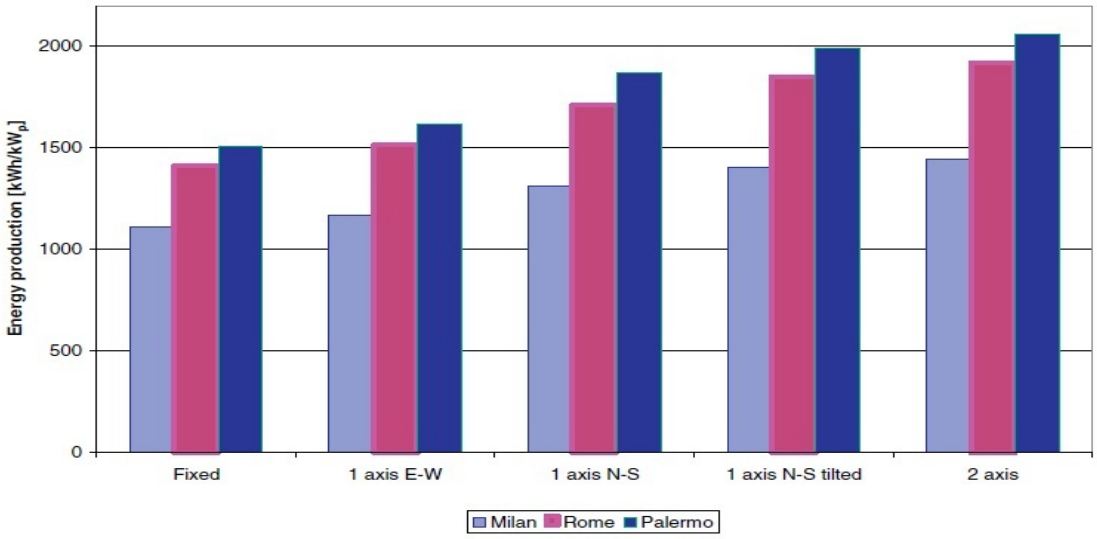

Figure 18: Milan, Rome and Palermo large scale PV power plants' performance with different tracking methods. [43]

As can be seen in the chart, the two-axis tracking device delivers the greatest amount of power in all three cities. The one-axis north-south tilted tracker, however, has slightly lower but comparable results. The image also depicts the difference in power production due to location. It can clearly be concluded that double-axis tracking devices are the best option for power producing capabilities. Other issues, such as cost and land use, need to be considered when selecting a tracking system. Aste and Pero choose the single-axis north-south tracking device as their best option after completing their analysis and taking all of these issues into consideration. [43]

Angle of Incidence:
Collection of solar radiation depends on the angle of incidence, θ, which is the angle between the beam radiation on a surface and the normal to the surface. The angle of incidence can be solved for with equation 6.

$$cos\theta = (sin\delta\ sin\phi\ cos\beta) - (sin\delta\ cos\phi\ sin\beta\ cos\gamma) + (cos\delta\ cos\phi\ cos\beta\ cos\omega) + (cos\delta\ sin\phi\ sin\beta\ cos\gamma\ cos\omega) + (cos\delta\ sin\beta\ sin\gamma\ sin\omega)[4] \quad (6)$$

Declination (δ) is the angular position of the sun at solar noon with respect to the plane of the equator. (ϕ) is latitude. (β) is the slope or the angle between the plane of the surface in question and the horizontal. (γ) is the surface azimuth angle or the deviation of the projection on a horizontal plane of the normal to the surface from the local meridian (zero is due south, east is negative and west is positive) and (ω) is the hour angle or the angular displacement of the sun east or west of the local meridian due to rotation of the Earth on its axis at 15 degrees per hour. [4]

Multiple factors affect the amount of solar radiation that can be collected. Specifically the location, as in the latitude, and the time of day and hour angle, are major factors. Tracking structures operate in a manner to minimize the angle of incidence, θ, of beam radiation on the surface of a photovoltaic device and thus maximize the incident beam radiation. [4]

Critical Issues and Problems:
Establishing the optimal distance between rows of modules, whether utilizing a tracking system or not, is extremely important. This is done to determine the effects of shading. Aste and Pero quantified this issue with the Shading Factor (SF) in their performance analysis of a large-scale ground-mounted PV plant. The shading factor is the percentage of solar radiation intercepted by the surface of the modules, compared to the total available radiation. A shading factor of 0.75 means that, on average, 25% of the incident solar radiation will be lost on the photovoltaic surface due to shading. Figure 19 illustrates this issue.

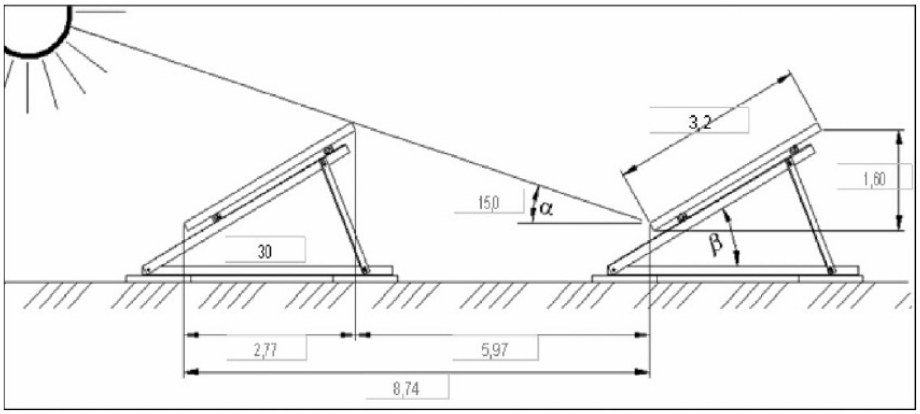

Figure 19: Placement of PV arrays to avoid array shading. [43]

One important piece of information for determining the distance between rows is the minimum solar height reached by the sun at twelve noon on the winter solstice. This value represents the lowest angle the sun will be at throughout the entire year. It is important to

make sure that full sun hits the photovoltaic units in the following row. Spacing between photovoltaic panels also depends on the tracking mechanism employed. More space is required between panels mounted on a double-axis tracking structure than a single-axis tracking structure to minimize to effect of shading. [41]

Another parameter that Aste and Pero used is the Ground Cover Ratio (GCR). It is the ratio of active photovoltaic area to the total ground surface occupied by the entire installation. Both of these values should be optimized when designing a large-scale photovoltaic plant. [43] Table 2 is from Aste and Pero's analysis and displays their results for both SF and GCR for each of the tracking systems.

Table 2: Covered surface, GCR and SF values. [43]

Plant type	Row/Column distance (m)	Covered Surface Area (m^2)	GCR	SF
Fixed	8.75	15000	0.39	0.98
1 axis E-W	12	20000	0.29	0.97
1 axis N-S	17	28000	0.21	0.965
1 axis N-S tilted	10x15	38000	0.15	0.95
2 axis	19x19	48000	0.12	0.94

Conclusions:
Following the literature review the decision has been made to use a single-axis tracking device for our design of an electrochemical energy storage integrated photovoltaic system. Each of the three chosen locations will utilize this tracking device on either a north-south or east-west orientation.

2.2. Electrochemistry

2.2.1. Electrochemistry Background

Electrochemistry is the study of chemical reactions in which an electron and/or ion is transferred during the reaction mechanism. Knowing that the thermodynamic parameters that govern reaction behavior (Gibbs energy, entropy) are state functions, we can in theory direct the change in chemical potential of reaction $\Delta_r G$ into the change in electrical potential (voltage) of an electron and/or ion being transferred in the reaction. The relationship between Gibbs energy and cell potential is shown in equation 7.

$$E_{eq} = -\frac{\Delta_r G}{zF} \tag{7}$$

Where E_{eq} is the cell potential (the voltage generated between the electrodes), $\Delta_r G$ is the Gibbs energy of reaction, z is the charge number of the reaction (the number of electrons transferred in the reaction), and F (96485.3 $C\ mol^{-1}$) is Faradays constant (the product of Avogadro's number and the elementary charge).

An electrochemical system can operate in equilibrium mode, in which no net electron transfer is occurring and voltage is maintained at the cell potential calculated in equation

7, the open-circuit potential. These systems are commonly used as sensors because the Gibbs energy of reaction is a function of the concentration of the reactants and products. In the case of a car's oxygen sensor, 21% oxygen is maintained at a Pt wire on one side of an oxygen-ion conductive membrane, while the car's exhaust is passed across a Pt wire on the opposite electrode, the concentration difference generates an measurable electrical potential. The relationship between chemical potential and chemical composition is shown in equation 8.

$$\Delta_r G = \Delta_r G^O + RT \sum_i \nu_i ln \alpha_i \tag{8}$$

In equation 8, $\Delta_r G$ is the Gibbs energy of reaction, $\Delta_r G^O$ is the standard Gibba energy of reaction (when all activities are 1.0), R is the gas constant, T is absolute temperature, α_i is the chemical activities of species i, and ν_i is the stoichiometric coefficient of species i (where reactants have a positive ν_i and products negative).

When equations 7 and 8 are combined the relationship between cell potential and chemical composition of reactants and products is represented, this is known as the Nernst equation and is given in equation 9.

$$E_{eq} = E_o - \frac{RT}{zF} \sum_i \nu_i ln \alpha_i \tag{9}$$

In equation 9, E_{eq} is the cell potential, E_o is the standard cell potential (when activities are 1.0), α_i is the chemical activities of species i, and ν_i is the stoichiometric coefficient of species i. The activity of a species is a unitless ratio of the concentration multiplied by an activity coefficient (a non-ideality correction) and divided by a standard state (1 mol liter, 1 atm partial pressure, mass or mol fraction of 1.0). Because there is no inherently correct concentration scale for activity, care must be taken in selecting the correct standard Gibbs energy, standard potential and activity coefficient.

We have now established the relationship between a change in chemical potential and an electrical potential difference between the electrodes of an electrochemical cell. The electrodes can be connected electronically in series with an external load or power supply. A schematic of a basic electrochemical cell, the Daniell cell, is represented in Figure 20.

In Figure 20, the following overall chemical reaction is occurring:

$$Cu^{+2}(aq) + Zn(s) \rightarrow Cu(s) + Zn^{+2}(aq) \tag{10}$$

This reaction is occurring in two half-reactions:

$$Cu^{+2}(aq) + 2e^- \rightarrow Cu(s) \qquad (reduction\ half-reaction) \tag{11}$$

$$Zn(s) \rightarrow Zn^{+2}(aq) + 2e^- \qquad (oxidation\ half-reaction) \tag{12}$$

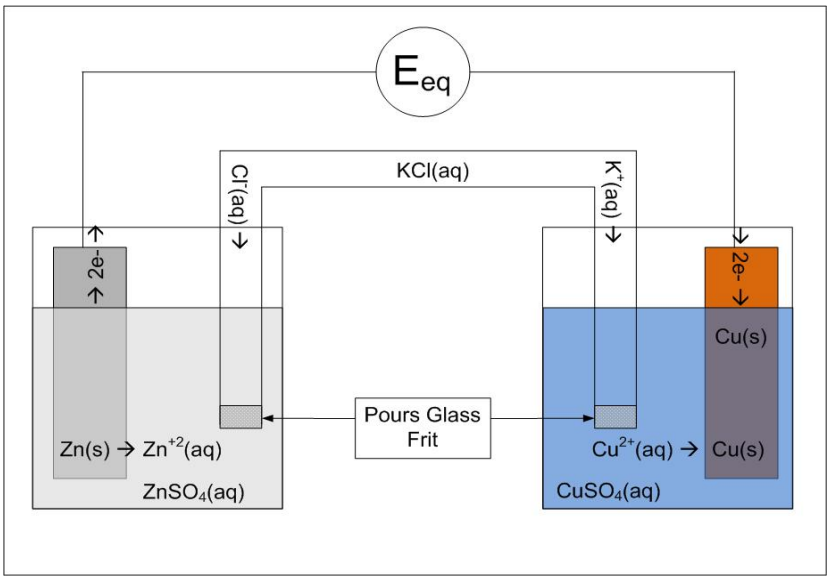

Figure 20: Daniell cell schematic.

These reactions are connected electronically through an external load or power supply and connected ionically via an ionically conductive aqueous salt bridge. The half-reactions are however physically separated and unique chemical environments are maintained. By convention the copper electrode in the Daniell cell is the positive electrode and the zinc is the negative electrode (this is determined because the reduction of Cu^{+2}(aq) ions has a more positive potential vs. a standard hydrogen electrode than the zinc reduction half reaction does).

When the reaction is allowed to occur in the spontaneous direction, electrical power is dissipated in the external load as the electrons travel from the negative electrode to the positive electrode. When a potential greater than E_{eq} is applied between the electrodes the electrons are forced from the positive electrode to the negative electrode, causing the electrochemical reaction to occur in reverse. A mass and charge balance allows us to equate the amount of material reacted directly with the total charge passed, this is known as Faraday's law and is represented in equation 13.

$$Q = \frac{m_i z F}{MW_i} \tag{13}$$

Where Q is the electrical charge passed (in coulombs), m_i is the mass of species i, MW_i is the molecular weight of species i, z is the charge number of the reaction and F (96485.3 $C\ mol^{-}1$) is Faradays constant.

The maximum electrical energy that can be stored in or extracted from an electrochemical reaction is the product of E_{eq} and the charge Q. Data collected from operating a Daniel cell in equilibrium, galvanic and electrolytic mode is shown in Figure 21.

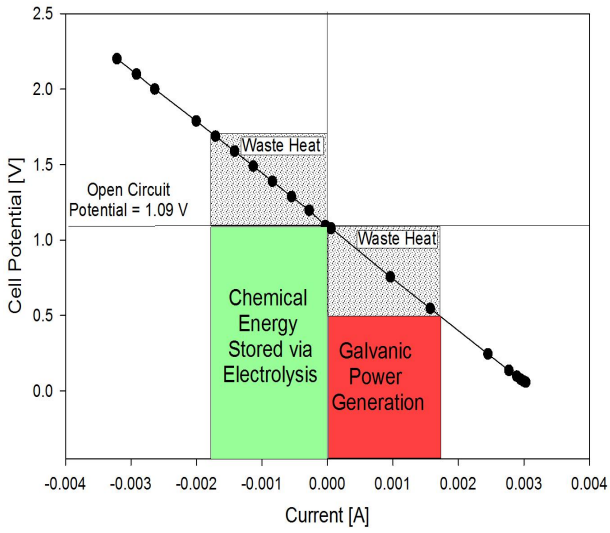

Figure 21: Voltage current relationship of Daniell cell. Data points with positive current represent electrical power being generated spontaneously (galvanic) across an external load; data points with negative current (electrolytic) represent electrical power being stored chemically in the system.

2.2.2. **Vanadium Redox Flow Cell Background**

The all-vanadium redox flow cell is an electrochemical system that can store and generate electrical power by altering the redox states of aqueous vanadium ions on opposite sides of a proton-conductive membrane. Figure 22 shows the all-vanadium redox flow cell.

The electrochemical processes that govern the behavior of the all-vanadium redox flow cell consist of two separate half-reactions that require the transfer of a proton across the membrane and an electron across an external load. The Gibb's free energy of that reaction is proportional to voltage, while the rate of reaction is proportional to amperage. From that electrical power can be extracted from or stored in the system, depending on the direction of the reaction.

The two electrochemical half-reactions are connected ionically via the membrane and electronically through an external load or power source. Therefore the extent of each reaction, or the number of protons and electrons reacted, must be identical for each electrode. However, the electrodes and half-reaction are physically separate and necessarily contain different chemical environments.

The chemical energy release from the system comes from the change in the redox state of the vanadium ions on both sides of the electrodes. When the vanadium cell is generating power (galvanic mode) the $VO^{2+}(aq)$ ions are converted to $VO^{+2}(aq)$ at the positive electrode shown in equation 14. The V^{+2} ions are converted to V^{+3} at the negative electrode shown in equation 15. The reverse reactions occur during the charging phase (electrolytic mode).

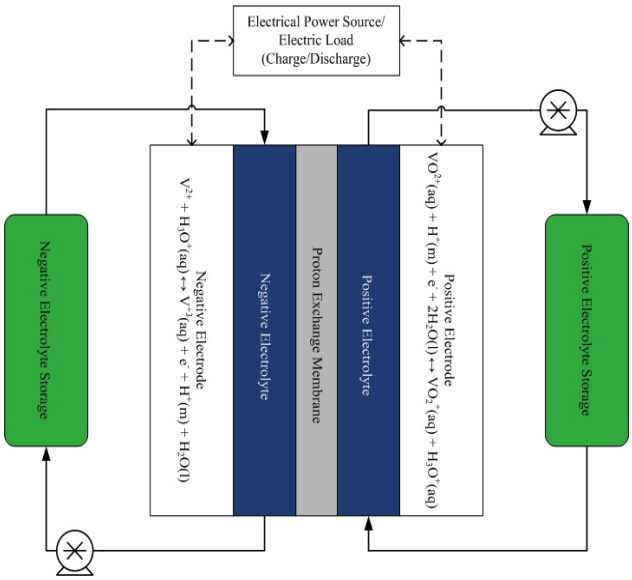

Figure 22: A schematic of the all-vanadium redox flow cell in bipolar plate geometry.

$$VO^{2+}(aq) + H^{+}(m) + e^{-} + H_3O^{+}(aq) \rightarrow VO^{2+}(aq) + 2H_2O(l) \tag{14}$$

$$V^{2+}(aq) + H_3O^{+}(aq) \rightarrow V^{+3}(aq) + H^{+}(m) + H_2O(l) + e^{-} \tag{15}$$

2.2.3. **Positive Electrode**

Solution:
Positive electrolyte solutions for vanadium redox cells can be generated by the oxidation of $VOSO_4$ in sulfuric acid solutions. Vanadium electrolyte used at the positive electrode must support concentrations of VO^{2+} and VO^{+2} in the range of 1.5 to 5.4 M and H_2SO_4 from 3.6 to 4.3 M. [44] [45] The active species in positive vanadium redox flow cell electrolyte solution are VO^{2+} and VO^{+2} aqueous ions where the redox numbers of vanadium are +5 and +4, respectively.

Increasing the concentration of electro-active species in the electrolyte solution is an integral component of reducing the volume and cost of the system. Precipitation inhibitors, such as KCl, have been used to prevent precipitation of solid vanadium species in the positive electrolyte solution. [46]

Electrode:
A variety of carbon-based electrodes have been studied for the positive electrode. These electrodes must be chemically stable towards VO^{2+}, VO^{+2} and H_2SO_4 in their aqueous saturated conditions up to 40°C. The species most responsible for chemical degradation in the system is the VO^{+2} ion. Carbon-felt electrodes are the most commonly utilized style. Pure carbon-felt and precious metal-doped carbon felts have been studied. [47] [48] Though carbon-felt remains the most commonly employed positive electrode in all

vanadium redox flow cells, a variety of novel carbon-electrode designs have also been shown to function, including: highly hydroxylated carbon fibers, graphite and carbon nano-tube composites, and several carbon-polymer designs such as polypropylene. [49] [50] [51]

2.2.4. Negative Electrode

Solution:
The negative electrolyte solution is very similar to the positive one with the exception of the active ions V^{+2} and V^{+3} (rather than VO^{2+} and VO^{+2} at the positive electrolyte). Generally, 3-4 M H_2SO_4 and 1.5-3.0 M V_2O_5 are prepared to maximize the concentration of V^{+2} and V^{+3} ions. However limitations to concentration and effects on chemical stability of the membrane and electrodes are not as limited as those in the positive electrolyte. The negative electrode and reaction are not limiting to system performance and are less studied than the positive electrode. [52] [44]

Electrode:
Carbon-felt and carbon-paper are the most common electrode material for the negative electrode of the flow cell. As the negative electrode kinetics and chemical stability are not limitations to system performance in all vanadium redox flow cells, carbon-felt electrodes are generally accepted as ideal in studies of the negative electrode. [44]

2.2.5. Full System

The all-vanadium redox flow cell systems are generally designed to produce and receive 1 kW to 10 MW of power for a full-system cycle duration of about 8 to 24 hours. They are typically utilized to level unstable power generation and demand or as uninterruptible back-up power for sensitive industrial facilities (semi-conductor fabrication).

The full system, shown in Figure 22, has two separate and simultaneous half-reactions at electrodes that are connected ionically via a proton-conductive membrane and electronically across an external load or power source. The system operates reversibly allowing for the storage and release of electrical power for over 10,000 cycles and has been shown to demonstrate overall charge to discharge efficiencies of more than 80% in operational systems. [53] The sum of the two half-reactions described above is shown in figure 16 for the galvanic power generation phase.

Overall Electrochemical Reaction:
Adding Reactions 14 and 15, above, the overall reaction corresponding to the galvanic power generation mode of the flow battery can be written as:

$$VO^{2+}(aq) + V^{2+}(aq) + 2H_3O^{+}(aq) \rightarrow VO^{2+}(aq) + V^{+3}(aq) + 3H_2O(l) \qquad (16)$$

The opposite direction of reaction 16 corresponds to the electrolytic mode of the flow battery.

Open-Circuit Potential and Thermodynamics:
The overall electrochemical reaction, shown above, has a corresponding change in Gibb's free energy, $\Delta_r G$, between the reaction products and reactants. The maximum electrical

potential (voltage) that can be extracted from the reaction can be calculated by the Nernst equation shown in equation 9.

The electrochemical reaction at unit activities shows a $\Delta_r G^o$ of -117.723 kJ/mol or a E^o of 1.241 V at 25°C. However, systems commonly operate with vanadium concentrations from 1.5 to 5.4 M and H_2SO_4 from 3.6 to 4.3 M and to maximize the open-circuit potential, these systems in practice show open-circuit potentials of 1.3 to 1.5 V. [52] [54] [55] The standard electrode potential for the all-vanadium redox couple from 0 to 100°C are calculated and given in Figure 23.

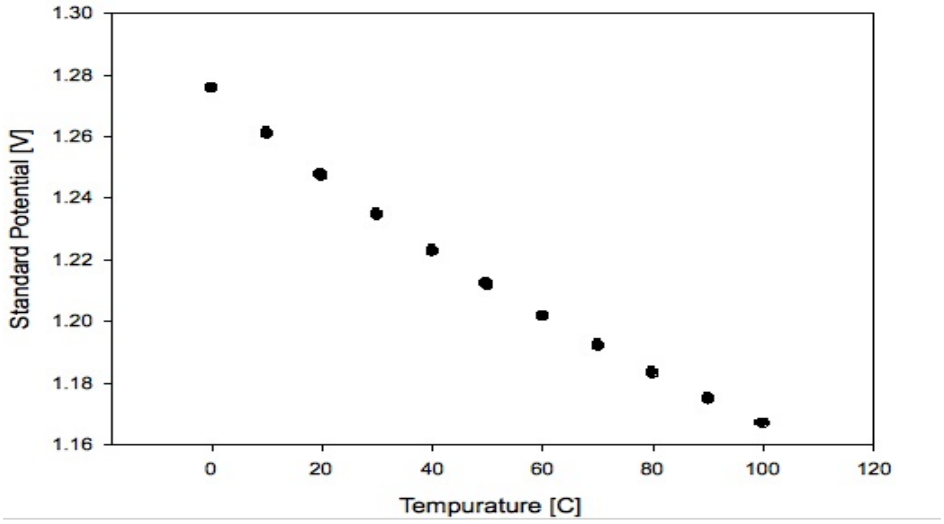

Figure 23: Standard Reaction Potential for All-Vanadium Redox Flow Cell. Any deviations from unit activity can be addressed via the Nernst equation.

Membrane:
All-vanadium redox flow cells require a proton-conductive membrane that minimizes vanadium and water crossover and resists chemical degradation from VO^{2+} (V^{+5}). [56] [47] [57] Nafion alone has been used in small-scale vanadium redox cells but shows high permeability to water and vanadium ions, and is not chemically stable for long periods of time with $VO^{2+}(aq)$ ions. The most frequently used membranes in Vanadium redox flow cells are composed of Daramic (a high-density micro-porous polyethylene separator) doped on the negative electrolyte side with a proton conductive polymer resin, such as Nafion. [58] This and similar designs have been well studied and show low permeability to vanadium species and water, as well as no chemical degradation from the positive electrolyte solutions. [59][60] [56]

A variety of other proton-conductive polymer-composite membranes have also been studied. Sulfonated poly(ether ether ketone) (SPEEK) and other similar sulfonated or chlorinated polymers, with and without Nafion impregnation, have been shown as viable alternatives to Daramic based membranes. [61] [56] [62] Several Nafion-silicate hybrid membrane composites have been shown to function as membranes with sufficient resistance

to vanadium and water permeation and chemical stability to electrolyte solutions. [63] [64]

Performance, Energy and Power Density:
Vanadium flow cells are used in full industrial-scale, uninterruptible power systems as well as for grid and wind farm power leveling. Power and energy densities of 100 mW/cm^2 and 25 Whrs are common in operational systems of up to 10 MW of electrical power. Due to membrane thermal stability, vanadium precipitation limitations and viscosity operational system, the operational temperature range is between -5 and 40°C [53] [65] [66]

2.2.6. Current Technology

Commercial Products:
Vanadium flow cells are beginning to enter the commercial market however energy density limitations caused by vanadium solubility limits significantly affect the cost of the system. The modern all-vanadium redox flow cells can generally be used where 1kW-10 MW power daily fluctuations need to be leveled. These systems are found in industry as back up power, in wind farms for stabilized power generation and in transforming stations to meet peak power demands without increasing power generation. [67] [68]

Challenges and Opportunities:
The limited volumetric energy density of the electrolyte solutions is the primary restraining factor to all-vanadium redox cells. Within membrane studies, preventing H_2O and vanadium crossover and chemical membrane degradation are the primary focus. A review of Nafion and Daramic could provide an avenue of study.

2.3. System Components

Based on the literature review, the components of the system we will design are as follows (see figure 24 for a similar system).

1. PV Array: CdTe and pc-Si modules. Cells are tabbed together in series to create modules. The modules are then strung together to form arrays. These convert solar irradiance to electrical energy.
2. Mounting Structure: Single-Axis Tracking. Support structure and angle of incidence minimization for PV arrays.
3. Charge Controller: DC-DC converter. Converts the DC output from PV arrays to the DC input for the redox flow cells and regulates the voltage-current ratio.
4. Redox Flow Cell: V_2SO_4, H_2SO_4. Converts electrical energy from the PV system to chemical energy for storage.
5. Storage Tanks. Reservoir for storing vanadium ions in solution.
6. Inverter - DC-AC three-phase converter. Converts the DC output from the PV arrays and flow cells to high-voltage AC for distribution.
7. Balance of Systems (BOS) Components: wiring, conduit, disconnects, pumps etc. All other minor components required for system installation that are not listed above are included in BOS.

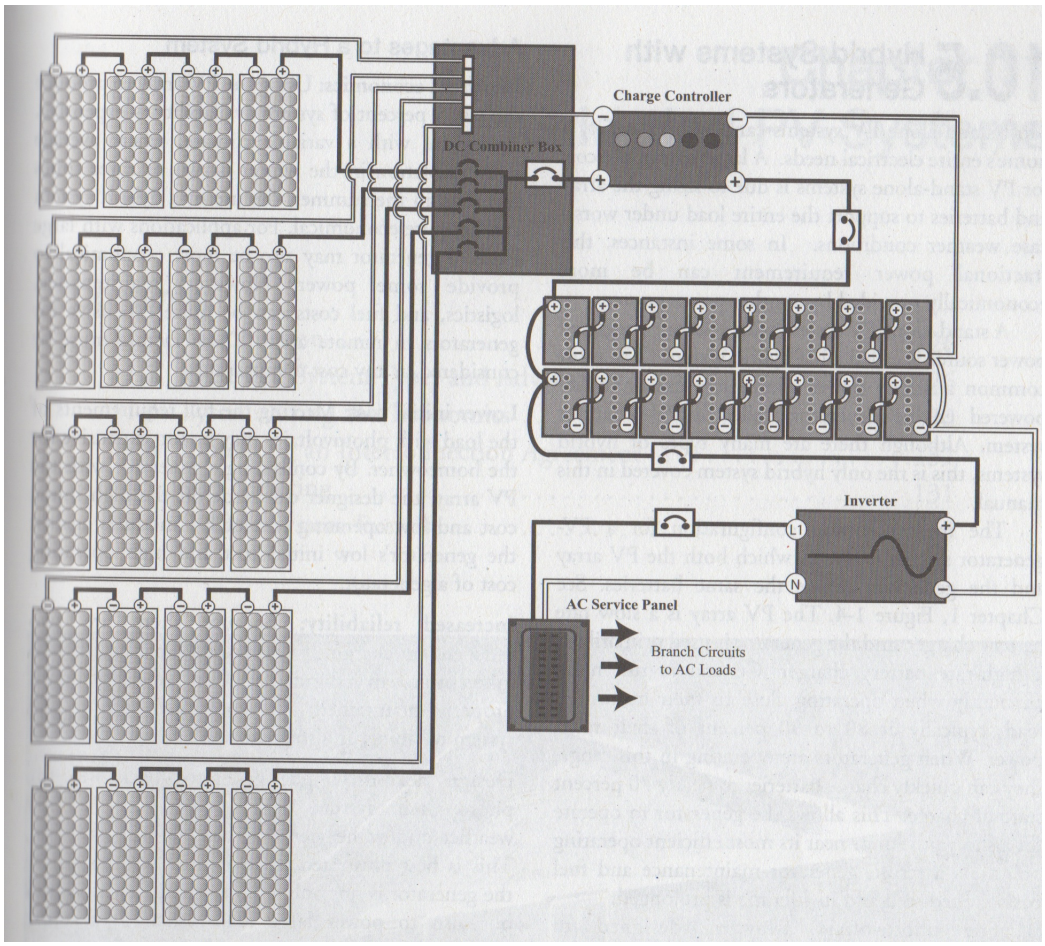

Figure 24: An illustration of an example stand-alone PV system and all of the electrical components. Not shown are installation materials and mounting systems. [69]

2.4. **Economic and Policy Analysis**

Costs and Benefits of the PV System:
For the economic concerns, we will consider the actual capital cost and annual cost within our system design. The capital cost includes the cost of modules, array field, fixed mounting structures, installation, design and accessories. A market survey will be performed to provide a complete evaluation of the capital cost for each part. Table 3 shows the average cost of various components in a PV system.

After determining the initial capital investment, it is also necessary to calculate the weight of annual maintenance and management as annual cost. On the basis of the above information, we can simulate the performance of the system for each year and sum over the system's life time.

Taking into consideration the impact of all involved costs (components, land, operation, maintenance etc.) in contrast to generated incomes, we can perform an economic assessment by determining the IRR (Internal Rate of Return). [70]

Table 3: Average cost of components for a PV system in $/kW. [43]

Component	Min Cost	Max Cost	Average
Modules	4000	4830	4416
Inverter	248.4	386.4	317.4
Fixed mounting structures	248.4	358.8	303.6
One-horizontal structures	552	828	690
One-tilted-axis mounting structures	828	1242	1035
Two-axis mounting structures	1242	1656	1449
Installation	345	483	414
Design and accessories	828	1380	1104

The levelized cost of energy was calculated for several solar reference units including: residential and commercial photovoltaic (PV) systems, and large scale PV and concentrating PV systems. It was also calculated for large scale solar thermal units including: solar parabolic troughs, solar parabolic dishes and central solar towers. Subsidies are still required to make solar power cost competitive with conventional generation systems. However, future reductions in solar equipment manufacturing costs and increases in solar system efficiencies will continue to make solar power even more cost competitive in the future. The competitiveness of solar electricity could be greatly improved by future spikes in the prices of fossil fuels used in generation since solar power has no fuels costs. In addition, coal generation could be negatively affected by restrictions on greenhouse gas emissions or taxes on emissions. This would make solar power even more competitive since it does not emit significant levels of greenhouse gases. Solar electricity production revenue could potentially be enhanced by selling carbon credit to other companies.

The levelized cost of energy from photovoltaics currently ranges from about 20 to 35 cents per kWh. This cost is mostly a function of the cost of solar photovoltaic modules. As module costs decrease other factors are likely to become more prominent. Module costs were $10-20 per watt in the 1980s and fell to $5-10 per watt in the 1990s. Currently, solar photovoltaic modules retail at around $4.80 per watt in the U.S., with some thin-film products retailing as low as $3.70. Figure 51 illustrates the historical and projected levelized cost of energy (LCOE).

Costs and Benefits of Vanadium Redox Flow Cells :
The vanadium flow battery has emerged as one of the most favorable and economical types of flow batteries. We will examine the cost of the storage system by three parts: 1) cost related to power, 2) cost related to energy, and 3) cost related to balance of the system. In a flow battery, cost/kW and cost/kWh can be related to the cost of power modules and the cost of electrolyte including tanks and sensors, respectively. Maintenance cost to keep the balance of the system will depend on the ratio between power and energy (kW/kWh). [72] Since this ratio varies for different designs, we would like to make the cost comparison among energy storage systems during the whole life time span (25 years for a reasonable estimation). Based on the cumulated energy delivered over the lifetime of the battery, the cost-benefit analysis will include initial investment, operation, replacement, maintenance

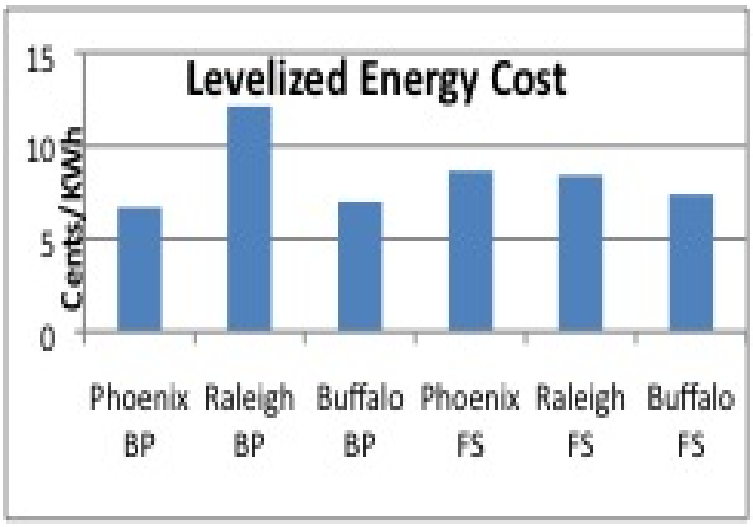

Figure 25: Levelized Cost of Photovoltaic Power, Historical (1980-2005) and Projected (2006-2025). [71]

and the costs of energy for the costumers.

We expect to quote sales price for the vanadium flow cell, stacks, tanks, electrolyte, pumps and controls. Typical depth of discharge (DOD) and cycle numbers were taken into account and the total number of kWh over the battery life will be estimated. Compared to other types of batteries, such as Pb-acid and Li-ion we expect the maximum energy may be achieved by a vanadium flow cell, for only one species of metal is applied in the electro-chemical redox reaction and the liquids can be reused without recycling. [73] Although the initial investment for a vanadium flow cell is relatively high, the electrolyte does not lose value and could be reused in another new installation. This counts for another benefit on the life cycle assessment for reuse. Vanadium flow cells require less investment per delivered kWh over the battery life. The strategy employed by the vanadium flow cell is to give the more efficient use of the stored energy than the standard single-stage operation.

In general, most of the cost of the vanadium flow cell materials are for the vanadium oxide and electrolytes. The labor costs account for approximately 10% of the total. Some cell components are still in the industrial-development stage; we expect the economy of a larger scale will lead to further cost reduction. As the design progresses we will use costs performance curves to illustrate the efficiency of the flow battery.

For the system, if the demand exceeds the solar production, electricity will be taken from the grid or the battery, depending on availability and costs. The management of the storage unit, the ownership, rights and duties are also important issues for the realization of the system. For evaluation, economic, social and the environmental issues are being considered.

Environmental and Social Impacts from Solar Energy Technologies:
Compared to conventional energy sources, solar energy systems provide significant benefits contributing to the sustainable development of human activities. When designing a solar energy system, potential environmental and social implications, especially any negative

impacts, must be considered. [74]

The macro-scale socio-economic benefits of exploitation for a solar energy system will be: 1) increase national/regional energy independency; 2) support of the deregulation of the energy market; 3) security and diversification of energy supply; and 4) acceleration of rural electrification in developing countries. There are some unfavorable effects: 1) loss of amenity; and 2) visual impact. Regarding the second point, appropriate siting of the solar systems involves careful evaluation of alternative locations and estimation of expected impact. Locations are often desired away from densely populated areas and not in protected areas with significant biodiversity or natural beauty. In order to ensure public acceptance, engagement of the public and relevant organizations in the early stages of planning is important.

One of the benefits from PV is that "it is one of the most viable renewable energy technologies for use in an urban environmental, replacing building cladding materials [sic][75]." Additionally to being used as building integrated photovoltaics (BIPV), PV systems have the avoidance of pylons and wires as a major advantage, making them an intriguing option for use in scenic areas and National Parks. The impact of land use on natural ecosystems is dependent upon specific factors such as the area of land covered by the PV system, topography of the landscape and the distance from areas of sensitive ecosystems. The "sentimental bind" of the cultivator and his cultivable land is likely to be the reason of several social displeasure and disagreements. [76] To avoid land-use complications, adding photovoltaics to the roof of existing buildings is solution if the PV scale is relatively medium or small. Since we are exploring large-scale PV, rooftop systems and BIPV are not an option.

Different types of PV systems lead to different visual intrusion. If a PV system is installed near an area of natural beauty, the visual impact would be significantly high. When it comes to the modules integrated into the facade of buildings, there might be positive aesthetic impact on modern buildings in comparison to historic buildings or buildings with cultural value. [77] A possible method to solve visual problems is to use color to assemble the PV modules in large-scale systems.

The manufacture of crystalline silicon solar cell is very energy intensive, especially for the poly crystalline and the mono-crystalline modules. In many thin films, large quantities of several scarce materials are used such as tellurium (Te), gallium (Ga), indium (In) and cadmium (Cd). [78] To minimize environmental impacts related to the production of the PV cells we can explore: 1) prospects for thinner cell layers; 2) the full potential of the concentrator PV technologies; 3) safer alternatives and materials; 4) module recycling technology; and 5) prospects for more efficient material utilization.

Complete System:
For each of the three locations we have decided on, we will collect policy information on construction permit regulation, land use, local incentives, feed-in tariff, possible commercial and residential issues, utility price and other parameters relative to the designed system. Such environmental and local aspects of information are very critical for determining the economic effectiveness for the system. Aside with the material and maintenance cost, we

can evaluate the capital cost and marginal cost of our system. By summing the local incentives and utility cash flow-in of our system, we will obtain the total benefit for each time period. The cost-benefit analysis is described in equation 17.

$$NPV = -C_o + \sum_{i=1}^{N} \frac{B_i - C_i}{(1+r)^i} \tag{17}$$

Where, NVP is the Net Present Value, C_o is the capital/initial cost (which include the material cost , installation cost, cost for construction permit and feed-in tariff); B_i is the benefit or revenue for each operating year (LCOE*total energy production); C_i is the annual cost for maintenance and operating; r is the interest or discounting rate and N is the total life time span.

Economic Parameters:
Feed-in tariff policies are driving rapid renewable energy growth for electricity generation. As shown in figure 26, there are currently 26 states with mandatory renewable portfolio standards (RPS) in the United States, and another six states have established non-binding renewable energy goals. In order to meet increasingly aggressive environmental and economic development goals, US policy makers are looking at new ways to accelerate renewable energy market growth. Among the emerging policy mechanisms that are being considered are feed-in tariffs. The rapid emergence of both federal and state feed-in tariff proposals in the US represent a significant opportunity for the development of the renewable energy industry. A federal feed-in tariff law could transform the US renewable energy market. [79]

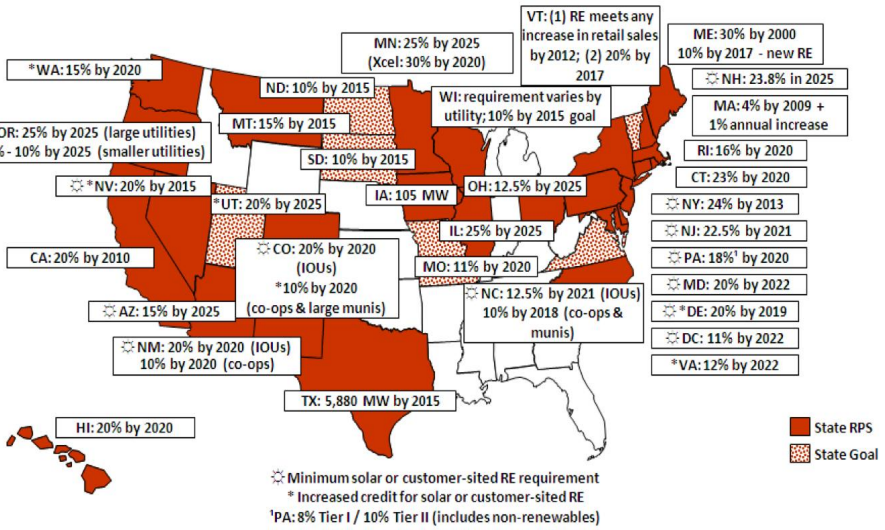

Figure 26: Renewable Portfolio Standards and Goals in the United States. [80]

Land-use is also an important factor that will be considered for photovoltaic deployment. The land-use for large-scale, grid connected solar power is large relative to that for other

electricity-generating technologies due to the large area of land needed to collect sufficient solar radiation for generation on the megawatt scale. In general large solar thermal and photovoltaic plants use about 5 acres of land per MW of peak capacity. Concentrating solar photovoltaic units use focused sunlight and thus use less land per unit of capacity, only 4 acres per MW. Distributed solar generation is used on site and does not require any additional land if the current roof or building facade is not an active surface. Table 4 illustrates the amount of land needed to support the solar generating requirement for Arizona to meet their 15% renewable energy goal by 2025 is all of that energy is generated from photovoltaics. The solar power industry would require 13,137 acres or 20.5 square miles of land to produce the amount of electricity. [80]

Table 4: Solar power incremental and total land use (in acres) projections to 2030 for the state of Arizona. Adapted from Frisvold et al. [80].

	2010	2015	2020	2025	2030
Incremental Land Use	47.4	209.9	804.8	1602.8	707.8
Total Land Use	47.4	675.0	3571.3	9858.1	13136.7

The subsidy and incentive will also be included in our analysis. A federal investment tax credit (ITC) is available to individuals or organizations that invest in solar power systems. The federal ITC offers a tax credit of 30% of the cost of purchasing and installing a solar power system for certain systems. This year, the federal government removed the maximum credit levels required in previous years. This has had a significant impact on the LCOE for solar power systems, particularly large-scale PV systems that previously had their subsidy limited by the maximum constraint. Residential and commercial customers have an additional incentive for purchasing and installing solar power units from their local utilities. All of the state's major utilities and electric cooperatives offer incentives for the purchase and installation of solar power systems. Unlike the federal and state investment tax credits, which are based on a percentage of the total cost of the solar system, these utility capacity based incentives (CBI) offer a fixed amount of incentive per installed kW capacity of solar units. Unisource Electric and the electric cooperatives also have similar programs, but Arizona Public service is used as an example to avoid excessive duplication of the example. [80]

Construction permit is required for the installation of a solar energy system and the costs for permit vary across states and cities. Local municipality may or may not require a building permit for installation of your solar PV system. Also, it may take up to a month to obtain the construction permit for solar system, although the time opportunity cost in the time waiting for the permit can be neglected, practically it is recommended to apply for the permit as soon as the solar design is finished.

System installation, completion and inspection: After all materials are delivered to the solar land, installation date will be dependent on the weather, our commitments to other installations, and any constraints that you may have. It is expected that installed system prices will approach $4.00 per watt by 2010 from their current level of $6.00 per watt as thin-film production volumes increase and new silicon refiners come on line. [81] Annual

inspection for the designed system will be calculated into part of the maintenance cost.

In addition to the aforementioned parameters, based on the literature several other important metrics to evaluate are levelized cost of energy (LCOE), payback time and net present value (NPV). In conclusion, the economic analysis will be based on cost-benefit analysis method and the assumption of a constant interest rate, including national as well as local economic parameters to assess the total costs and benefits over the life time of the system, and net present value of the projected income.

LCA stands for Life Cycle Assessment and is a "cradle to grave" approach for evaluating products, processes or services. It is used to assess the environmental aspects and potential impacts associated with these products, processes or services. Standards for an LCA must comply with the International Standards Organization (ISO) 14000 series set by the U.S. Environmental Protection Agency (EPA). The LCA framework consists of four components which are listed below and can been seen in figure 27.

- **Goal Definition and Scope:** This is where the product, process or activity is defined and described. The context in which the assessment is to be made is established. Also, the boundaries and environmental effects to be assessed are identified.
- **Inventory Analysis:** Energy, water and material usage along with environmental releases are identified and quantified in this step.
- **Impact Assessment:** The potential human and ecological effects of energy, water and material usage as well as the environmental releases identified in the inventory analysis are assessed in this step.
- **Interpretation:** The results of the inventory analysis and impact assessment are evaluated. The preferred product, process or service can then be selected fully knowing the uncertainties and assumptions used [82].

As mentioned above a Life Cycle Assessment is used to evaluate products, processes or services throughout their life cycle. Life cycle refers to the major activities in the course of the product or system's life-span from the acquisition of raw materials, manufacturing, use and maintenance to its final disposal. The four phases of a life cycle assessment are shown in the diagram below. They are Raw Material Acquisition, Manufacturing, Use/Reuse/Maintenance, and Recycle/Waste Management [82]. A fifth phase of Transportation should also be included but is not required by ISO.

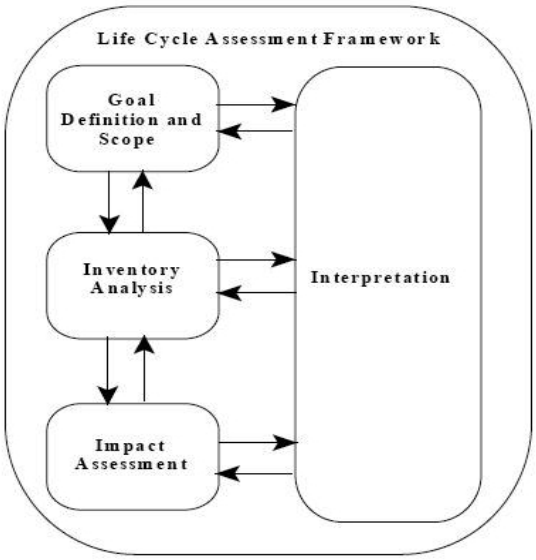

Figure 27: Lifecycle Assessment Framework [82]

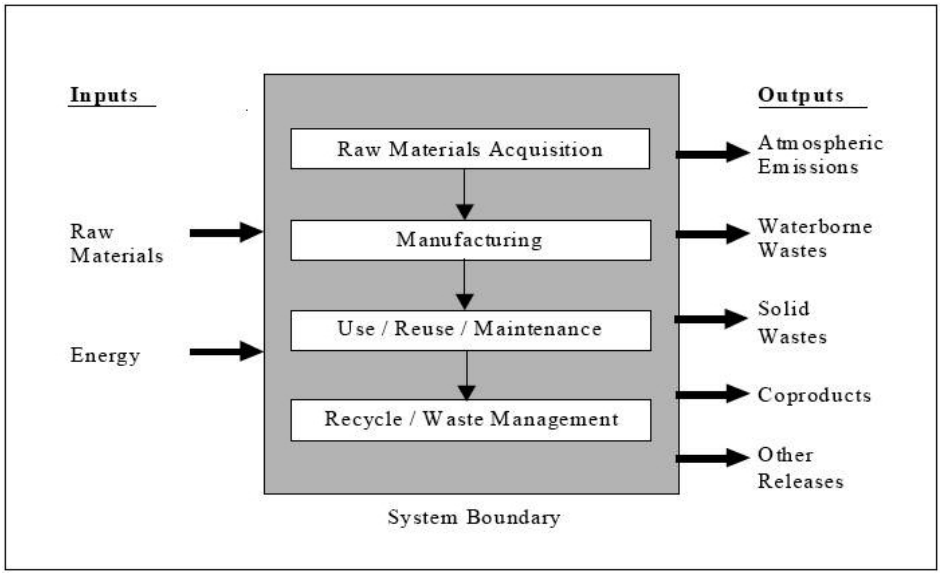

Figure 28: Life Cycle Stages [82]

3. Preliminary Conclusions

The preliminary conclusions from each section in the above literature review will be used to determine our final design of an electrochemical energy storage integrated photovoltaic system.

Economic, environmental and policy analyses will be performed after the final system design to determine the viability of the project. Also, a life cycle assessment of all system components will be performed to determine the specific cradle-to-grave impacts. Specifications for the project follow:

- Location: Phoenix, AZ (high irradiance), Rayleigh, NC (medium irradiance) and Buffalo, NY (low irradiance)
- PV materials: Cadmium Telluride and Polycrystalline Silicon
- Mounting Systems: Single-axis tracking (either N-S axis or E-W axis)
- Energy Storage: Vanadium Oxide Redox Flow Cell
- PV-Storage daily duty cycle: as illustrated by figure 29

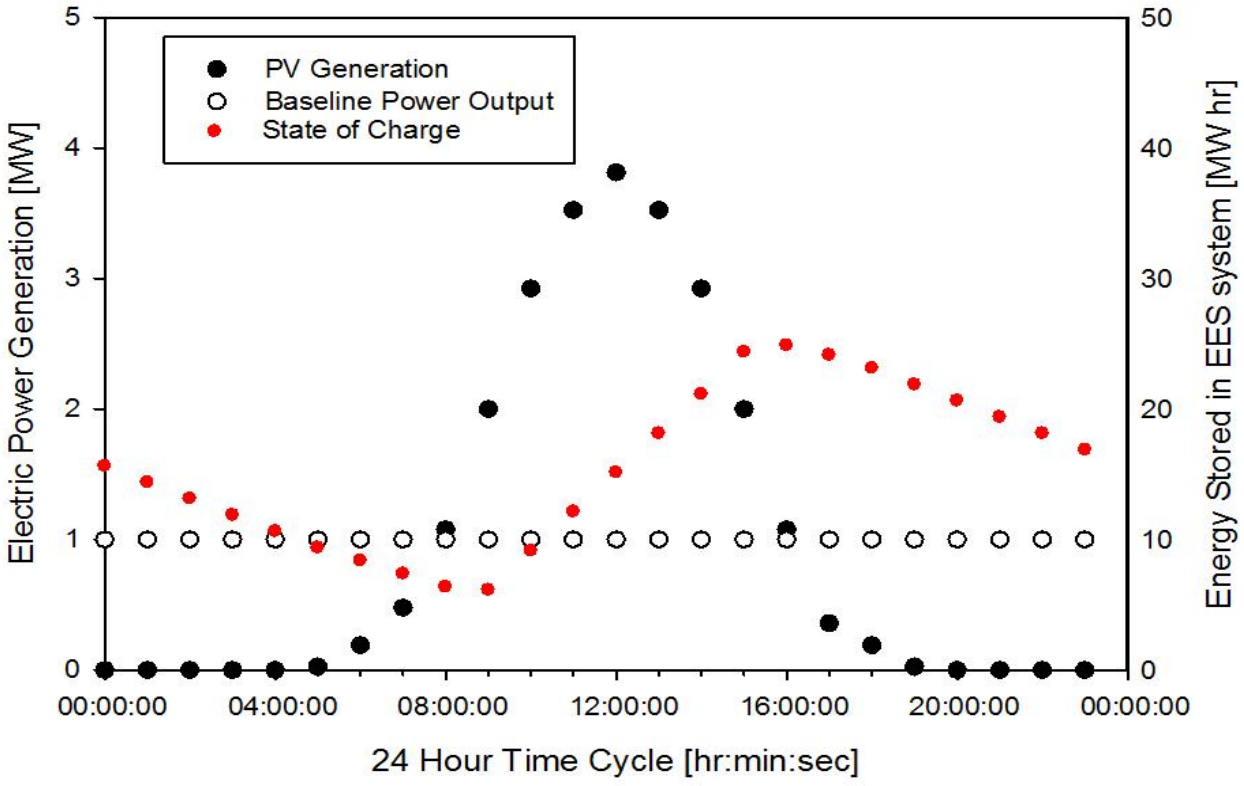

Figure 29: The daily duty cycle for the electrochemical energy storage integrated photovoltaic system.

4. Engineering Assessment

4.1. Methodology

4.1.1. Insolation and Weather

The solar resource at each location was modeled using Typical Meteorological Year (TMY2) data. TMY2 data sets were produced by the National Renewable Energy Laboratory under the Resource Assessment Program. They are generated from weather and insolation values from the National Solar Radiation Data Base (NSRDB) for the years 1961 to 1990. TMY2 provides a good estimate for average energy generation since the values are compiled as climate averages. As we are interested in the long term performance of the system rather than exact performance each day, TMY2 datasets are an appropriate data source. In order to further predict the exact performance of the system a different type of data would be required. Table 5 provides a complete list of TMY2 parameters.

Table 5: TMY2 Data Elements and Their Degree of Completeness. Adapted from [83].

Element	Data Completeness	
	Class A	Class B
Extraterrestrial Horizontal Radiation	1	1
Extraterrestrial Direct Normal Radiation	1	1
Global Horizontal Radiation	1	1
Direct Normal Radiation	1	1
Diffuse Horizontal Radiation	1	1
Global Horizontal Illuminance	1	1
Direct Normal Illuminance	1	1
Diffuse Horizontal Illuminance	1	1
Zenith Luminance	1	1
Total Sky Cover	1	1
Opaque Sky Cover	1	1
Dry Bulb Temperature	1	1
Dew Point Temperature	1	1
Relative Humidity	1	1
Atmospheric Pressure	1	1
Wind Direction	1	1
Wind Speed	1	1
Horizontal Visibility	2	2, 3, 4
Ceiling Height	2	2, 3, 4
Present Weather	2	2, 3, 4
Precipitable Water	1	1
Broadband Aerosol Optical Depth	1	1
Snow Depth	1	5
Days Since Last Snowfall	1	5

Notes:

1. Serially complete, no missing data.
2. Data may be present only every third hour.
3. Nighttime data may be missing.
4. Data may be missing for up to 47 hours.
5. Serially complete, except for Colorado Springs, CO.

The data is composed of hourly values of insolation and meteorological parameters for a 1-year period based on hourly time-steps. Not all of the values shown are measure; the direct and diffuse radiation are calculated from the global radiation; the illuminance values are calculated from the respective radiation values.

TRNSYS reads the entire TMY2 file and allows each parameter to be utilized as an input to any number of devices. The necessary values for each site are temperature, relative humidity, wind speed, direct and diffuse irradiance and total irradiance on the horizontal. These values are fed into TRNSYS for use in the energy simulation. Additionally, the weather importer can calculate the energy incident on a surface based on the horizontal values.

4.1.2. Photovoltaic System

The photovoltaic systems were modeled using TRNSYS, the Transient Energy System Simulation Tool, a Fortran component-based transient energy simulation engine. TRNSYS was developed by the University of Wisconsin and Colorado State University in 1975. It was originally for thermodynamic energy systems but was later expanded to include a wide variety of energy systems.

The simulation consists of a weather processor (Type109), photovoltaic modules (Type 94a and 94b for crystalline and thin film respectively), DC-DC and DC-AC converters (Type 48), batteries (Type 47), and data plotters (Type 65). Simple equations were used for conversions between units. The EESiPV system was able to be modeled properly using the standard TRNSYS component library.

The analysis consisted of calculating the potential of both thin film (First Solar's FS3 77.5 watt modules) and monolithic silicon modules (BP Solar's PB3235N 235 watt modules) at each location. Table 6 lists both of the modules parameters. Module voltages are determined by the material band structure and the number of cells tabbed in series. The next parameter, module current, is proportional to the surface area of the cells.

Table 6: Photovoltaic Device Parameters

Parameter	Units	BP	First Solar
P_{max}	watts	235	77.5
I_{sc}	amps	8.48	1.84
V_{oc}	volts	37.2	60.7
T_{ref}	Kelvin	298	298
I_{mp}	amps	7.89	1.61
V_{mp}	volts	29.8	48.3
I_{sc} Temp coefficient	$\frac{\%I_{sc}}{^\circ C}$	0.00105	0.0004
V_{mp} Temp coeficient	$\frac{\%V_{mp}}{^\circ C}$	-0.0036	-0.0027
Cells in series	#	60	154
Module Area	m^2	1.667	0.72
Semiconductor Bandgap	eV	1.12	1.44

The arrays all followed maximum power point tracking routines, and the maximum power output linked directly to the electrochemical storage system. The physical system would consist of a switching mechanism that changes the series and parallel connections of the redox flow cells to match the PV system voltage in a 98% efficient process. In the simulation, the desired switching mechanism could not be modeled so a DC-DC regulator

was used to simulate the actual mechanism. In the TRNSYS simulation, the PV system voltage was stepped to match the constant voltage of the flow-cell battery system.

4.1.3. Energy Storage

This section addresses the flow of electrical energy from the photovoltaic array to the grid. The energy flow analysis of the system considers electricity stored and released from the vanadium redox flow battery as well as the excess photovoltaic electricity sent to the grid without storage. Conversion efficiencies of transferring electricity from the photovoltaic array to the flow battery and grid, as well as electrochemical efficiency losses are addressed. Each of the three locations are considered on a month to month basis to maximize profit in peak production months while guaranteeing a minimum base load of 1 MW in the lowest solar resource months. The efficiencies of polycrystalline silicon and cadmium telluride photovoltaic arrays are also addressed.

The energy output of each system will vary as a function of time of day, month of year, location, and photovoltaic materials. In all cases the system will provide a minimum of 1 MW of base-load power 24 hours per day, 365 days per year. The peak electrical power generated by each system will fluctuate based on the solar resource and material choice of each individual system.

Electrical power generated by the photovoltaic array will be sent to the electrochemical battery via a DC voltage that is matched by a flexible voltage system with series to parallel switching. This component has a regulating efficiency of 98%. Electrical power generated by the photovoltaic array in excess to that used to charge the flow battery will be inverted and sold directly to the grid with a 95% power efficiency. Within the vanadium redox flow cell, an operational charge to discharge efficiency of 94% is predicted, this drop will come only in the form of voltage reduction. Direct current power generated by the flow battery will be inverted and sold to the grid with a 95% power efficiency.

Vanadium redox flow cells are scalable to both the power and energy requirements of the system. Based on the energy storage needs of the EESiPV system a maximum of 25 MWh of energy storage will be supplied by the system, this allows the storage of 42% more electrical power than the average day in the worst performance month of any location and PV design modeled. The oversized storage tanks allow for continuous power generation with short term PV outages due to maintenance as well as local weather. The two electrolyte storage tanks will hold 225,000 liters of solution each; and will have cylindrical dimensions of 4 meters heigh with a 4.24 meter diameter. Each tank will be made of high density polyethylene (HDPE) with secondary containment and indoor storage.

In order to generate the electrolyte solutions required for 25 MWh of energy storage in a vanadium flow cell 125,000 kg of V_2O_5 will be dissolved into 450,000 liters of 2.0 M H_2SO_4. The temperature and pH of the solution during preparation will determine the redox states of the ions in solution. However the preparation and installation of this system and its materials will be handled by the commercial supplier (Prudent energy e.g.).

The power demands of the EESiPV system call for a maximum charging rate of 4.0 MW. The membrane active area is directly proportional to the maximum power it can receive or

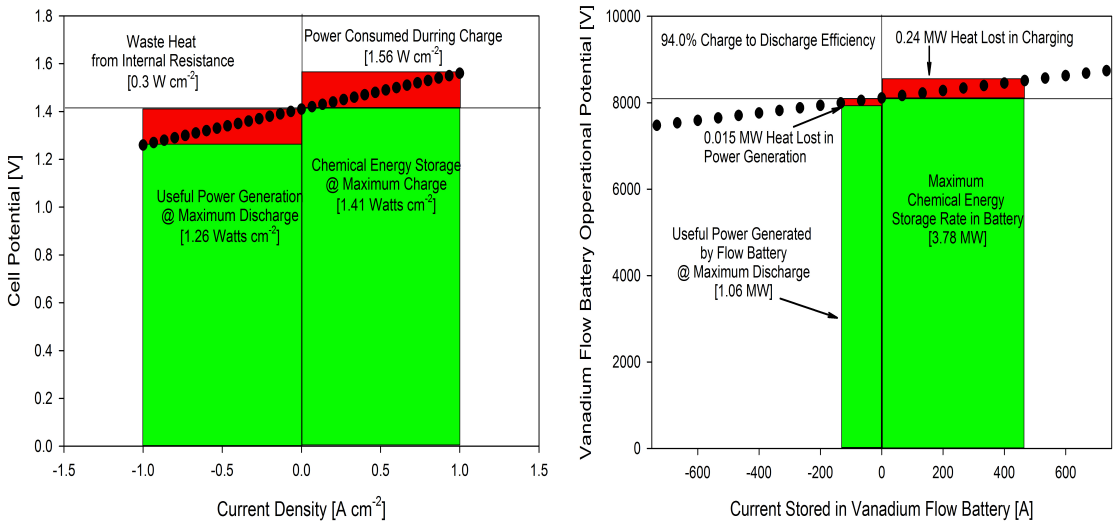

Figure 30: Area specific performance curve for vanadium redox flow cell (left). System design performance curve for redox flow battery to be implemented (right).

dissipate. The system will never need to generate power in excess of 1MW, or 1.02 MW delivered from the storage system to the inverter. A membrane area of 575 m^2 is chosen, this will both allow for charging in excess of 4 MW but will also provide a charge/discharge efficiency of 94% (the loss comes in the form of voltage drop). Two 200 $\frac{liter}{min}$ pumps will be required to deliver the liquid electrolyte solutions to the active area.

4.2. Results

4.2.1. PV System Results

The main challenge with sizing the photovoltaic systems was to maximize energy production throughout the entire year while maintaining significant energy production during the lowest producing months. Due to the locational and seasonal variability in the solar resource, each location required different sized systems in order to meet the minimum generation requirements. Phoenix, AZ required 22,100 BP Solar panels with a peak power of 5.194MW$_{dc}$ or 51,200 First Solar panels with a peak power of 3.968MW$_{dc}$. Raleigh, NC required 27,300 BP Solar panels with a peak power of 6.416MW$_{dc}$ or 48,000 First Solar panels with a peak power of 3.720MW$_{dc}$. Buffalo, NY required 45,500 BP Solar panels with a peak power of 10.639MW$_{dc}$ or 60,800 First Solar panels with a peak power of 4.712MW$_{dc}$. The slopes for the three locations are listed in table 7.

Table 7: Slope (β) of the photovoltaic arrays.

Location	BP3235N	FS3 77.5
Phoenix	60°	35°
Raleigh	60°	35°
Buffalo	75°	45°

Figure 31 illustrates the average power production for each of the three locations by hour for the polycrystalline module system. The general trends follow what would be expected from a fixed slope single-axis (N-S) tracking PV system. [4] The dual peaks are consistent with two times of a minimized angle of incidence each day. All three locations demonstrate the increase in the length of day by the increase in power generation earlier in the day and later into the evening during the summer months as compared to the winter months.

Phoenix, AZ:

In Phoenix (a), the results indicate dual optimum angles of incidence between April and August while the angle of incidence has one maximum in January through March and September through December. This effect is amplified by the high array slope required for the winter month optimization. Phoenix shows the highest power generation throughout the course of the year based on the system size.

Raleigh, NC:

In Raleigh (b) a similar effect to Phoenix is observed. Raleigh showed fewer months with two peaks in optimum angles of incidence. This is largely due to more daily variability between the mornings and evenings (asymetry) in the power generation. In general Raleigh showed a smaller decrease in solar noon production from the tracking system than Phoenix.

Buffalo, NY:

Buffalo (c) had the most dramatic change in energy production between the summer and winter months. For November and December, the maximum average power barely surpasses 4MW while in July the peak power reached is over 8MW. The high latitude of Buffalo causes very low angles of incidence during the winter months. The high slope of the system (75°) produces larger angles of incidence during the summer. The peak average power never reached 80% of the maximum system power. Had the system slope been decreased to a summer optimum we would have seen power levels closer to the maximum system power.

(a)

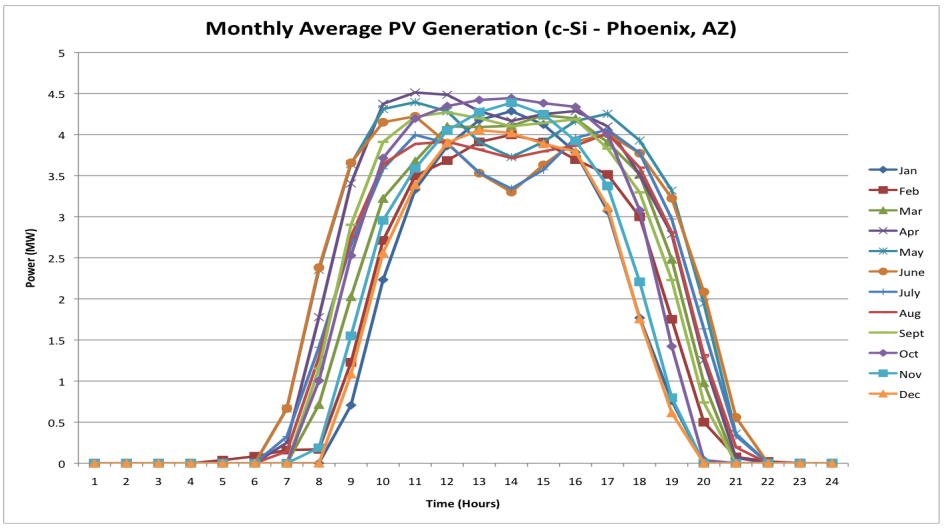

(b)

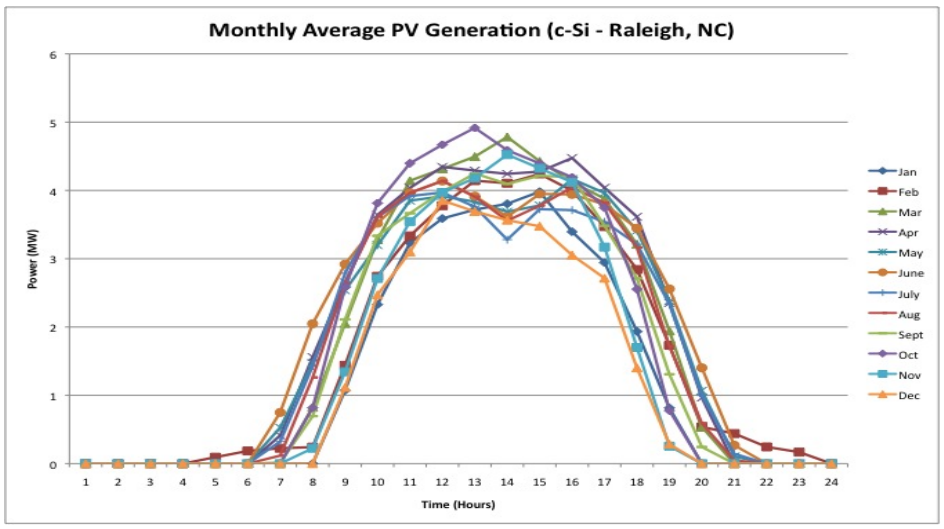

(c)

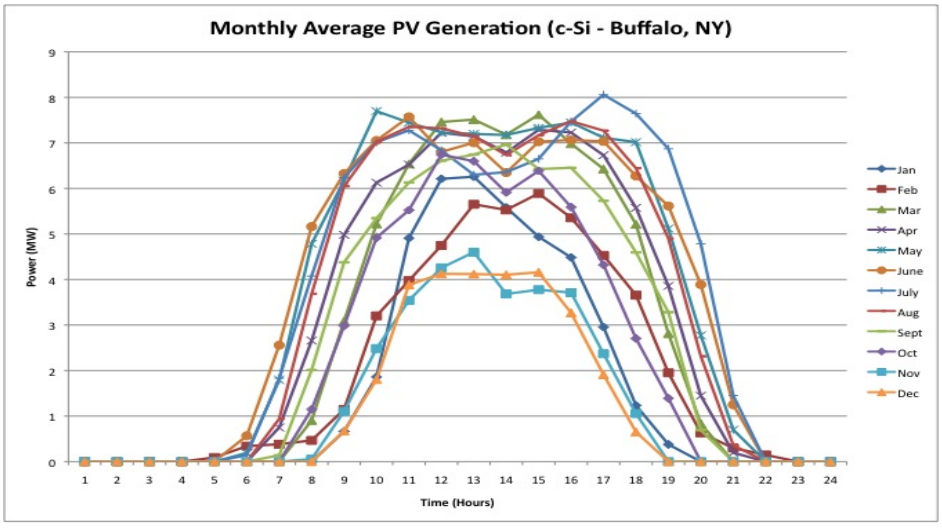

Figure 31: Average hourly power production by month for (a) Phoenix, AZ, (b) Raleigh, NC and (c) Buffalo, NY systems with the BP3235N modules.

Figure 32 illustrates the average power production for each of the three locations by hour for the Cadmium Telluride module system. All three CdTe systems we able to be sized significantly smaller than their equivalent poly-Si systems. Unlike the polycrystalline silicon modules, the Cadmium Telluride modules show less evidence of the tracking system in that the dual optimum angles of incidence are less noticeable due to other performance impacts.

Phoenix, AZ:

Phoenix (a) shows a very interesting phenomena occurring during the middle of the day. The power production decreases after an initial peak followed by a slow increase. This can be explained by the power's dependance on temperature. The CdTe modules suffer more severe voltage loss due to high temperatures. While the percentage decrease (per degree K) is less than the poly-Si modules, the voltage of the CdTe modules accounts for a larger portion of the module power, hence, the overall power drops faster due to temperature increases. The high level of direct irradiance in Phoenix also increases the cell operating temperature adding to the power loss. The temperature dependance is most prominent in June, July, August and September. These months also showed the lowest power production during solar noon.

Raleigh, NC:

Raleigh (b) shows significantly less temperature degradation than Phoenix due to less extreme temperatures. This was the only case that Raleigh, rather than Phoenix, required the smallest array. The temperature effect is still very prominent however. The maximum production in Raleigh occurs during February despite lower levels of irradiance. The summer production is still more than sufficient for daily energy requirements due to the increased duration of daylight. Raleigh shows the most consistent power production throughout the year.

Buffalo, NY:

Buffalo (c) again has the widest range of power production. The seasonal changes in irradiance levels caused the most significant change in power production since temperature issues are less of a problem in cooler climates. The highest power production occurs during May through June. Temperature becomes more of an issue during July, August and September but causes much less of a decrease in maximum power than either Phoenix or Raleigh. Of the three locations, the Buffalo CdTe power generation shows the strongest correlation to the poly-Si power generation.

In general, the CdTe systems performed better than the pc-Si systems throughout the year. This is due to the better performance of CdTe under high angles of incidence. The winter months show improved performance as compared with the poly-Si despite the lower system slopes. With the exception of Phoenix the CdTe systems are preferable to the pc-Si systems.

(a)

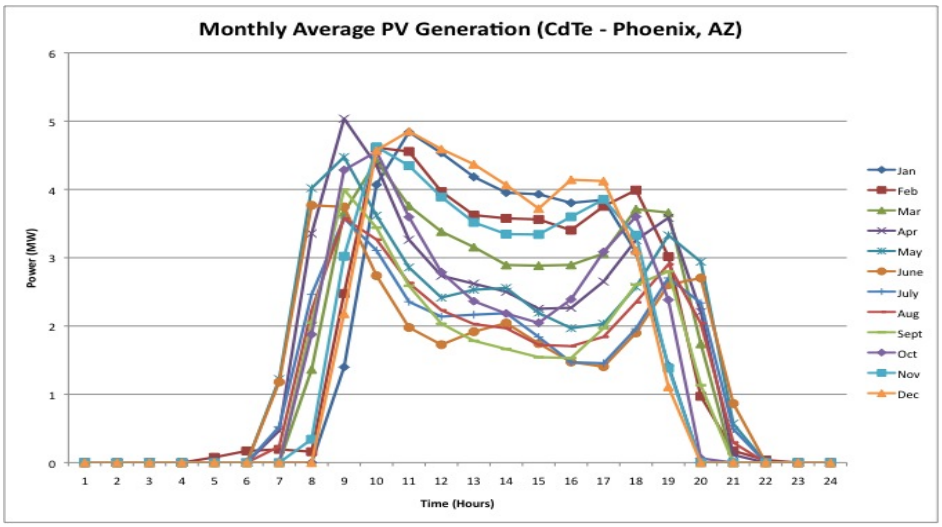

(b)

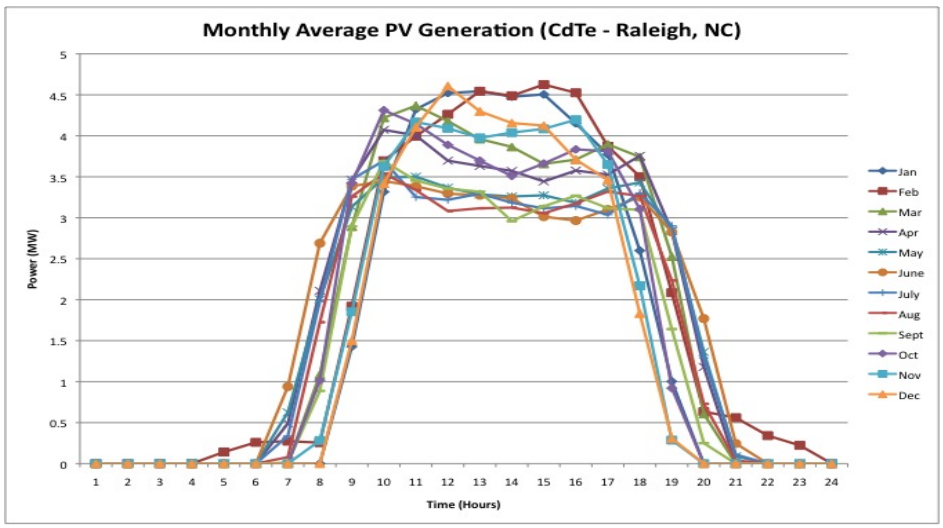

(c)

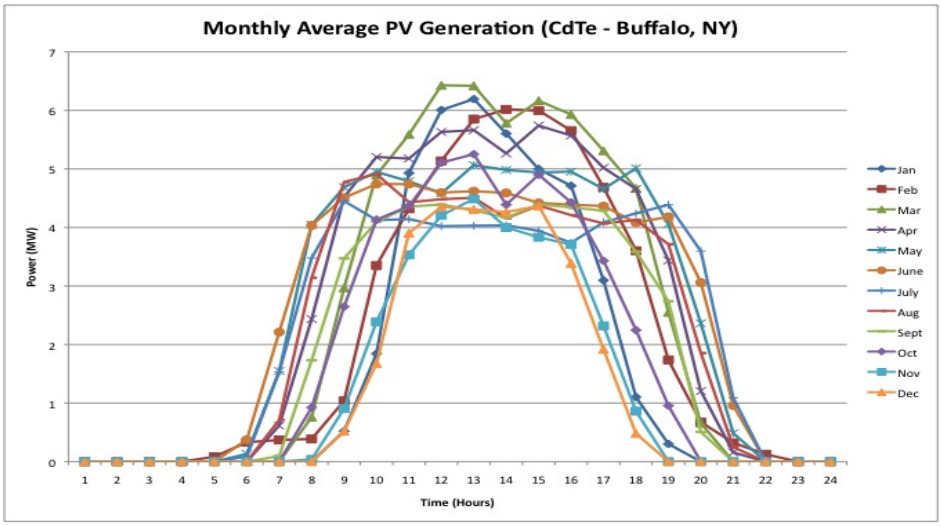

Figure 32: Average hourly power production by month for (a) Phoenix, AZ, (b) Raleigh, NC and (c) Buffalo, NY systems with the FS3 77.5 modules.

4.2.2. Energy Storage

Three locations are modeled for implementation of the EESiPV system. Each site must supply a minimum of 1 MW of electrical power delivered to the grid at all times. Due to the annual solar cycles at each site, as well as differences in temperature and solar intensity at each site, a significant amount of electrical power beyond the minimum requirements can be supplied directly from the PV array to the grid bypassing any efficiency losses within the electrochemical energy storage battery. For each location we will compare the energy outputs from both polycrystalline silicon (pc-Si) and cadmium telluride (CdTe) PV arrays. The annual fluctuation is also addressed by modeling the average daily output of each system during each month of the year. The locations chosen for this modeling provide a representative sampling of the nation's solar resource: Buffalo, NY; Raleigh, NC and Phoenix, AZ.

Buffalo, NY:

The area modeled with the least favorable solar resource and coldest temperatures due to its northern latitude was Buffalo, NY. December was found to be the lowest producing month due mostly to the late sunrise and early sunset. During an average December day in Buffalo, NY the modeled EESiPV system would supply a total of 27.8 MWh per day of electrical power (15.1 MWh of which is directly from the PV array) using the pc-Si array; and 28.3 MWh/day (15.3 MWh of which directly from the PV array) using the Cd-Te array.

The peak performance of Buffalo's EESiPV system comes in July for the pc-Si array and May for the CdTe array; this difference is a result of the differing temperature dependence on PV system efficiency. Due to the relatively large change in sunrise and sunset times between summer and winter in Buffalo, the PV array sized to generate a minimum of 1 MWh continuously in the winter will generate significantly more than 24 MWh/day in summer (this also requires significantly larger capital investment). In the month of July the pc-Si PV array sized for Buffalo will generate 73.1 MWh/day of electrical power (62.6 MWh of which will go directly from the PV array to the grid); however if using the CdTe array only 60.4 MWh/day (47.9 MWh direct from PV to grid) will be produced.

Figure 33 displays daily average performance for the peak and minimum monthly EESiPV power production for pc-Si PV design in Buffalo. Figure 34 displays daily average performance for the peak and minimum monthly EESiPV power production for CdTe PV design in Buffalo.

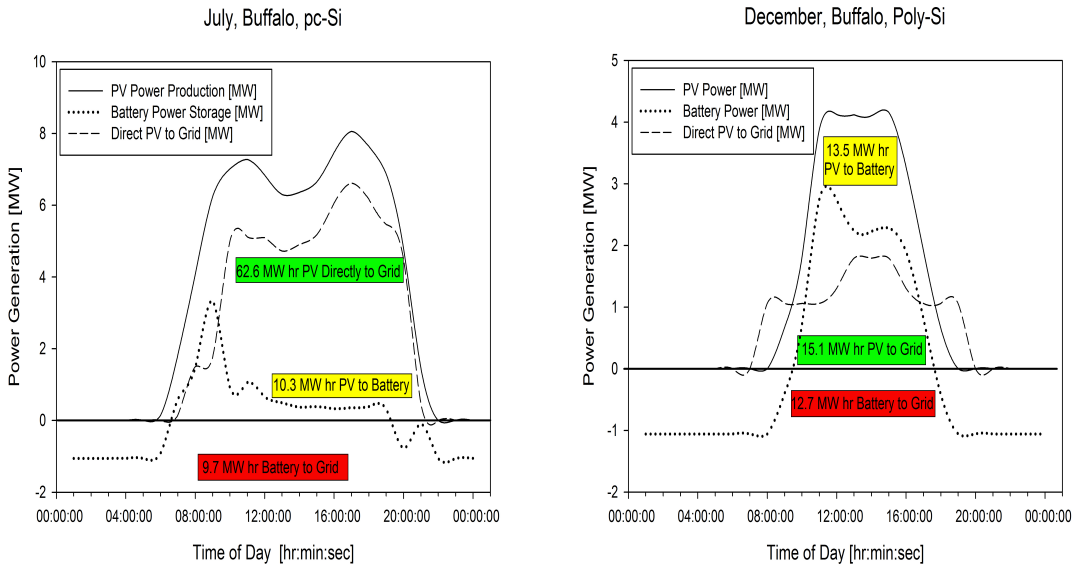

Figure 33: Average daily energy performance modeling for Buffalo, NY based polycrystalline silicon EESiPV system during its peak (left) and minimum(right) monthly performances.

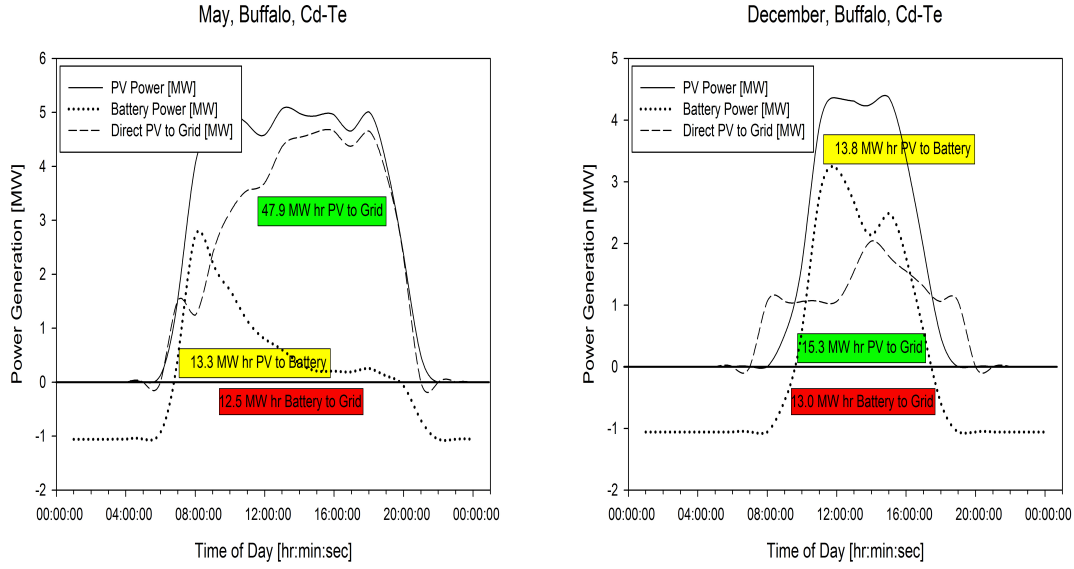

Figure 34: Average daily energy performance modeling for Buffalo, NY based cadmium telluride EESiPV system during its peak (left) and minimum (right) monthly performances.

Raleigh, NC:

The solar resource available in Raleigh, NC was greater than that available in Buffalo but less than Phoenix. Raleigh also had the most moderate climate. Because of temperature dependence the poorest performance month was different with each PV array design modeled. Using pc-Si December proved to be the minimum production month in Raleigh with only 27.9 MWh/day of average electricity production (15.1 MWh direct PV to grid).

In the CdTe model however, September proved least productive with 34.2 MWh/day average production (21.3 MWh direct PV to grid).

The peak performance months for EESiPV implementation in Raleigh, NC also varied with array design. Using a pc-Si array, April proved to be the most productive month with an average daily power generation of 44.1 MWh/day (31.7 MWh direct PV to grid). The CdTe array model generated its peak performance in February (due to low temperatures) with an average daily output of 43.4 MWh/day (29.9 MWh direct PV to grid).

Because of its more southern latitude, the change in useful solar hours between summer and winter are less extreme than Buffalo; however temperature variation between winter and summer in Raleigh are significant enough to have an effect on PV power production.

Figure 35 displays the EESiPV performance on an average day in the peak and minimum performance months in Raleigh for pc-Si PV array. Figure 36 shows the EESiPV performance on an average day of the peak and minimum performance months in Raleigh for CdTe PV array.

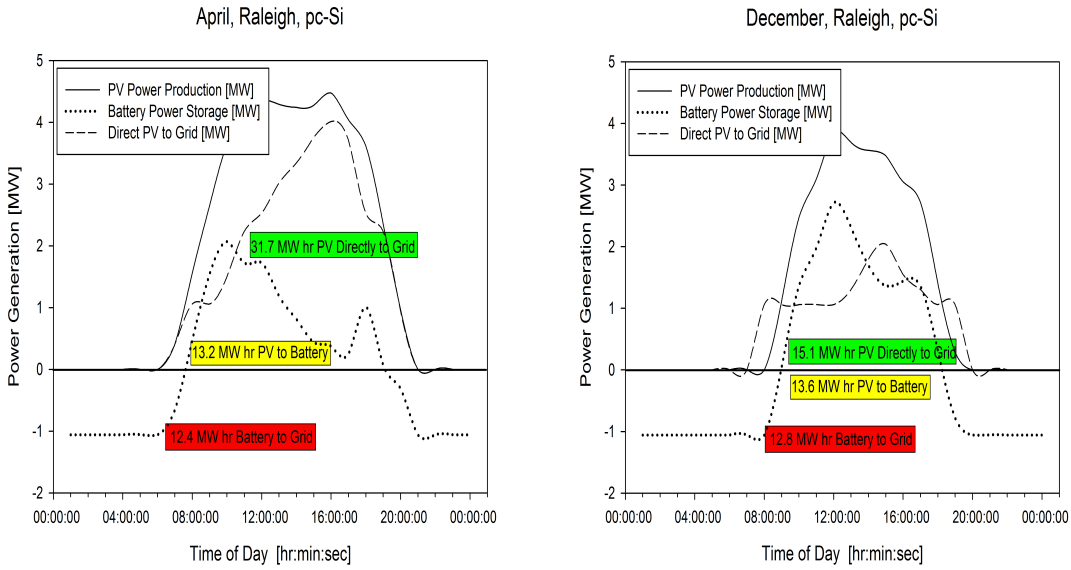

Figure 35: Average daily energy performance modeling for Raleigh, NC based polycrystalline silicon EESiPV system during its peak (left) and minimum (right) monthly performances.

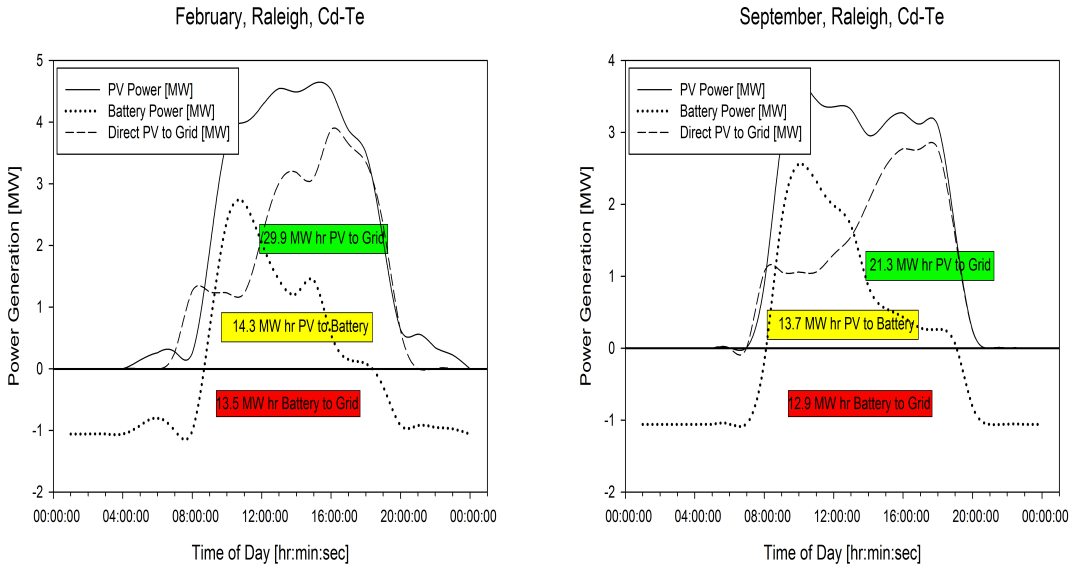

Figure 36: Average daily energy performance modeling for Raleigh, NC based cadmium telluride EESiPV system during its peak (left) and minimum (right) monthly performances.

Phoenix, AZ

The solar resource available in Phoenix, AZ is the most powerful of all locations modeled. However the high temperatures make some PV array designs less efficient. The lowest performance month for our EESiPV system in Phoenix using a pc-Si PV array is December with 31.4 MWh/day average power production (18.9 MWh direct PV to grid). The extreme heat was very unfavorable to CdTe array design making September the lowest performance month with 29.1 MWh/day average power output (16.4 MWh direct PV to grid).

The peak performance months for EESiPV implementation in Phoenix, AZ also varied with array design. Using a pc-Si array, May was to be the most productive month with an average daily power generation of 48.1 MWh/day (36.5 MWh direct PV to grid). The CdTe array model generated its peak performance in February (due to low temperatures) with an average daily output of 39.8 MWh/day (28.9 MWh direct PV to grid).

Because of its southern latitude the change in useful solar hours between summer and winter is significantly less than the other sites. Temperature variation between winter and summer in Phoenix however has a notable influence on PV power production.

Figure 37, displays the EESiPV performance on an average day in the peak and minimum performance months in Phoenix for pc-Si PV array. Figure 38 shows the EESiPV performance on an average day of the peak and minimum performance months in Phoenix for Cd-Te PV array.

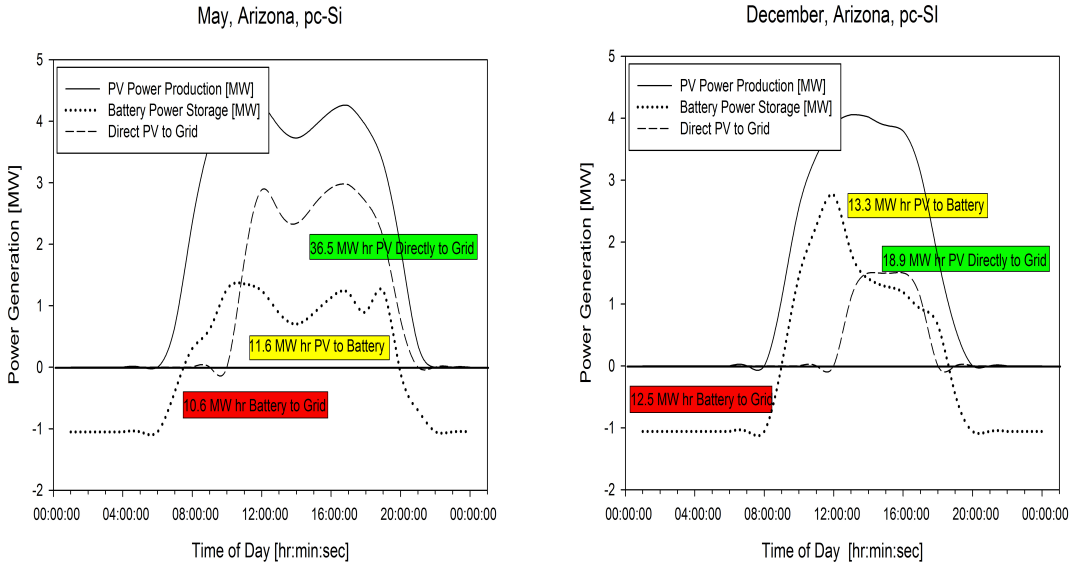

Figure 37: Average daily energy performance modeling for Phoenix, AZ based polycrystalline silicon EESiPV system during its peak (left) and minimum (right) monthly performances

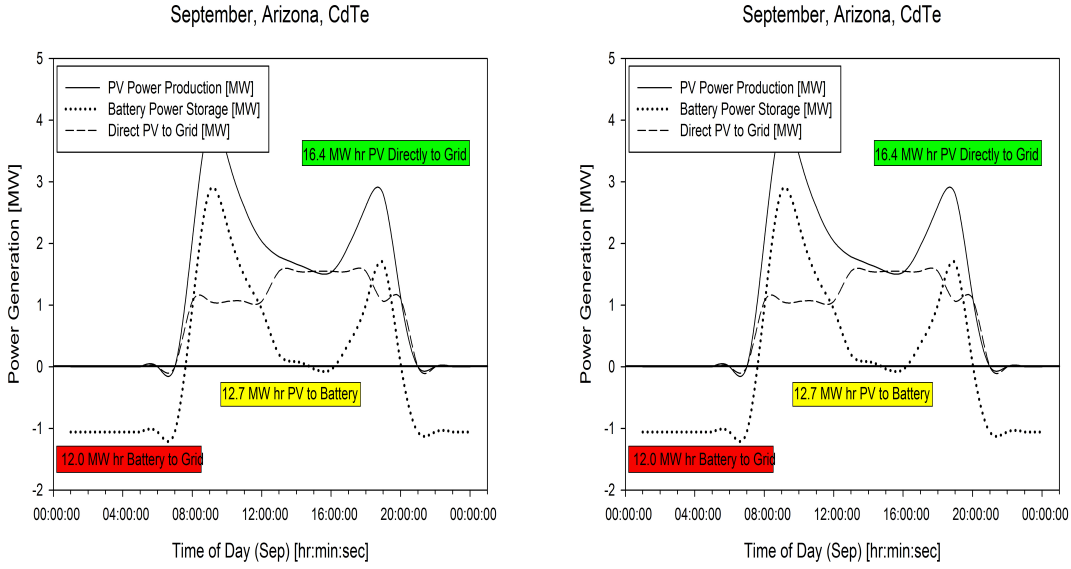

Figure 38: Average daily energy performance modeling for Phoenix, AZ based cadmium telluride EESiPV system during its peak (left) and minimum (right) monthly performances.

4.2.3. **Electricity Generation and Conversion Efficiency**

Figures 39 illustrate the average energy production per day by month at several different stages of conversion throughout the system for the polycrystalline silicon system. The five series represent the total energy generated by the PV system, the total energy from the redox flow cell to the energy control unit, the PV energy dumped directly to the grid, the PV energy, the redox flow cell energy to the grid and the total energy sent to the grid (the

sum of the dumped PV energy and the redox flow cell energy). The average total energy sent to the grid is also displayed in table 8.

Phoenix (a) illustrates the maximum energy generation during March to July. The decrease in energy output corresponds to the extreme temperature effects on the photovoltaic performance. This effect is significantly less for the polycrystalline silicon modules. Raleigh (b) shows a very consistent energy generation throughout the year with only small decreases during the winter months. Buffalo (c) showed the largest increase in energy generation during the summer. Due to this, the largest amount of energy of any of the three systems of either material was generated during the summer in Buffalo.

All three system show a similar trend in the average energy delivered to the grid from the redox flow cell system. The flow cell energy is consistently between 15MWh and 20MWh per day. This is exactly in the desired range from our initial concept selection. The different between the daily energy requirement and the redox flow cell energy is produced from the PV system. This energy is ultimately more profitable due to a higher system efficiency than first being stored in the flow cell. The flow cells average 85% charge to discharge rate with an additional 95% inversion efficiency from DC to AC. The energy produced directly by the photovoltaics only undergo the 5% inversion losses.

Figures 40 illustrate the average energy production per day by month at several different stages of conversion throughout the system for the cadmium telluride system.

Phoenix (a) illustrates severe losses during the hottest months (June, July, August and September) from decreased photovoltaic performance. Despite the decrease in PV energy generation, the flow cell system still achieve ideal energy generation. There is, however, a slight decrease in the total flow cell energy during these months. The decrease in photovoltaic energy is lessened slightly due to the higher system efficiencies. This excess energy is still significant enough to sell to the grid. Raleigh (b) also shows a slight decrease in performance during the hottest months. This is visible in both the PV energy and the flow cell energy.

Buffalo (c) shows the largest decrease in both the photovoltaic energy generation and the flow cell energy generation during the winter months. Since both energy sources undergo system losses and are at a minimum the total energy to the grid is significantly decreased with average daily energy provided at 25.06MWh and 24.20 MWh in November and December.

(a)

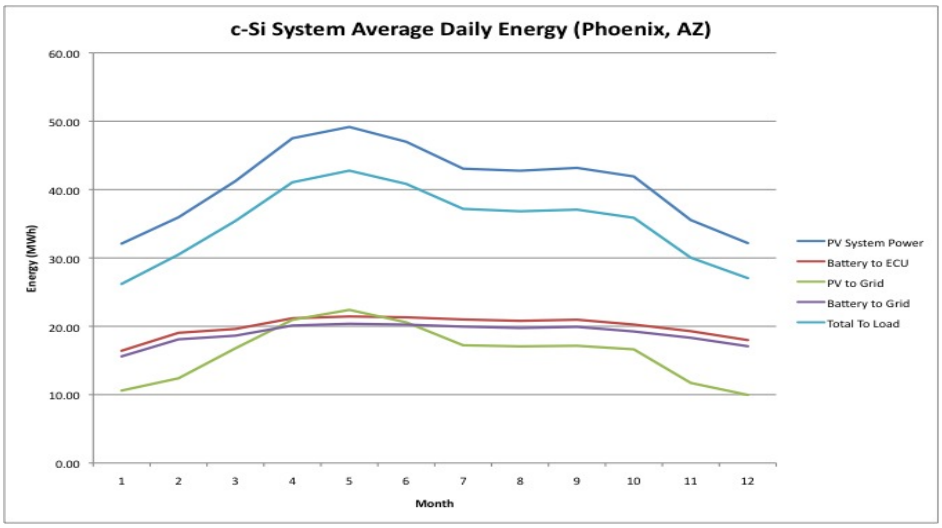

(b)

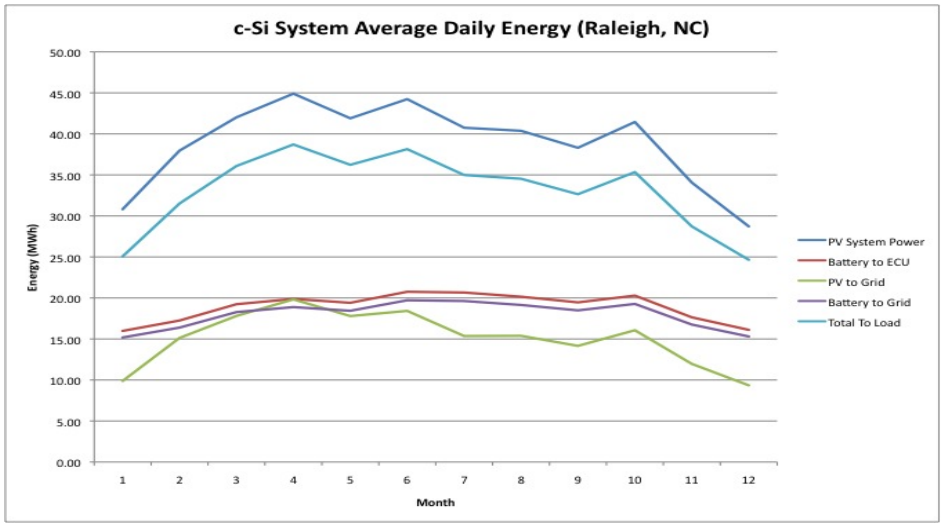

(c)

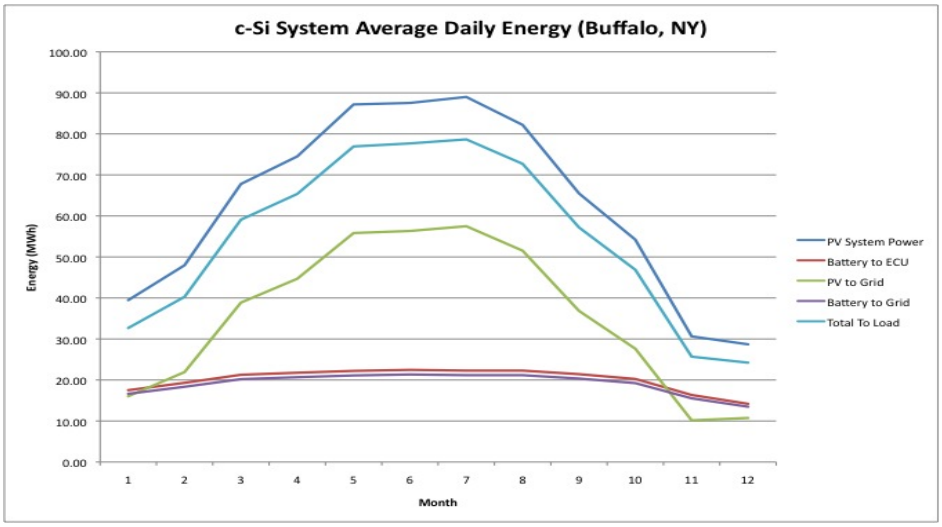

Figure 39: System average energy production per day by month for (a) Phoenix, AZ, (b) Raleigh, NC and (c) Buffalo, NY systems with the BP3235N modules.

(a)

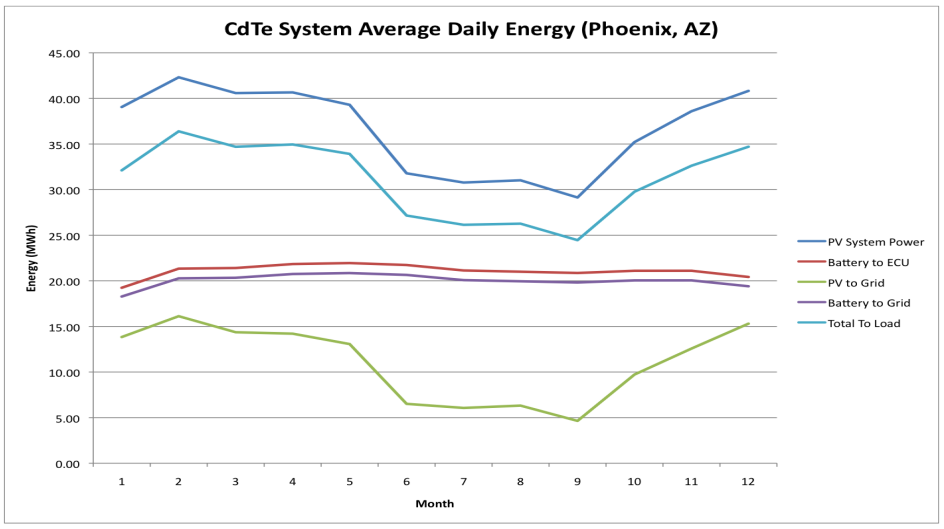

(b)

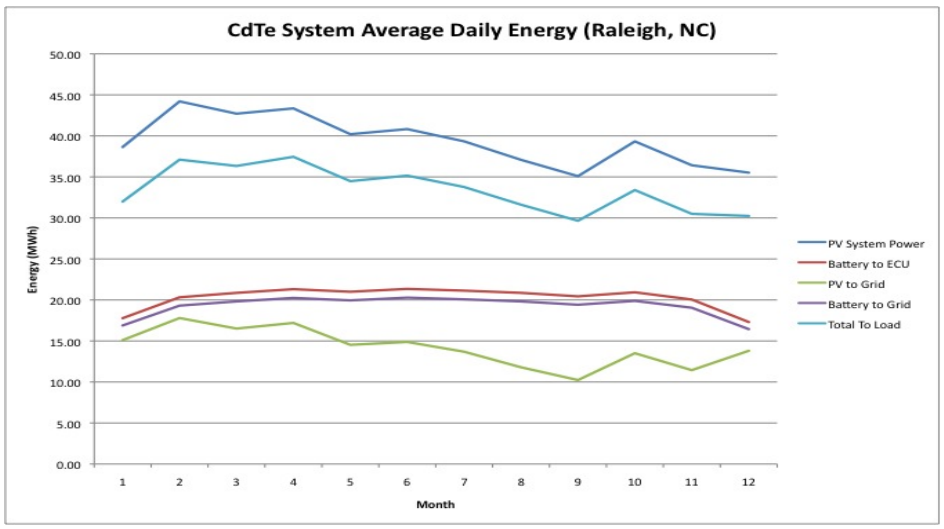

(c)

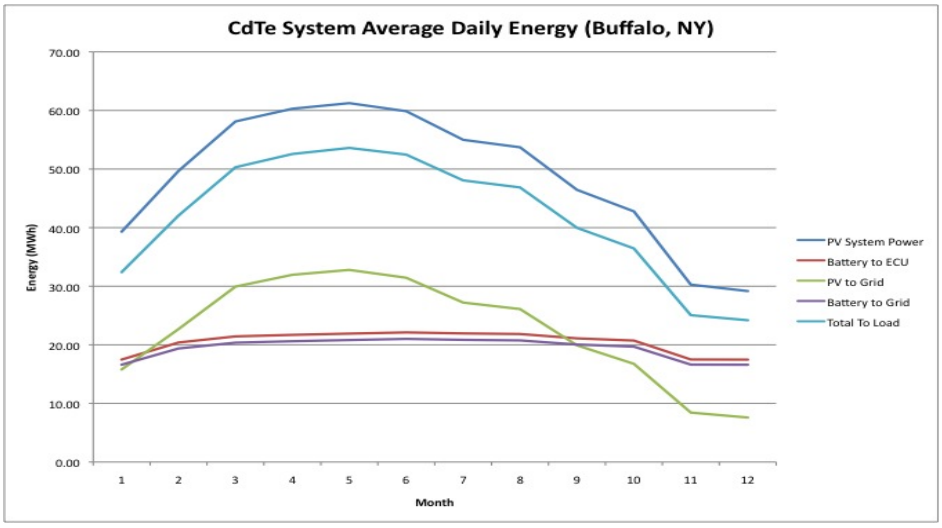

Figure 40: System average energy production per day by month for (a) Phoenix, AZ, (b) Raleigh, NC and (c) Buffalo, NY systems with the FS3 77.5 modules.

Table 8: Average daily energy (MWh) sent to the grid for each panel type and location.

Month	Phoenix BP	Phoenix FS	Raleigh BP	Raleigh FS	Buffalo BP	Buffalo FS
January	26.20	32.11	25.07	31.99	32.67	32.40
February	30.49	36.39	31.52	37.11	40.28	42.07
March	35.42	34.70	36.09	36.33	59.08	50.31
April	41.06	34.95	38.71	37.45	65.37	52.57
May	42.77	33.92	36.23	34.48	76.94	53.61
June	40.83	27.16	38.14	35.16	77.68	52.46
July	37.18	26.14	34.99	33.77	78.66	48.06
August	36.82	26.27	34.53	31.61	72.70	46.86
September	37.07	24.46	32.65	29.65	57.20	39.97
October	35.87	29.77	35.34	33.40	46.87	36.45
November	30.04	32.62	28.72	30.50	25.69	25.06
December	27.05	34.71	24.65	30.24	24.22	24.20
Yearly Total	12804.13	11340.82	12062.72	12208.23	20031.51	15328.46

5. Economic and Policy Assessment

5.1. Electricity Pricing

Electricity price is the primary parameter that determines whether the EESiPV system design is economically feasible. Utilities across the United States have been raising power prices for years, mostly to pay for increasing fuel costs, but also to build new generators and refurbish aging power grids. More dramatic rate increases are ahead, and the increasing trend has showen no sign of slowing down. Moreover, because of inflation in the United States, energy crises and the increasing demand to meet the nation's development, we expect an upward trend for electricity prices within next 25 years (the lifetime for the EESiPV system).

To make estimates of the future electricity prices in Arizona, New York and North Carolina, the historical 10 years prices data are collected. Figure 41 is the plot of this data, which is from the US Energy Information Administration [84].

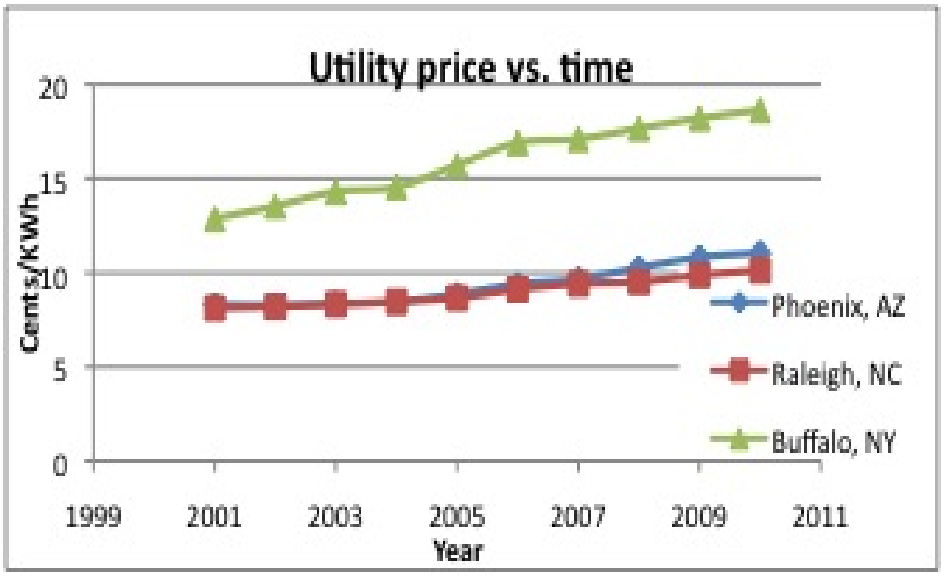

Figure 41: Historical electricity prices from 2001 to 2010 for the the localities. [84]

As we can observe from the graph during the concerned period, Buffalo, NY has the highest electricity price and increase rate. Raleigh, NC and Phoenix, AZ have relatively similar utility price in the early years of the century, but the rate increase in Phoenix is higher, which effects the results of the cost-benefit and sensitivity analysis significantly.

The price trend details illustrate the upward tendency during the years of quick economic growth, such as 2005 to 2007. The increase rate slowed down when there was a financial crisis in 2008 and 2001. The energy demand and supply relationship is affected by the background of the global/national economy. Also, energy price is a good indicator and index for GDP growth. [85] The relationship between macroeconomics and energy price is beyond the scope of this project, but for our design, the economic feasibility of the whole system, even for the development of solar industry, is significantly affected, or determined

by the nation's economic status and energy price volatility.

Based on above historical electricity prices, the future 25 years prices can be estimated by figuring out the average geometric increasing rate, rather than a linear regression model. The linear regression method is not statistically accurate or effective for future prices estimation. This analysis calculates the average geometric increasing rate by calculating the price increase rate for each year and taking the average for them as the future increasing rate. Mathematically, it is based on the following formula for each site:

$$r = \frac{\sum_i^n r_i}{n} \tag{18}$$

By conducting above analysis for each site, we get the standard rate increase illustrated by figure 42.

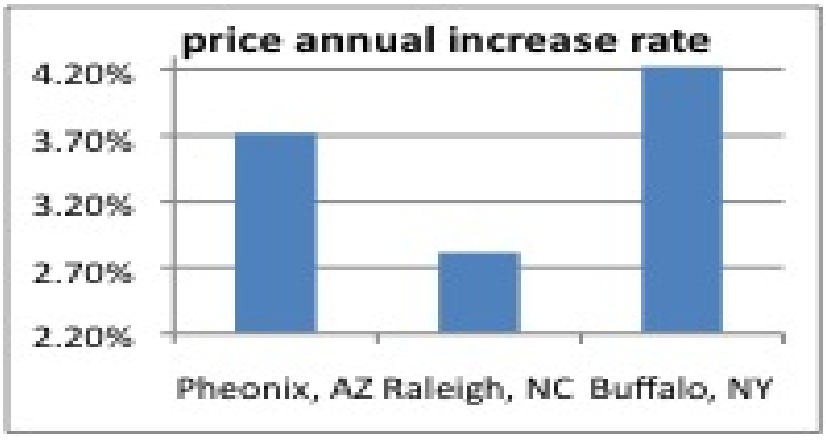

Figure 42: Average rate increase (per year) in energy prices for the three localities.

With the 2010 price and the average increasing rate for each site, the expected future electricity price for 25 years is shown in figure 43.

The above information will be critical input data for later calculations. It should be noted that the predicted utility price in Buffalo, NY will be over 50 cents/kwh after 2035, which is a surprising number. In the macroeconomic sense, however, this is highly possible for the price to peak above 50 cents/kwh within 25 years considering both the common energy shortage and the USD annual inflation rate. The increase in price is an exponential pattern, which may not be realistic compared to the volatility increase trend for the practical situation.

5.2. Federal, State and Local Incentives

Feed-in tariffs (FIT), is a policy mechanism designed to encourage the adoption of renewable energy sources and to help promote the transition toward grid parity, providing significant economic development benefits. By using a variety of design variables to provide incentives, FIT policies can help encourage a variety of renewable energy technologies and various sizes of projects. Feed-in tariff policies are implemented in more than 45 countries

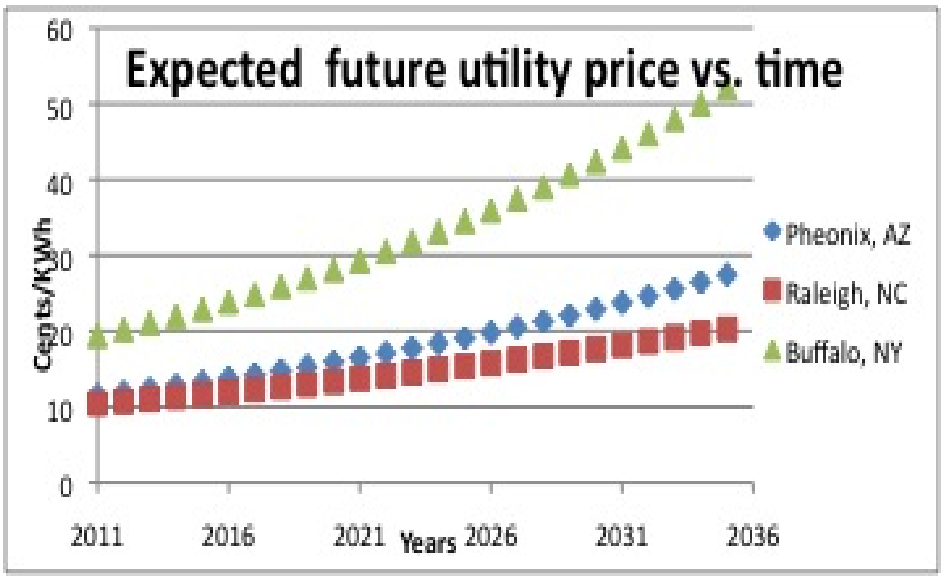

Figure 43: Estimation of the future cost of energy at each locality.

all around the world and are cited as the primary reason for the success of Germany and Spain's renewable energy markets. [86] As a result of that success, FIT policy proposals are starting to gain traction in several states and municipalities in the U.S. A number of states have considered or are considering FIT legislation and regulation, including Florida, Hawaii, Illinois, Indiana, Maine, Arizona, Massachusetts, Oregon, Michigan, Minnesota, New Jersey, New York, Rhode Island, Virginia, North Carolina, Washington and Wisconsin. Feed-in tariffs basically guarantee electricity grid access under long term contracts, and offer purchase prices that make renewable energy economically acceptable.

As shown in the literature review, there are several models for Fit policy including the Fixed-price FIT model, the Non-variable premium-price FIT model and the Spot-Market Gap Model. In these calculations, the Non-variable premium-price FIT model, in which FIT payments are offered as a premium on top of the spot-market electricity price, was used. The price guarantees long-term policy certainty. Figure 44 illustrates the non-variable premium-price FIT model.

The magnitude of FIT reflects the different levels of the states' incentive to all sizes of renewable energy and overall cost-efficiency. Also, not all of these three have passed the FIT incentive, and it is expected they will be available within at most three years. For the simplicity of calculation, it was assume the FIT policy is available right now, and the FIT policy is the high level of solar energy incentive, compared to the 10 years incentive. The 10 years incentive will be considered as a medium level of incentive. Figure 45 is a comparison of the FIT premium that have been or will be proposed by three states.

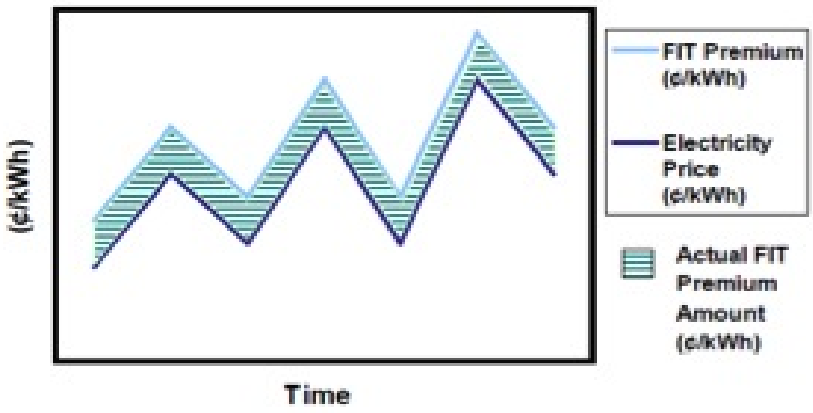

Figure 44: Non-variable premium-price FIT model description. [86]

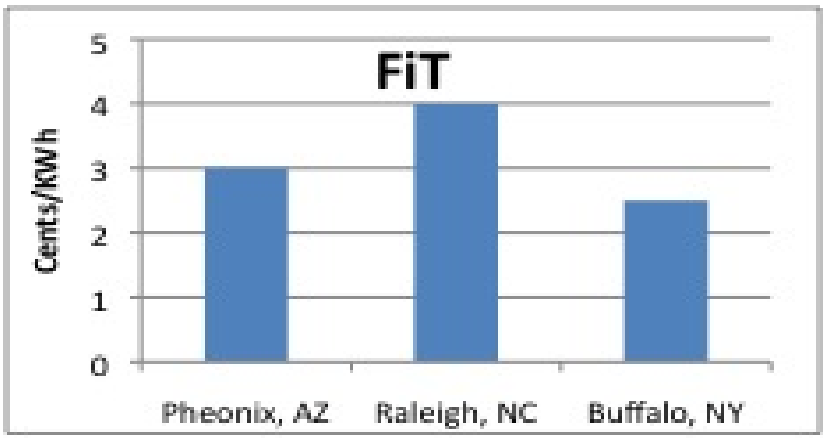

Figure 45: Proposed of accepted FIT rates for the localities. [87]

There have been a series of renewable energy incentives throughout recent years, especially for solar energy. In this context, the policies that are applicable orpotentially applicable for the EESiPV system in Phoenix, Raleigh and Buffalo will be discussed, based on the Database of State Incentive for Renewables and Efficiency. [87].

Phoenix, AZ:
Renewable Energy Production Tax Credit: Qualified renewable energy systems installed on or after December 31, 2010, may be eligible for a tax credit based on the amount of electricity produced annually for a 10-year period. The maximum tax credit that can be claimed for a qualified system in any one year is $2 million.

Renewable Energy Business Tax Incentives: To be eligible the business must meet certain minimum requirements for the quantity and quality of new jobs created. The amount of the tax credit is up to 10% of the taxpayer's total capital investment.

Property Tax Assessment for Renewable Energy Equipment: Renewable energy equipment owned by utilities and other entities operating in Arizona is assessed at 20% of its

depreciated cost for the purpose of determining property tax.

Solar and Wind Equipment Sales Tax Exemption: Arizona provides a sales tax exemption for the retail sale of solar energy devices and for the installation of solar energy devices by contractors. However, the sales tax exemption does not apply to batteries, controls, etc.

Raleigh, NC:
Renewable Energy Tax Credit: North Carolina offers a tax credit equal to 35% of the cost of eligible renewable energy property constructed, purchased or leased by a taxpayer and placed into service in North Carolina during the taxable year.

Renewable Energy Equipment Manufacturer Tax Credit: The credit is worth 25% of the eligible costs and must be claimed in five equal annual installments beginning with the year the facility is placed in service.

Buffalo, NY:
NYSERDA - Clean Energy Business Growth and Development: Providing clean energy business projects with grants of up to 50% of a project's cost, with a maximum of $200,000 per project.

NYSERDA - PV Incentive Program: NYSERDA provides an incentive of $1.75 per watt (DC) to eligible installers for the installation of approved, grid-connected photovoltaic systems.

Local Option - Solar, Wind & Biomass Energy Systems Exemption: Section 487 of the New York State Real Estate Property Tax Law provides a 15-year real property tax exemption for solar, wind energy, and farm-waste energy systems constructed in New York State.

5.3. Land Use and Other Economic Parameters

Land use for utility-scale grid connected solar power systems is large relative to that for other generating technologies due to the fact that a large area of land is needed to collect sufficient solar radiation. Considering the large dimension of PV panels, land use is a critical parameter affecting the economic feasibility. When choosing the sites, three benchmarks arose: 1) the location is compatible with power grid without any difficulties, 2) The topography is suitable for the PV and storage system and 3) the land use cost is as low as possible.

Construction permits are required for installing solar energy systems with costs for permits varying across states and cities. Local municipalities may or may not require a building permit for installation of solar PV systems. Also, it may take up to a month to obtain the construction permit for a solar system, although the opportunity cost in waiting for the permit can be neglected. For practicality purposes, it is recommended to apply for the permit as soon as the solar design is finished. The permit fee is also an effective indicator the solar energy incentive level.

System installation, completion and inspection: After all materials are delivered to the site, the installation date will be dependent on the weather, commitments to other installations, and any constraints that may have arisen. Annual inspection for the designed system will

Table 9:

	Buffalo, NY	Phoenix, AZ	Raleigh, NC
Solar Resource	2.3 kWh/m^2/day	5.6 kWh/m^2/day	3.5 kWh/m^2/day
Construction Permit	$358	$250	$500
Land Use	$3400/acre	$4809/acre	$5701/acre
Local Utility	National Grid Plc	AZ Public Service	Progress Energy

be calculated into part of the maintenance cost. Table 9 is a summary of the parameters for the capital costs of the EESiPV system.

For the annual maintenance cost, 3 engineers for the technical work and 4 staff for the daily operation will be recruited. Yearly salary for engineers and staff is estimated to be $75,000 and $45,000, respectively. The total cost for maintenance is given by $75,000*3+$45,000*4=$405,000 which is the variable cost each year. The difference in salary levels for the three locations (for cost of living expenses) are not considered here.

5.4. Cost Benefit Analysis

The capital cost consist of PV panels and associated BOS, battery storage system, land use and installation and construction cost. Figure 46 illustrates a breakdown of the capital cost for Phoenix, AZ. The Buffalo and Raleigh sites' share of PV and battery storage cost will be a little bit higher, but overall similar to Phoenix.

Table 10:

Component	Cost ($)
BP 3235N	539/unit
FS3 77.5	168/unit
V_2SO_4	1,930,000 million
Nafion	400,000
2.0 M H_2SO_4	90,000
HDPE storage tank	50,000
Pumps	20,000
Balance of Plant	50,000
Total	**2,540,000**

The maintenance cost of solar energy systems is relatively low compared to other renewable energy systems. There is barely any energy input and a low rate of material cycling. Staff and engineers' salary along with material cycling make up most of the annual cost (approximately $500,000). Table 10 shows the breakdown of costs for the systems.

The major economic benefit occurs from selling electricity to the grid. Figure 47 illustrates the averages for daily energy generation.

As the BP panels have a higher price than the First Solar panels, a large capital cost is observed, especially in Buffalo, where there is the lowest solar resources among the three locations. The capital cost is about $30 million. As shown in figure 48, without considering

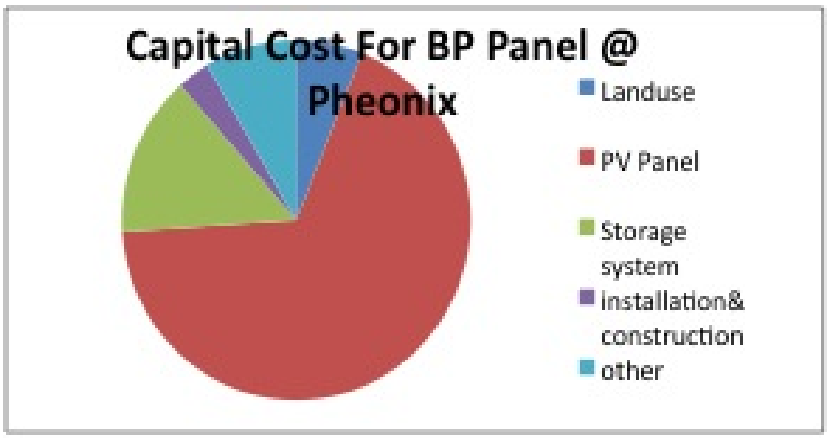

Figure 46: Breakdown of the capital costs for Phoenix, Arizona for the BP 3235N EESiPV system.

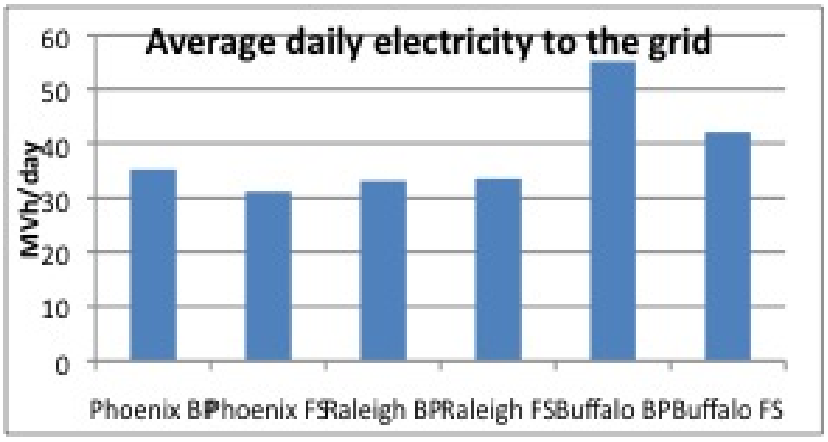

Figure 47: Average daily energy generation sold to the grid.

incentives the design passes the cost-benefit test in every location except for Raleigh due to lower utility prices and lower electricity cost increasing rate. With 10 years of incentives all of the scenarios pass the test, although Raleigh just breaks even at the end of 25 years. Feed-in tariffs are a strong incentive for the solar industry. Within 3 years, when all the feed-in tariffs are available, solar energy will become extremely economically feasible.

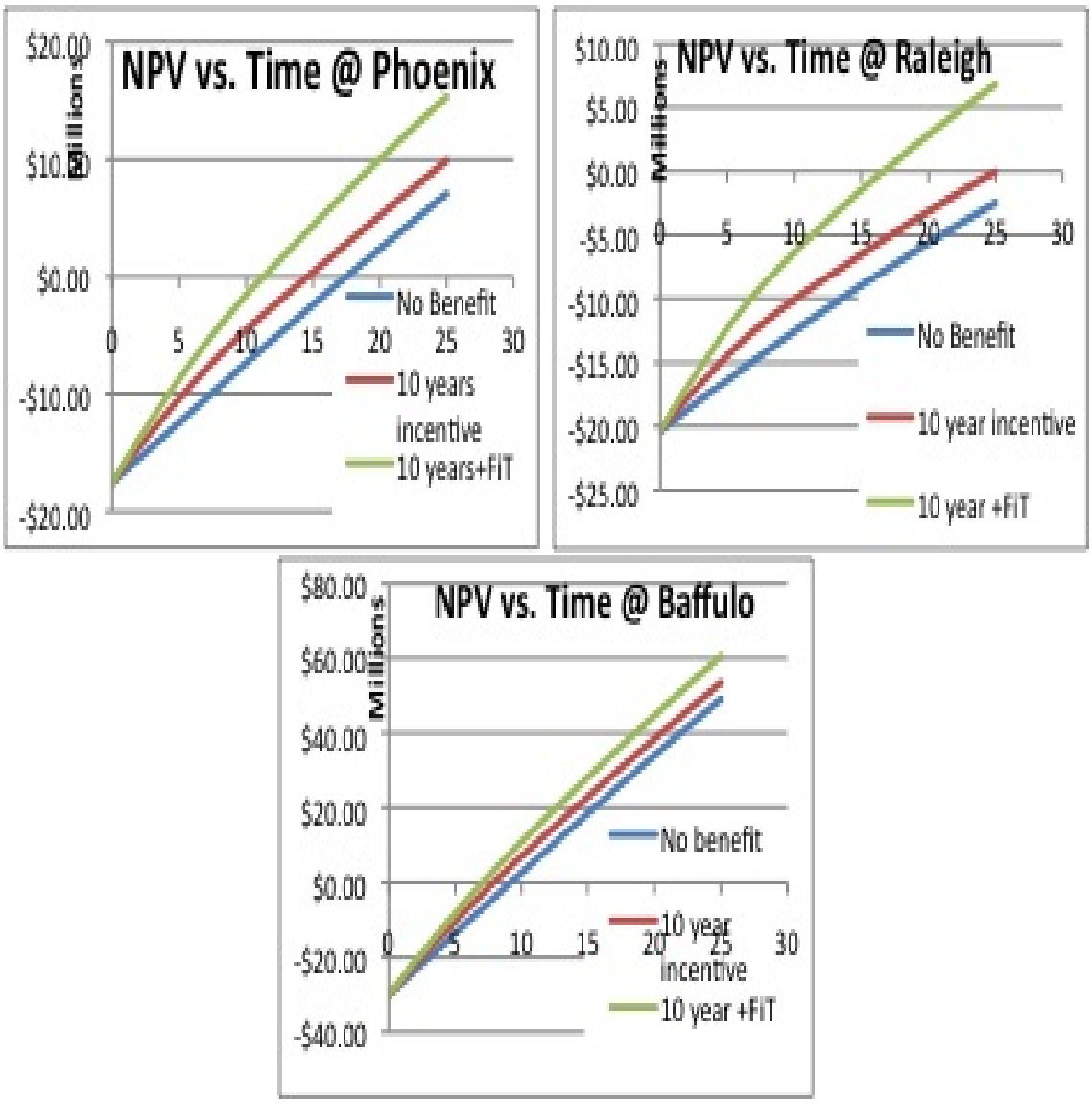

Figure 48: NPV for the polycrystalline silicon systems at each of the locations.

Figure 49 illustrates the NPV for the First Solar module systems.

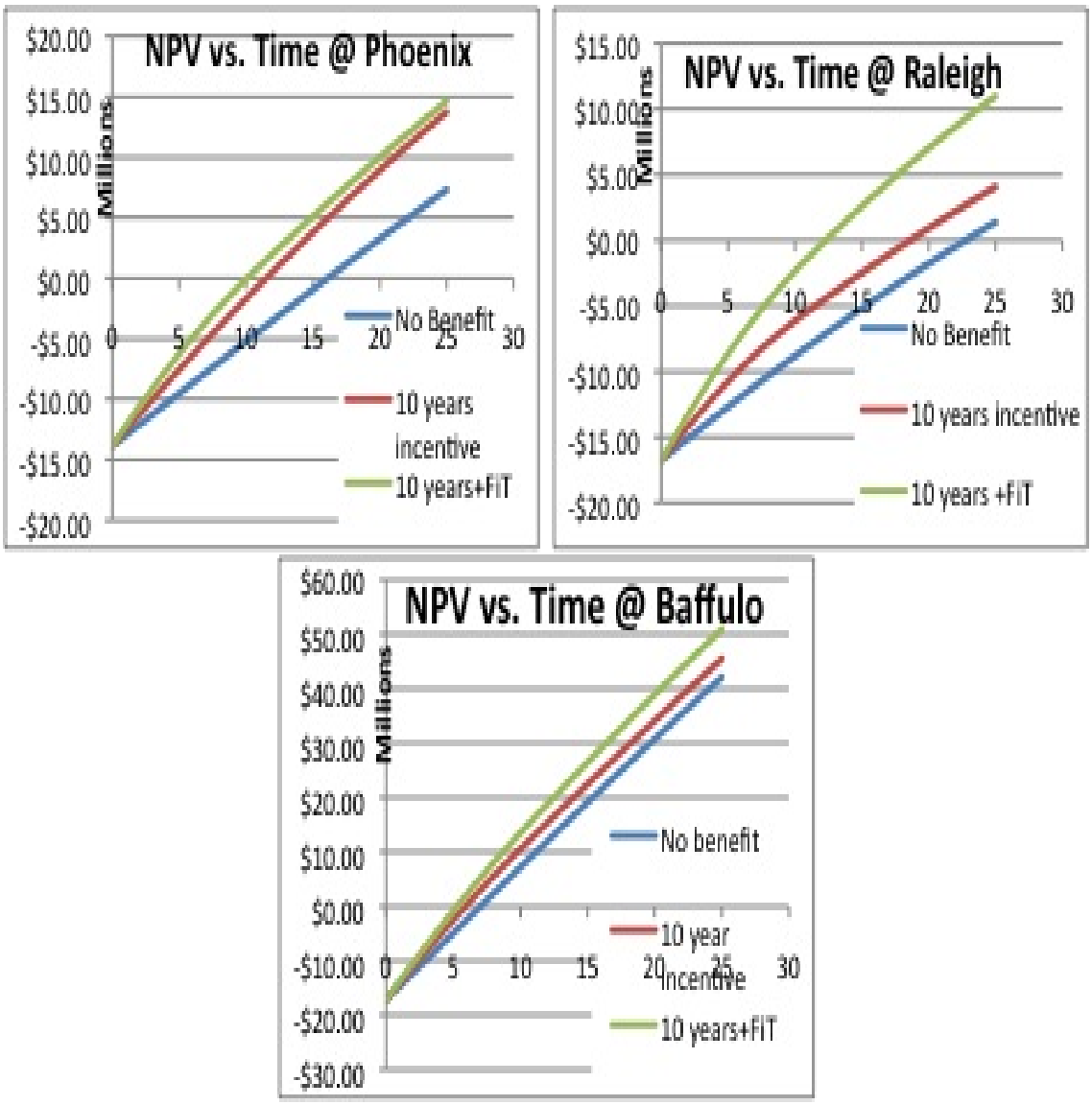

Figure 49: NPV for the cadmium telluride systems at each of the locations.

All of the scenarios for the First Solar system pass the cost-benefit analysis. In addition to the previous analysis, an interest rate sensitivity analysis was conducted for both BP modules and First Solar modules in Phoenix based on the work by Tucker shown in figure 50. [88]

From the results, we assert that the average annual return rate for the EESiPV in Phoenix is between 5% and 10%. For the First Solar module system, we observe the average annual return rate for EESiPV in Phoenix to be a little above 10%. This evidence also supports the First Solar modules over the BP modules.

5.5. Levelized Cost of Energy

LCOE is another economic indicator for feasibility of an energy system. It is defined by the

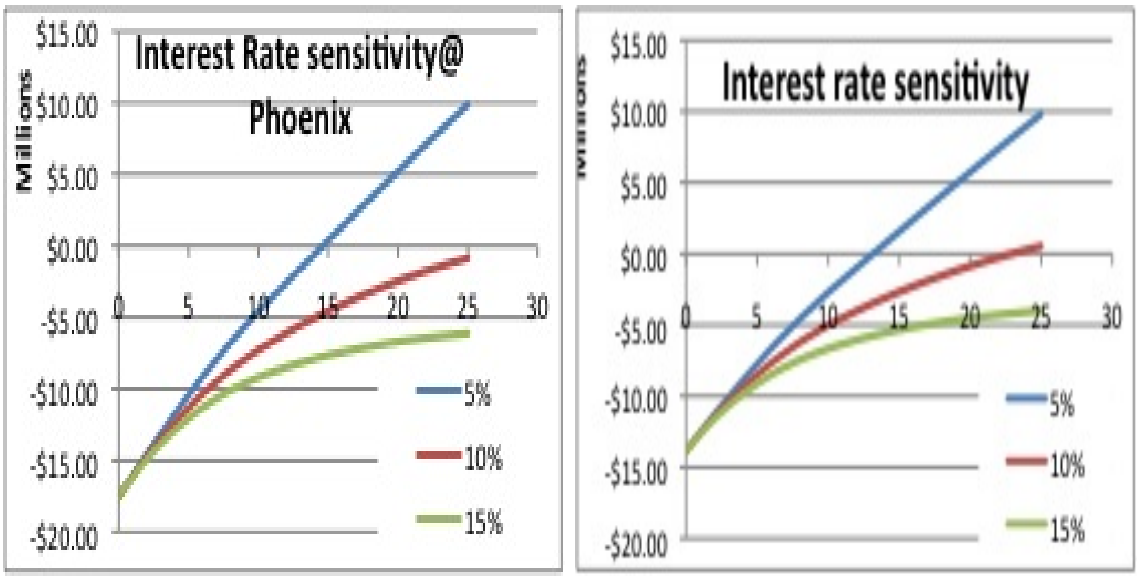

Figure 50: Interest rate sensitivity analysis for BP 3235N system (left) and FS3 77.5 system (right).

total capital cost divided by the total amount of energy generated during the whole lifespan. [89] The LCOE allows a comparison to be made between energy generation methods. The results for BP panels and FS panels for the three locations are shown in figure 51.

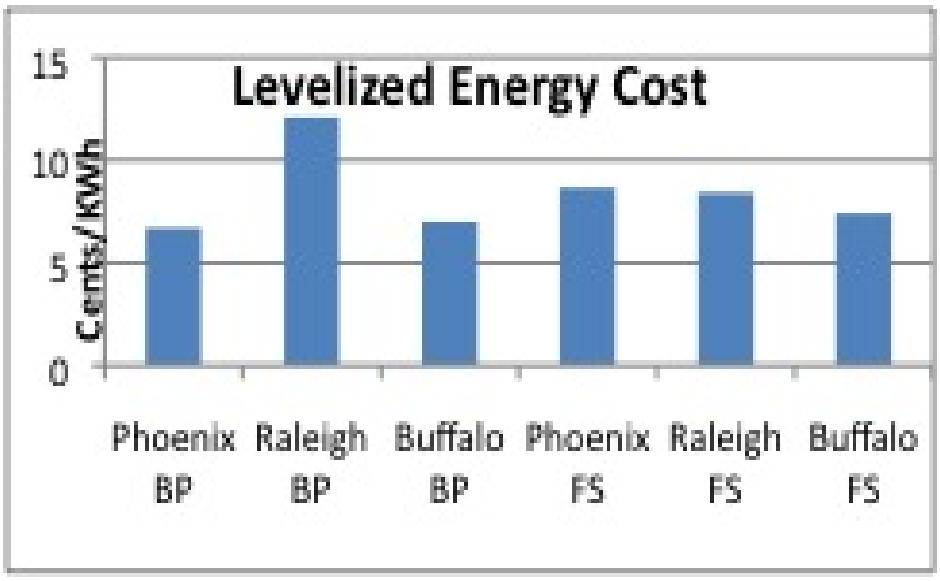

Figure 51: LCOE comparison for each location and panel type.

Using BP panels in Raleigh results in the highest LCOE, which fails the cost-benefit analysis when compared to the estimated electricity prices. The LCOEs for other scenarios

are all well within the national average electricity prices. In general, the First Solar panels perform better than BP panels under this specific assessment.

5.6. Carbon Offsets and Future Speculation

The definition of a carbon offset is usually the reduction in emissions of carbon dioxide or other greenhouse gases made in order to compensate for or to offset an emission made elsewhere. [90] For renewable energy such as a solar PV system, we calculate the offset of total life time CO_2 tonnage by each of our designed systems, which should have been emitted to the atmosphere by the traditional coal fire plants. Both systems would generate the same amount of electricity. Using the capital cost multiplied by the total tonnage of CO_2, we get an index of capital investment for per metric ton of CO_2. This number can be compared with other renewable energies. If this number is below $30 per metric ton of CO_2, the design is considered as carbon neutral. [91] Figure 52 illustrates the carbon offsets for the various EESiPV locations and several other energy generation methods.

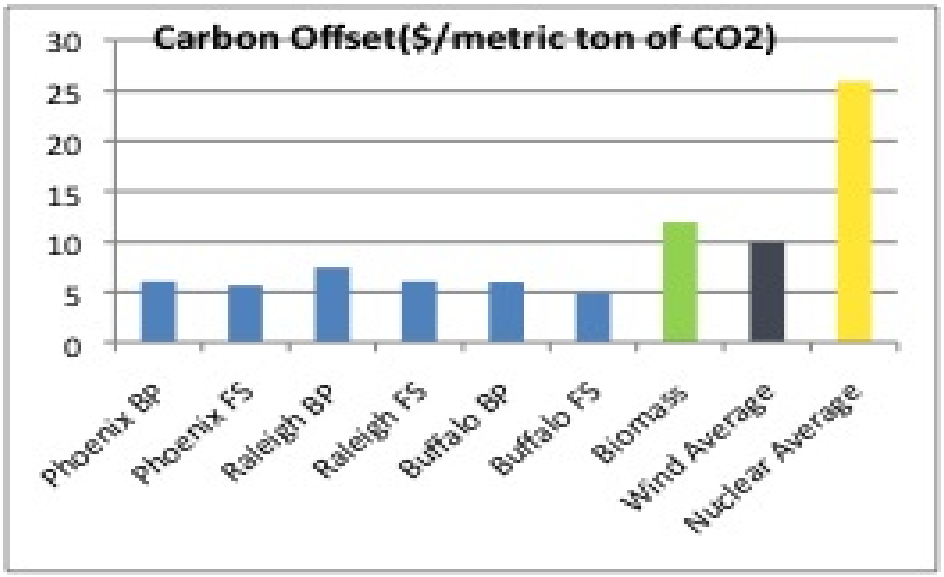

Figure 52: Carbon offsets for EESiPV and several other alternative energy technologies.

First Solar panels perform better than BP panels in this carbon offset comparison. Based on our analysis, EESiPV is the most environmental friendly option compared to other renewables. Comparing the EESiPV system to nuclear energy, nuclear energy requires large capital investment. Moreover, out of all the listed renewables, solar energy appears more favorable both for economic and environmental reasons.

Table 11:

Years to Break Even:	Phoenix, BP	Raleigh, BP	Buffalo, BP	Phoenix, FS	Raleigh, FS	Buffalo, FS
No Benefit	16	N	9	16	24	8
10 year incentive	14	N	8	13	17	6
10 years + FIT	12	17	7	11	14	6

5.7. Conclusions

Due to the largest advantage of the solar resource, Phoenix passes the Cost-Benefit test. For the relatively high electricity price, the design in Buffalo is the most economically favorable, despite the smallest solar resource. Raleigh, due to lower energy costs, did not pass the C-B test without substantial incentives for BP panels. In general, First Solar is the better option for our design than BP panel in all three sites according to the economic analysis.

Based on the sensitivity analysis, we conclude that the EESiPV has an annual return rate range from 8% to 11%, which will be profit-desirable. The carbon offset work proves that EESiPV is carbon neutral and performs better than other renewable energies.

Most solar energy systems are designed to operate between 25-30 years. This does not mean the EESiPV system must be shut down after 25 years, but rather the energy production will slowly decrease after that lifetime. Due to the volatility of the electricity market, the costs cannot be accurately estimated past 2035. It is highly possible that EESiPV will still provide stable cash flow after 2035, especially for the conservative electricity projections used here.

The material scarcity will be another important issue, not only for the solar industry, but for all energy industries. In recent years, PV panel costs have been reduced, but this trend can be changed if scarcity increases for PV materials.

6. Life Cycle Assessment

To analyze the environmental issues associated with the Electrochemical Energy Storage integrated Photovoltaic (EESiPV) system a Life Cycle Assessment (LCA) was completed for the three main items (products) involved. These items include CdTe photovoltaic panels, polycrystalline Silicon photovoltaic panels and a Vanadium Redox flow cell. A larger Life Cycle Assessment was completed for the entire ESSiPV system using an online LCA Calculator tool [92]. The results from this assessment were then compared to the results of a Life Cycle Assessment performed by NREL on coal-fired power production.

An LCA was performed for each of the three main items composing the EESiPV system. The scope of the assessment included five phases, which are Materials, Manufacturing, Transportation, Use and Disposal. The impacts for each item were assessed according to the effects on material resources, energy use, global warming and human health. Each of the four impacts were scored -4 (extremely high benefit) to +4 (extremely high impact) for each phase. The lowest and best score possible is -80 while the highest and worst possible score is +80.

6.1. Cadmium Telluride PV Panel

Goal Definition and Scope:
The goal was to perform a life cycle assessment on a cadmium tellurium photovoltaic panel. Material and energy usage along with impacts on global warming and human health were assessed from the acquisition to disposal of materials comprising a CdTe PV panel.

Inventory Analysis:
Table 12 through 16 contain lists of resources/inputs and emissions/outputs involved in each of the five phases for a CdTe photovoltaic panel.

Materials Phase:

Table 12: Inputs and emissions from the Material phase for CdTe.

Resources/Inputs:	Emissions/Outputs:
Fuel oil/gasoline	Carbon dioxide
(for mining equipment)	Nitrogen oxides
	Sulfur dioxide
	Other air pollutants

Manufacturing:

Table 13: Inputs and emissions from the Manufacturing phase for CdTe.

Resources/Inputs:	Amount	Emissions/Outputs:
Electricity (coal) [93]	$236 kWh/m^2$	Carbon dioxide [94]
Water [93]	1250 g/m^2	Nitrogen oxides [94]
Glass [93]	24,960 g/m^2	Sulfur dioxide [94]
EVA-sheet [93]	630 g/m^2	Other air pollutants [94]
Cd (smelted Zn & Pb) [95]	230 g/m^2	Metal wastes [94]
Te (leached Cu slimes) [95]	↑	Wastewater [94]
CdS layer (CdS powder) [93]	↑	
TCO layer [93]	↑	
Al (frame) [93]	1900 g/m^2	
Steel (support cable) [93]	25,000 g/m^2	
Cu (cables and contact boxes) [93]	40 g/m^2	
Plastics (cables and contact boxes) [93]	40 g/m^2	
Fuel oil/gasoline (for installation purposes) [93]	10.8 MJ/m^2	

Transportation:

Table 14: Inputs and emissions from the Transportation phase for CdTe.

Resources/Inputs:	Emissions/Outputs:
Fuel oil/gasoline	Carbon dioxide
(for transportation of consumer-ready and inactive PV panels)	Nitrogen oxides
	Sulfur dioxide
	Other air pollutants

Use:

Table 15: Inputs and emissions from the Use phase for CdTe.

Resources/Inputs:	Emissions/Outputs:
Sun (solar radiation)	Electricity (solar energy)
Acidic/Basic Solution (for washing purposes) [93]	Wastewater [96]
Water (for washing purposes) [96]	

Disposal:

Table 16: Inputs and emissions from the Disposal phase for CdTe.

Resources/Inputs:	Emissions/Outputs:
Electricity (coal) to recycle	Carbon dioxide
	Nitrogen oxides
	Sulfur dioxide
	Other air pollutants
	Liquid metal emissions (into the ground)
	Solid (metal) wastes

Impact Assessment:

Material Phase: There are many material resources used, as noted above, so a score of 4 was given for the acquisition of these materials. The acquisition of cadmium and telleruim, however, are the main concern. Cadmium is generated by smelting zinc or lead ores while tellurium is recovered by leaching slimes from the electrolytic refining of copper [95]. These are both energy intensive processes, but the materials are considered byproducts thus lessening the impact to a value of 3. Due to the high amounts of energy used during extraction, emissions are greatest during this phase [94]. Cadmium is considered a toxic element, while tellurium is mildy toxic. A score of 2 was given to the global warming and human health impacts because of the emissions and toxicity factor.

Manufacture Phase: As with the material phase, the manufacturing phase is energy intensive resulting in a value of 4. It is assumed that fossil fuels, such as coal, are used for electricity purposes [93]. Because of fossil fuel usage the impact on global warming and human health are high but not as great as in the Materials phase. The compound Cadmium tellurium is toxic if the solid is ingested or the dust is inhaled. Precautions must be taken during the encapsulating process of CdTe PV modules. Once secured in the module, it is deemed harmless [97]. A value of 1 was given to the human health impact because only manufactures would be exposed to the Cadmium tellurium compound.

Transportation Phase: Transportation of materials, consumer-ready CdTe PV panels, and inactive PV panels will most likely occur by large freight trucks. First Solar CdTe photovoltaic panels are manufactured in the United States at the Perrysburg, Ohio plant [98]. Materials will be transported to this location, and consumer-ready PV panels will be transported from this location to the ESSiPV system sites. Transportation distances increase as the following shows for the 3 ESSiPV system locations: Buffalo, NY (303 miles), Raleigh, NC (619 miles) and Phoenix, AZ (1,931 miles). Distance values were obtained from Google Maps. Fuel oil/gasoline is used to power these trucks and tailpipe emissions will be produced. These values can be comparable to those in other industries and are thus lower on the scale.

Use Phase: Not many added material resources are needed during the operation of photovoltaic panels. An acidic/basic solution [93] along with water [96] is used to clean the panels once a year [96]. External electricity (energy) is not required during use. The PV panel actually produces electricity during this phase resulting in a score of -4 for the energy use impact. Also environmental emissions are not an issue during this phase. They would

be considered in the case of an accidental fire, which is highly unlikely [95]. Because small amounts of materials are used as well as low amounts of wastes and emissions, a score of 0 was given to the global warming and human health impact areas.

Disposal Phase: If the entire CdTe PV module were to be disposed of in a landfill some of the materials, specifically the cadmium tellurium compound, would pose a threat to human health. Many parts of the PV module, however, can be recycled while some will inevitably end up in a landfill [93]. To score this phase the assumption was made that materials will go in both directions. A score of 2 was given to material resource and energy use impacts based on recycling. A score of 1 was given to the global warming and human health impact because even though the materials are harmful little amounts of them exist in the PV panel.

Table 17: CdTe PV Panel Assessment

	Materials	*Manufacture*	*Transportation*	*Use*	*Disposal*
Material resources	4	3	1	0	2
Energy Use	3	4	1	-4	2
Global Warming	3	2	1	0	1
Human Health	3	1	1	0	1
Column Totals	13	10	4	-4	6
				Sum across column totals	29

Interpretation:
A score of 29, on the range of -80 to +80, was received by the CdTe PV panel in the ESSiPV system. Impacts are greatest during the acquisition of materials and manufacturing phase, especially for material resources and energy use. The use phase showed the least impact and resulted in a benefit of producing energy/electricity. Information is scarce on the disposal phase because current photovoltaic panels have not reached this stage. Also, full life cycle assessments are not available for photovoltaic panels based on the statement above along with limited research performed in this area.

6.2. Polycrystalline Silicon PV Panel

Goal Definition and Scope:
The goal was to perform a life cycle assessment on a polycrystalline Silicon photovoltaic panel. Material and energy usage along with impacts on global warming and human health were assessed from the acquisition to disposal of materials comprising a pc-Si PV panel.

Inventory Analysis:
The tables below contain a list of resources/inputs and emissions/outputs involved in each of the five phases for a polycryrstalline Silicon photovoltaic panel. As can be seen in the tables, many of the phases for this panel are similar to a CdTe PV panel. The main difference is in the active photovoltaic materials used. Differences also exist with the impact these materials have in each of the five phases.

Materials Phase:

Table 18: Inputs and emissions from the Material phase for pc-Si.

Resources/Inputs:	Emissions/Outputs:
Fuel oil/gasoline (for mining equipment)	Carbon dioxide
	Nitrogen oxides
	Sulfur dioxide
	Other air pollutants

Manufacturing:

Table 19: Inputs and emissions from the Manufacturing phase for pc-Si.

Resources/Inputs:	Amount	Emissions/Outputs:
Electricity (coal) [95]	N/A	Carbon dioxide[94]
Water [95]	N/A	Nitrogen oxides[94]
Glass (front cover) [95]	24,960 g/m^2	Sulfur dioxide [94]
EVA-sheet [95]	1250 g/m^2	Other air pollutants [94]
EG Silicon (silica sand) [96]	1120 g/m^2 [96]	Wastewater [94]
White Polyester (back cover)	N/A	
Al (frame) [95]	1900 g/m^2	
Steel (support cable) [95]	25,000 g/m^2	
Cu (cables and contact boxes) [95]	40 g/m^2	
Plastics (cables and contact boxes) [95]	40 g/m^2	
Fuel oil/gasoline (for installation purposes) [93]	10.8 MJ/m^2	

Note: Exact amounts of electricity, water and white polyester could not be determined due to insufficient available information.

Transportation:

Table 20: Inputs and emissions from the Transportation phase for pc-Si.

Resources/Inputs:	Emissions/Outputs:
Fuel oil/gasoline	Carbon dioxide
(for transportation of consumer-ready and inactive PV panels)	Nitrogen oxides
	Sulfur dioxide
	Other air pollutants

Use:

Table 21: Inputs and emissions from the Use phase for pc-Si.

Resources/Inputs:	Emissions/Outputs:
Sun (solar radiation)	Electricity (solar energy)
Acidic/Basic Solution (for washing purposes) [93]	Wastewater [96]
Water (for washing purposes) [96]	

Disposal:

Table 22: Inputs and emissions from the Disposal phase for pc-Si.

Resources/Inputs:	Emissions/Outputs:
Electricity (coal) to recycle	Carbon dioxide
	Nitrogen oxides
	Sulfur dioxide
	Other air pollutants
	Liquid metal emissions (into the ground)
	Solid (metal) wastes

Impact Assessment:
Material Phase: Many material resources are used in creating pc-Si PV panels. Silicon for wafer production is obtained in one of two possible ways. Silicon can be off-grade and come from the semiconductor industry (EG-Si) or it could be direct solar grade silicon (SoG-Si) used only for photovoltaic purposes. BP Solar, Inc. purchases Silica that is reduced in an arc furnace and further purified to the equivalent of EG silicon [99]. Fewer types of materials are used in constructing pc-Si PV panels than CdTe PV panels. However, the amount of material used is greater [95]. Because of this factor a score of 4 was given to the impact of material resources in this phase. The same type of energy source is used to extract these resources as in CdTe PV panels, so a score of 4 was given to the energy use impact. Emissions are great during the Materials and Manufacturing phase [94], and are higher for pc-Si PV panels than CdTe PV panels so a global warming impact value of 4 was assigned. Toxicity isn't much of a concern with the material resources, so a value of 2 was assigned to the human health impact.

Manufacture Phase: The production of silicon wafers is the most energy intensive step during the manufacturing process [95]. Since off-grade silicon is used, some of the impacts can be allocated to the electronic industry resulting in a lower impact score [96]. Pieces of silicon are melted together to form an ingot, which is further cut into smaller bricks then wafers [99]. It is this extremely inefficient wafer cutting step that uses most of the energy [95]. As with the material phase, the manufacturing phase is energy intensive resulting in a value of 4. Because of fossil fuel usage the impact on global warming is high. The impact on human health isn't as high because silicon is not toxic.

Transportation Phase: Transportation of materials, consumer-ready pc-Si photovoltaic panels, and inactive PV panels will most likely occur by large ocean vessels and freight trucks. Polycrystalline silicon PV panels are manufactured in Madrid, Spain, Sydney, Australia, and Bangalore, India [99]. PV panels for the ESSiPV system will come from one of these three locations, most likely Madrid, Spain. Fuel oil/gasoline will be used to power both the freight vessels and trucks. Vessel and tailpipe emissions will be produced. Once again these values can be comparable to those in other industries, but the overall impact will be greater than that of CdTe PV panels.

Use Phase: Not many added material resources are needed during the operation of

photovoltaic panels. An acidic/basic solution [93] along with water [96] is used to clean the panels once a year [96]. External electricity (energy) is not required during use. The PV panel actually produces electricity during this phase resulting in a score of -4 for the energy use impact. Also environmental emissions are not an issue during this phase. They would be considered in the case of an accidental fire, which is highly unlikely [95]. Because small amounts of materials are used as well as low amounts of wastes and emissions, a score of 0 was given to the global warming and human health impact areas. The same discussion was made for the CdTe PV panel.

Disposal Phase: Many parts of the pc-Si PV panel can be recycled while some will inevitably end up in a landfill [93]. To score this phase the assumption was made that materials will go in both directions. A score of 2 was given to material resource and energy use impacts based on recycling. A score of 1 and 0, were given to the global warming and human health impact, respectively, because the materials aren't as harmful as in other PV panels.

Table 23: pc-Si PV Panel Assessment

	Materials	*Manufacture*	*Transportation*	*Use*	*Disposal*
Material resources	4	3	1	0	2
Energy Use	4	4	2	-4	2
Global Warming	4	3	2	0	1
Human Health	2	2	1	0	0
Column Totals	14	12	6	-4	5
				Sum across column totals	33

Interpretation:
A score of 33, on the range of -80 to +80, was received by the pc-Si PV panel in the ESSiPV system. Impacts are greatest during the Acquisition of Materials and Manufacturing phase, especially for material resources and energy use. The same result occurred for the CdTe PV panel showing that these phases are of concern for PV panels in general. Exact information wasn't available for all material amounts during the Manufacturing phase; this brought about some uncertainty in scoring. The use phase showed the least impact and resulted in a benefit of producing energy/electricity. Also, information is scarce on the disposal phase because current photovoltaic panels have not reached this stage. Full life cycle assessments are not available for photovoltaic panels based on the statement above along with limited research performed in this area.

6.3. Vanadium Redox Flow Cell

Goal Definition and Scope:
The goal was to perform a life cycle assessment on a Vanadium Redox Flow Cell. Material and energy usage along with impacts on global warming and human health were assessed from the acquisition to disposal of materials comprising a vanadium redox flow cell with 10,000 cycles. The main issues with performing an LCA on this item is that, information on systems of this size is not readily available.

Inventory Analysis:

The tables below contain a list of resources/inputs and emissions/outputs involved in each of the five phases for a Vanadium Redox Flow Cell.

Materials Phase:

Table 24: Inputs and emissions from the Materials phase for the RFC.

Resources/Inputs:	Amount	Emissions/Outputs:
Electricity (coal) [100]	17.5 MWh	Carbon dioxide [100]
Other Energy [100]	75 MWh	Carbon monoxide [100]
		Methane [100]
		Nitrogen oxides [100]
		Sulfur dioxide [100]

Note: Values for electricity and energy use were scaled up from Rydh's 4000-cycle flow cell system to the ESSiPV's 10,000-cycle flow cell system. This was also done for the Manufacturing, Transportation and Disposal phase.

Manufacturing:

Table 25: Inputs and emissions from the Manufacturing phase for the RFC.

Resources/Inputs:	Amount	Emissions/Outputs:
Electricity (coal) [100]	72.5 MWh	Carbon dioxide [100]
Other Energy [100]	25 MWh	Carbon monoxide [100]
		Methane [100]
		Nitrogen oxides [100]
		Sulfur dioxide [100]

Transportation:

Table 26: Inputs and emissions from the Transportation phase for the RFC.

Resources/Inputs:	Amount	Emissions/Outputs:
Fuel oil/gasoline		Carbon dioxide [100]
Other Energy [100]	7.5 MWh	Carbon monoxide [100]
		Methane [100]
		Nitrogen oxides [100]
		Sulfur dioxide [100]

Use:

Table 27: Inputs and emissions from the Use phase for the RFC.

Resources/Inputs:	Amount	Emissions/Outputs:
$V_2O_{5(s)}$	125,000 kg	Liquid emissions
Positive Electrolyte (3.5M VO_2^- & VO^{-2} in H_2SO_4)	225,000 L	
Negative Electrolyte (3.5M V^{+2} & V^{+3} in H_2SO_4)	225,000 L	
Ion membrane (Nafion/Daramic)	575 m^2	
carbon paper electrode	2	
HDPE (high density polyethylene) storage tanks	2	
Steel (pumps, motors, racks, bolts, etc.) [100]	2516 kg	
Copper (connectors, electrode ends, etc.) [100]	184 kg	

Disposal:

Table 28: Inputs and emissions from the Disposal phase for pc-Si.

Resources/Inputs:	Amount	Emissions/Outputs:
Electricity (coal) to recycle [100]	7.5 MWh	Air Emissions:
		Carbon dioxide [100]
		Carbon monoxide [100]
		Methane [100]
		Nitrogen oxides [100]
		Sulfur dioxide [100]
		Liquid metal emissions (into the ground)
		Solid (metal) wastes

Note: Values for air emissions are grouped for all phases in Rydh's assessment [100] and proved difficult to be separated so exact values were not listed above.

Impact Assessment:
Material Phase: Vanadium, the main electrolyte component, can be extracted by mining or recovered from petroleum residues. H_2SO_4, which is also used in the electrolyte solutions can be obtained as waste from other industrial processes. Ryhd completed an environmental assessment of vanadium redox and lead-acid batteries for 4000-cycle systems. He showed that greater amounts of energy are needed during the material acquisition phase for lead-acid batteries than vanadium redox batteries. Energy/electricity information, however, is not available for the photovoltaic panels to make a direct comparison between the three products. A value of 3 was given to the energy use impact. Many materials are needed, some of which pose a concern to humans. Specifically, vanadium oxide, V_2O_5. is considered to be a toxic and harmful chemical. It possess irritant properties and is dangerous to the environment. It has a NFPA 704 Health Value of 3 [101]. For this fact, a value of 4 was given to the human health impact.

Manufacture Phase: As with the materials phase, the manufacturing phase is energy intensive mainly because it will occur at two locations; in a factory and at the EESiPV

system site. Materials and chemicals will be manufactured in China while the flow cell will be constructed on site. It is assumed that fossil fuels, such as coal and oil, are used for electricity/energy purposes. Because of fossil fuel usage and construction occurring at multiple locations the impact on global warming and human health are higher than in the materials phase. A score of 2 was given to the material resources area, 3 to global warming and human health areas, and 4 to the energy use area.

Transportation Phase: Materials and chemicals for the Vanadium Redox flow cell will be shipped from China to the west coast of the United States. This distance is approximately 6,500 miles, and the items will be shipped via an ocean freight vessel. Once in the United States, transportation of all materials, for use and disposal purposes, will most likely occur by large freight trucks. Fuel oil/gasoline will be used to power the freight vessel and trucks. Also, vessel and tailpipe emissions will be produced. Once again these values can be comparable to those in other industries, but will be greater than those for the photovoltaic panels.

Use Phase: Materials used during the operation of a Vanadium Redox Flow Cell are listed in the Inventory Analysis section. Numerous materials are used with a lifespan of approximately 30 years. Energy is not produced directly from the flow cell, but it is used to store the photovoltaic energy. Once again, the toxicity of Vanadium oxide is an issue for human health along with the possible leakage of other liquids. Atmospheric emissions contributing to global warming are not a major concern during this phase.

Disposal Phase: The vanadium redox flow cell is disassembled after operation and the materials are either re-used or deposited in a landfill [**?**]. Rydh allocated 50 percent of the materials to re-use and recycling and the other 50 percent to hazardous waste/landfill disposal. Recycling along with the transportation phase are the least energy intensive phases with little material usage, resulting in low scores for these areas. The toxicity of vanadium oxide, however poses a threat to humans if disposed of in a landfill resulting in a higher human health impact score.

Table 29: Vanadium Redox Flow Cell Assessment

	Materials	*Manufacture*	*Transportation*	*Use*	*Disposal*
Material resources	2	2	1	3	1
Energy Use	3	4	2	0	1
Global Warming	2	3	2	0	2
Human Health	4	3	2	3	3
Column Totals	11	12	7	6	7
				Sum across column totals	43

Interpretation:
A score of 43, on the range of -80 to +80, was received by the vanadium redox flow cell in the ESSiPV system. Impacts are greatest during the acquisition of materials and manufacturing phase, especially for energy use and human health concerns. These two phases also resulted in the greatest impact for CdTe and pc-Si photovoltaic panels. It can concluded that for the entire system, these two phases will result in the greatest impact

values while the use phase will have the lowest values. The transportation, use and disposal phase all had similar values. Information for air emissions was difficult to extract from Rydh's study and resulted in uncertainty for assessing the global warming impact. Also, the unavailability of a full life cycle assessment for a vanadium redox flow cell of this size limited the depth of our assessment.

6.4. ESSiPV System LCA

An online LCA Calculator tool [92] was used to perform a life cycle assessment for the entire ESSiPV system. This calculator computes the impact in grams of carbon dioxide produced based on four phases: manufacture, transport, product use and disposal. The acquisition of raw materials, or materials, phase was not included in the LCA Calculator tool but was included in the individual product assessments. Three assemblies representing the CdTe photovoltaic panels, pc-Si photovoltiac panels and vanadium redox flow cell were included in the ESSiPV system LCA. Final results were based on average values for the three chosen system locations in the United States.

Information for the Phases of the LCA Calculator tool:
Manfuacture: Specific parts of the assemblies (or products) were listed along with the materials involved in each one. The mass of these materials according to the g/m^2 and m^2 of the products needed were entered into the calculator. It was assumed that one panel is approximately 1667 m^2 and an average area of CdTe panels for a site is 38,000 m^2 and an average area of pc-Si panels for a site is 52,000 m^2. Materials such as water and electricity usage could not be entered into the calculator and were thus not included in this phase. At the end, the mass of each assembly was added to a final manufacturing total.

Transport: Transportation for each assembly was accounted for in this phase. The type and distance traveled in miles were entered into the calculator. The distance values were average between the three locations and were taken from the individual product LCA's completed above.

Product Use: It was assumed that the ESSiPV system would have a lifespan of 25 years. This value was used in the Economic Analysis as well. No electricity use occurs for any of the three assemblies, so values of zero were entered into this phase. A downfall with the LCA Calculator is that the electricity produced by the system could not be added in as a benefit to the assessment.

Disposal: As noted in the individual product life cycle assessments, the materials for each assembly will go in both directions - landfill waste and recycling matter. For simplicity, it was assumed that fifty percent of the material will be recycled while the other fifty percent will be disposed of in a landfill. This fifty percent recycled value was entered into the LCA Calculator.

ESSiPV System LCA Calculator Conclusions:
A total impact of 354,000,000 g or 3540 metric tons of CO_2 will result from the ESSiPV system over it's lifetime of 25 years. As with the individual product LCA's performed, the manufacturing phase had the greatest impact. Specifically within this phase, the Vanadium oxide resulted in the greatest concern because of the amount needed and toxicity issues.

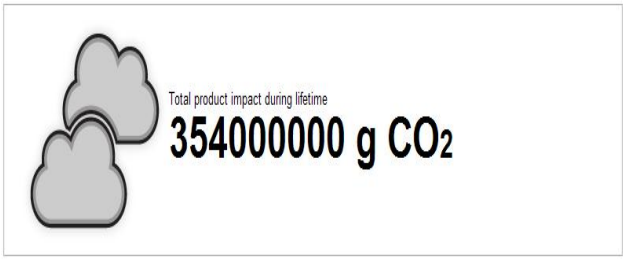

Figure 53: Total CO_2 Impact [92]

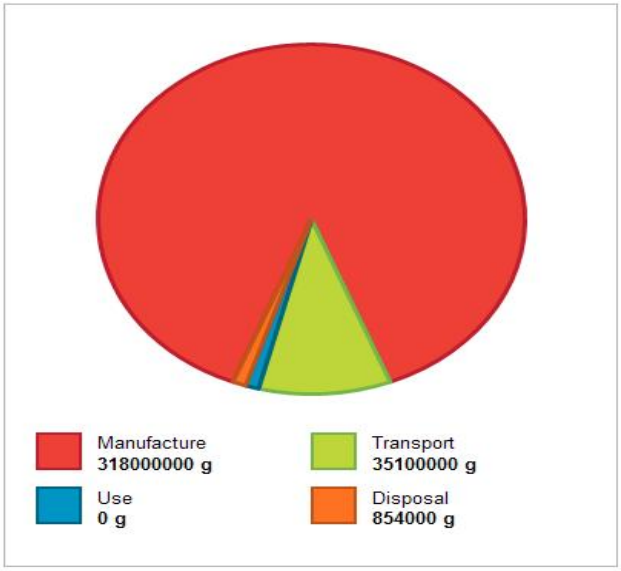

Figure 54: Breakdown of the Impact from the Four Phases [92]

Transportation had the second greatest impact, most likely because of the oceanic and inland freight for the pc-Si photovoltaic panels and vanadium redox flow cell materials and chemicals. The disposal phase had a lower impact than both the manufacturing and transportation phase. The Use phase resulted in no impact with electricity use being zero. The LCA Calculator confirmed many conclusions obtained from the individual product LCA's previously performed. The phases with the greatest and least impact were found to be the same.

Comparison to Coal-fired Power Generation:
Total metric tons of CO_2 produced per kWh of electricty from our ESSiPV system is calculated below. The total metric tons of CO_2 was first divided by 25 to get the amount produced per year of operation. The assumption was made that the system would generate an average of 12.96 GWh, or $1.396 * 10^7$kWh.

$$\frac{141.6t}{1.396 * 10^7 kWh} = 1.014 * 10^{-5} \frac{t}{kWh} \tag{19}$$

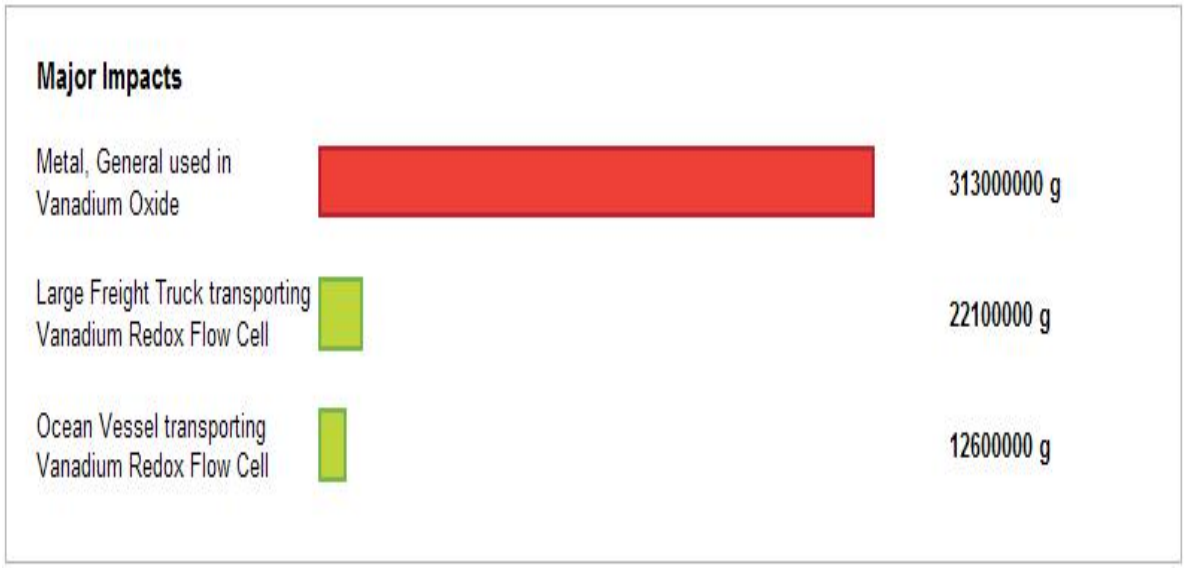

Figure 55: Major Impacts [92]

Data from a report by the Environmental Protection Agency concluded that in 1999, 1,787,910 thousand metric tons of CO_2 were emitted by 1,881,571 million kWh of coal-fired power. The output rate of CO_2 is 2.095 lb/kWh [102].

$$\frac{2.095lb}{kWh} * \frac{0.00045359237t}{1lb} = 9.5 * 10^{-4} \frac{t}{kWh} \tag{20}$$

From the calculations above, it is shown that the ESSiPV system has a lower environmental impact than coal-fired power generation based on carbon dioxide emissions.

7. Final Conclusions

The analysis of both polycrystalline silicon and cadmium telluride photovoltaic systems in Phoenix, Raleigh and Buffalo shows that both materials can be preferable in different situations. The pc-Si has some temperature issue in hot climates, but performs well under direct irradiance associated with hotter climates. The CdTe modules performed very well in all three locations except for the summer in Phoenix.

The seasonal variations in irradiance has less of an impact on the performance of the redox flow cell system. Since the flow cell's purpose is to provide baseline electricity generation, the lack of seasonal variations in a very important performance metric. The redox flow cells deliver consistent energy to the grid throughout the entire year for all of the system designs and locations.

The main assumption in the economic assessment was the future cost of energy. As the global energy demand increases more and more in the coming decades, the cost of energy will change drastically. This has the potential to increase the economic feasibility of the EESiPV system even further. Overall the CdTe modules proved to be the more cost effective photovoltaic module. This is consistent with the current market trend that First Solar has achieved the lowest production cost ($/W) of photovoltaic modules.

The LCA of the photovoltaic modules concluded that cadmium telluride modules have less of an impact than polycrystalline silicon modules. Of all the components in the EESiPV system the vanadium redox flow cell has the most significant environmental impact. It is significant to note that recycling of the EESiPV system after its lifetime would significantly decrease the total impact of all system components.

Bibliography

[1] S. Kalogirou, *Solar Energy Engineering Processes and Systems*. Elsevier, 2009.

[2] C. Honsberg and S. Bowden. (2010) Standard solar spectra. [Online]. Available: http://www.pveducation.org/pvcdrom/appendicies/standard-solar-spectra

[3] (2011) Introduction to solar radiation. Newport Corporation. Global Headquarters, 1791 Deere Avenue, Irvine CA 92606, USA. [Online]. Available: http://www.newport.com/store/genContent.aspx/Introduction-to-Solar-Radiation/411919/1033

[4] J. A. Duffie and W. A. Beckman, *Solar Engineering of Thermal Processes*, 3rd ed. John Wiley & Sons, Inc., 2006.

[5] (2008) Weather resources for teachers: The solar spectrum. North Carolina School of Sciences and Mathematics. PO Box 2418, Durham NC 27715. [Online]. Available: http://www.dlt.ncssm.edu/resources/wxresources.htm

[6] (2011, January) Solar maps. online. National Renewable Energy Laboratory (NREL). [Online]. Available: http://www.nrel.gov/gis/solar.html

[7] Surfrad (surface radiation) network. online. [Online]. Available: http://www.srrb.noaa.gov/surfrad/

[8] A. Goetzberger and V. U. Hoffmann, *Photovoltaic Solar Energy Generation*, W. T. Rhodes, Ed. Springer, 2005.

[9] B. G. Streetman and S. K. Banerjee, *Solid State Electronic Devices*. Prentice Hall series in solid state physical electronics, 2006.

[10] Hyperphysics: Electron volts. online. Department of Physics and Astronomy at Geogia State University. [Online]. Available: http://hyperphysics.phy-astr.gsu.edu/hbase/electric/ev.html#c2

[11] S. J. Fonash, *Solar Cell Device Physics*, 2nd ed. Academic Press, 2010.

[12] C. Honsberg and S. Bowden. Pvcdrom. online. PVeducation. [Online]. Available: http://www.pveducation.org/pvcdrom

[13] E. Becquerel, "Recherche sur les effets de la radiation chimique de la lumiere solaire, au moyen des courants electriques," *Compte rendus hebdomaclaires des seances de l'academie des seances*, vol. 9, pp. 145–149, 1839.

[14] J. Perlin, *The Silicon Solar Cell Turns 50*, The National Center for Photovoltaics Std.

[15] S. Clavenna, Ed., *The Solar Industry's Monthly Market Monitor*, vol. 29, no. 10, PV News, October 2010.

[16] L. L. Kazmerski, "Solar photovoltaics r& d at the tipping point: A 2005 technology overview," *Journal of Electron Spectroscopy*, vol. 150, pp. 105–135, 2006.

[17] D. G. F. Sonnenenergie, *Planning and Installing Photovoltaic Systems*, 2, Ed. Earthscan Publications Ltd., 2008.

[18] J. A. Carlin, S. A. Ringel, A. Fitzgerald, and M. Bulsara, "High-lifetime gaas on si using gesi bu!ers and its potential for space photovoltaics," *Solar Energy Material and Solar Cells*, vol. 66, pp. 621–630, 2001.

[19] A. Luque and V. Andreev, *Concentrator Photovoltaics*, W. T. Rhodes, Ed. Springer, 2007.

[20] S. Semiconductors. (2010, 10) Spire produces worldÕs most efficient solar cell. online. Optics.org. [Online]. Available: http://optics.org/press/222

[21] D. Zubia, L. Romo, J. Cruz-Campa, B. Aguirre, and J. McClure, "Photovoltaics of ordered cdte/cds nanoarrays," in *Conference Record of the IEEE Photovoltaic Specialists Conference*, 2009.

[22] P. V. Meyers and S. P. Albright, "Technical and economic opportunities for cdte pv at the turn of the millennium," *Progress in Photovoltaics: Research and Applications*, vol. 8, pp. 161–169, 2000.

[23] (2011) First solar. online. First Solar. [Online]. Available: http://www.firstsolar.com/en/index.php

[24] E. Fortunato, D. Ginley, H. Hosono, and D. C. Paine, "Transparent conducting oxides for photovoltaics," *MRS Bulletin*, vol. 32, pp. 242–247, 2007.

[25] Quality and sustainability. online. Solyndra. [Online]. Available: http://www.solyndra.com/about-us/quality-sustainability/

[26] A. K. Pandey and J.-M. Nunzi, "Rubrene/fullerene heterostructures with a half-gap electroluminescence threshold and large photovoltage," *Advanced Materials*, vol. 19, pp. 3613–3617, 2007.

[27] B. O'Regan and M. Gratzel, "A low-cost, high efficiency solar cell based on dye-sensitized colloidal tio2 films," *Letters to Nature*, vol. 353, pp. 737–740, 1991.

[28] P. V. V. Jayaweera, A. G. U. Perera, and K. Tennakone, "Why gratzel's cell works so well," *Inorganica Chimica Acta*, vol. 361, pp. 707–711, 2008.

[29] (2011) Power plastic. online. Konarka. [Online]. Available: http://www.konarka.com/index.php/power-plastic/about-power-plastic/

[30] K. Kawanoa, R. Pacios, D. Poplavskyy, J. Nelson, D. D. Bradley, and J. R. Durrant, "Degradation of organic solar cells due to air exposure," *Solar Energy Material and Solar Cells*, vol. 90, pp. 3520–3530, 2006.

[31] R. Garcõa-Valverde, J. A. Cherni, and A. Urbina, "Lide cycle analysis of organic photovoltaic technologies," *Progress in Photovoltaics: Research and Applications*, vol. 18, pp. 535–558, 2010.

[32] N. Senthilkumara, H.-S. Kanga, D.-W. Parka, and Y. Choe, "Improving efficiency of organic photovoltaic cells using pedot:pss and mwcnt nanocomposites as a hole conducting layer," *Journal of Macromolecular Science, Part A*, vol. 47, pp. 484–490, 2010.

[33] Y. Kim, S. A. Choulis, J. Nelson, D. D. C. Bradley, S. Cook, and J. R. Durrant, "Composition and annealing effects in polythiophene/fullerene solar cells," *Photovoltaic Materials and Phenomena SCell*, vol. 40, pp. 1371–1376, 2004.

[34] B. L. Oksengendler, N. N. Turaeva, and S. S. Rashidova, "Statistical theory of multiple exciton generation in quantum dot solar cells," *Applied Solar Energy*, vol. 45, pp. 162–165, 2009.

[35] A. J. Nozik, "Nanoscience and nanostructures for photovoltaics and solar fuels," *Nano Letters*, vol. 10, pp. 2735–2741, 2010.

[36] A. J. Nozik, M. C. Beard, J. M. Luther, M. Law, R. J. Ellingson, and J. C. Johnson, "Semiconductor quantum dots and quantum dot arrays and applications of multiple exciton generation to third-generation photovoltaic solar cells," *Chemical Review*, vol. 110, pp. 6873–6890, 2010.

[37] S. E44.09. Astm e1036 - 08 standard test methods for electrical performance of nonconcentrator terrestrial photovoltaic modules and arrays using reference cells. [Online]. Available: http://www.astm.org/Standards/E1036.htm

[38] G. Klise and J. Stein, "Models used to assess the performance of photovoltaic systems," Sandia National Laboratories, Tech. Rep., 2009.

[39] M. Ito, K. Kato, K. Komoto, T. Kichimi, and K. Kurokawa, "A comprative study on cost and life-cycle analysis for 100 mw very large-scale pv (vls-pv) systems in deserts using m-si, a-si, cdte, and cis modules," *Progress in Photovoltaics: Research and Applications*, vol. 16, pp. 17–30, 2008.

[40] L. M. Moore and H. N. Post, "Five years of operating experience at a large, utility-scale photovoltaic generating plant," *Progress in Photovoltaics: Research and Applications*, vol. 16, pp. 249–259, 2008. [Online]. Available: http://www.greentops.co.il/Portals/0/Article%20about%20Schott.pdf

[41] K. Komoto, M. Ito, P. van der Vleuten, D. Faiman, and K. Kurokawa, Eds., *Energy From the Desert. Very Large Scale Photovoltaic Systems: Socio-economic, Financial, Technical and Environmental Aspects*. Earthscan, 2009.

[42] D. Gomes, L. Pina, and J. Martins. (2010, October) Comparison between astronomical and light sensor feedback sun-tracking algorithms. WS Energia. [Online]. Available: http://concentrating-pv.org/pdf/papers/V-22-Gomez.pdf

[43] N. Aste and C. D. Pero, "Technical and economic performance analysis of large-scale ground-mounted pv plants in italian context," *Progress in Photovoltaics: Research and Applications*, vol. 18, pp. 371–384, 2010. [Online]. Available: http://onlinelibrary.wiley.com/doi/10.1002/pip.984/abstract

[44] M. Skyllas-Kazacos, C. Menictas, and M. Kazacos, "Thermal stability of concentrated v(v) electrolytes in the vanadium redox cell," *Journal of Electrochemical Society*, vol. 143, pp. L86–L88, 1996.

[45] M. Vijayakumar, S. Burton, C. Huang, L. Li, Z. Yang, G. Graff, J. H. J. Liu, and M. Skyllas-Kazacos, "Nuclear magnetic resonance studies on vanadium(iv) electrolyte solutions for vanadium redox flow battery," *Journal of Power Sources*, vol. 195, pp. 7709–7717, 2010.

[46] M. Skyllas-Kazacos, C. Peng, and M. Cheng, "Evaluation of precipitation for supersaturated vanayl electrolytes for vanadium redox battery," *Electrochemical and Solid State Letters*, vol. 2, pp. 121–122, 1999.

[47] T. Mohammadi and M. S. Kazacos, "Evaluation of the chemical stability of some membranes in vanadium solution," *Journal of Applied Electrochemistry*, vol. 27, pp. 155–160, 1996.

[48] W. Wang and X. Wang, "Investigation of ir-modified carbon felt as the positive electrode of all vanadium redox flow battery," *Electrochemica Acta*, vol. 52, pp. 6755–6762, 2007.

[49] L. Yue, W. Li, F. Sun, L. Zhao, and L. Xing, "Highly hydroxylated carbon fibres as electrode materials of all-vanadium redox flow battery," *Carbon*, vol. 48, pp. 3079–3090, 2010.

[50] H. Zhu, Y. Zhang, L. Yue, W. Li, G. Li, D. Shu, and H. Chen., "Graphite-carbon nanotube composite electrodes for all vanadium redox flow battery," *Journal of Power Sources*, vol. 184, pp. 637–640, 2008.

[51] V. Haddadi-Asl, M. Kazacos, and M. Skyllas-Kazacos, "Conductive carbon-polypropylene composite electrodes for vanadium redox battery," *Journal of Applied Electrochemistry*, vol. 25, pp. 29–33, 1995.

[52] C. Fabjan, J. Garche, B. Harrer, L. Jorissen, C. Kolbeck, F. Philippi, G. Tomazic, and F. Wagner, "The vanadium redox-flow battery: and efficient energy storage unit for photovoltaic systems," *Electrochemica Acta*, vol. 47, pp. 825–831, 2001.

[53] P. Zhao, H. Zhang, H. Zhou, J. Chen, S. Gao, and B. Yi., "Characteristics and performance of 10 kw class all-vanadium redox-flow battery stack," *Journal of Power Sources*, vol. 162, pp. 1416–1420, 2006.

[54] B. Fang, Y. Wei, T. Arai, S. Iwasa, and K. Kumagai, "Development of a novel redox flow battery for electricity storage system." *Journal of Applied Electrochemistry*, vol. 33, pp. 197–203, 2003.

[55] Y. Qin, J. Liu, Y. Di, C. Yan, C. Zeng, and J. Yang, "Thermodynamic investigation of electrolytes of the vanadium redox flow battery (ii)," *Journal of Chemical Engineering Data*, vol. 55, pp. 1276–1279, 2010.

[56] D. Chen, S. Wang, M. Xiao, D. Han, and Y. Meng, "Sulfonated poly (fluorenll ether ketone) membrane with embedded silica rich layer and enhanced proton selectivity for vanadium redox flow battery," *Journal of Power Sources*, vol. 195, pp. 7701–7708, 2010.

[57] T. Sukkar and M. Skyllas-Kazacos, "Water transfer behavior across cation exchange membranes in the vanadium redox battery," *Journal of Membrane Science*, vol. 222, pp. 235–247, 2003.

[58] Daramic polyethylene separators, deep-cycle low water loss applications. [Online]. Available: http://www.daramic.com/products/daramic_deep_cycle.cfm

[59] B. Tian, C. Yan, and F. Wang, "Proton conductive composite membrane from daramic/nafion for vanadium redox flow battery," *Journal of Membrane Science*, vol. 234, pp. 51–54, 2004.

[60] F. Mohammadi, P. Timbrell, S. Zhong, C. Padeste, and M. Skyllas-Kazacos., "Overcharge in the vanadium redox battery and changes in electrical resistivity and surface functionality of graphite-felt electrodes," *Journal of Power Sources*, vol. 52, pp. 61–68, 1994.

[61] Q. Lou, H. Zhang, J. Chen, P. Qian, and Y. Zhai, "Modification of nafion membrane using interfacial polymerization for vanadium redox flow battery applications," *Journal of Membrane Science*, vol. 311, pp. 98–103, 2008.

[62] J. Zeng, C. Jiang, Y. Wang, J. Chen, S. Zhu, B. Zhao, and R. Wang., "Studies on polypyrrole modified nafion membrane for vanadium redox flow battery," *Electrochemistry Communications*, vol. 10, pp. 372–375, 2008.

[63] X. Teng, Y. Zhao, J. Xi, Z. Wu, X. Qiu, and L. Chen, "Nafion/organically modified silicate hybrids membrane for all vanadium redox flow battery," *Journal of Power Sources*, vol. 189, pp. 1240–1246, 2009.

[64] J. Xi, Z. Wu, X. Qiu, and L. Chen, "Nafion/sio2 hybrid membrane for vanadium redox flow battery," *Journal of Power Sources*, vol. 166, pp. 531–536, 2007.

[65] K. Huang, X. Li, S. Liu, N. Tan, and L. Chen, "Research progress of vanadium redox flow battery for energy storage in china," *Renewable Energy*, vol. 33, pp. 186–192, 2008.

[66] M. Rychick and M. Skyllas-Kazacos, "Charicteristics of a new all-vanadium redox flow battery," *Journal of Power Sources*, vol. 22, pp. 59–67, 1988.

[67] Deeya energy, deeya energy 24k energy storage platform fact sheet. [Online]. Available: http://www.deeyaenergy.com/product/

[68] Prudent energy, prudent energy 10 mw class product specification sheet. [Online]. Available: http://www.pdenergy.com/products_mwclasssystems.html

[69] S. E. International, *Photovoltaic Design and Installation Manual*. New Society Publishers, 2007.

[70] J. Berwind, "Impact of credit crisis on solar industry," 2009.

[71] Solar energy incentives. State Energy Conservation Office. [Online]. Available: http://www.seco.cpa.state.tx.us/re_solar_incentives.htm

[72] M. Schreiber, M. Harrer, A. Whitehead, H. Bucsich, M. Dragschitz, E. Seifert, and P. Tymciw, "Practical and commercial issues in the design and manufacture of vanadium flow batteries," *Journal of Power Sources*, 2011.

[73] P. Butler and S. Klassen, "Materials for advanced rechargeable batteries," Sandia National Laboratory, Tech. Rep., 1993.

[74] A. Bascetim, S. Tuylu, and A. Nieto, "The study of relationship between economical and environmental parameters for sustainable resources management," 2009.

[75] A. G. Hestnes, "Building integration of solar energy systems," *Solar Energy*, vol. 67, pp. 181–187, 1999.

[76] V. Fthenakis, "End-of-life management and recycling of pv modules," *Energy Policy*, vol. 28, pp. 2051–1058, 2000.

[77] T. Tsoutsos, N. Frantzeskaki, and V. Gekas, "Environmental impacts from the solar energy technologies," *Energy Policy*, vol. 33, pp. 289–296, 2005.

[78] ——, "Environmental implications from the use of solar systems. examples of the potential impact mitigation in a sustainable perspective," in *7th National Conference for Solar Energy Sources*, November 2002.

[79] W. Rickerson, F. Bennhold, and J. Bradbury, "Feed-in tariffs and renewable energy in the usa Đa policy update," May 2008.

[80] G. Frisvold, W. P. Patton, and S. Reynolds, "Arizona solar energy and economics outlook," 2009.

[81] Projection of pv system prices: Australia, europe, japan, usa 2004-2030. online. The European PV Technology Platform, PV Platform Working Group 2. [Online]. Available: http://www.eupvplatform.org/fileadmin/Documents/WG2_061124_Rudek_03_PVSystemsPrice.pdf

[82] "Life cycle assessment: Principles and practice," NATIONAL RISK MANAGEMENT RESEARCH LABORATORY: OFFICE OF RESEARCH AND DEVELOPMENT,

U.S. ENVIRONMENTAL PROTECTION AGENCY, Tech. Rep., May 2006. [Online]. Available: http://www.epa.gov/nrmrl/lcaccess/pdfs/600r06060.pdf

[83] W. Marion and K. Urban. (1995, June) User's manual for tmy2s. National Renewable Energy Laboratory. [Online]. Available: http://rredc.nrel.gov/solar/pubs/tmy2/tab1-1.html

[84]

[85] E. L. Bacha, "A three-gap model of foreign transfers and the gdp growth rate in developing countries," 1990.

[86] P. Grace, K. Cory, T. Couture, and C. Kreycik, "Feed-in tariff policy: Design, implementation, and rps policy interactions."

[87] Dsire (database of state incentives for renewable energy) for federal, state & local incentives. [Online]. Available: http://www.dsireusa.org/

[88] W. R. Tucker, "Effective interest rate," 2000.

[89] K. Cory and P. Schwabe, "Wind levelized cost of energy: A comparison of technical and financing input variables," 2009.

[90] Renewable carbon offsets. Carbon Fund. [Online]. Available: www.Carbonfund.org

[91] K. Smith, "The carbon neutral myth," Department of Energy, Tech. Rep., 2010.

[92] (2011) Lca calculator: The sustainable design tool. LCA Calculator. Southbank Technopark, 90 London Road, London SE1 6LN. [Online]. Available: http://www.lcacalculator.com/

[93] M. Raugei, S. Bargili, and S. Ulgiati, "Life cycle assessment and energy pay-back time of advanced photovoltaic modules: Cdte and cis compared to poly-si," *Science Direct: Energy*, vol. 32, pp. 1310–1318, 2007.

[94] V. M. Fthenakis, H. C. Kim, and E. Alsema, "Emissions from photovoltaic life cycles," *Environmental Science & Technology*, vol. 42, pp. 2168–2174, 2008.

[95] V. M. Fthenakis and H. C. Kim, "Cdte photovoltaics: Life cycle environmental profile and comparisons," *Science Direct: Thin Solid Films*, vol. 515, pp. 5961–5963, 2007.

[96] N. Jungbluth, "Life cycle assessment of crystalline photovoltaics in the swiss ecoinvent database," *Progress in Photovoltiacs: Research and Applications*, vol. 13, pp. 429–446, 2005.

[97] (2011, March) Cadmium telluride. Wikipedia: The Free Encyclopedia. [Online]. Available: http://en.wikipedia.org/wiki/Cadmium_telluride

[98] (2011) First solar contact information. First Solar, Inc. [Online]. Available: http://www.firstsolar.com/en/contact.php

[99] (2011) How solar works. BP Solar, Inc. [Online]. Available: http://www.bp.com/

[100] J. J. Rydh, "Environmental assessment of vanadium redox and lead-acid batteries for stationary energy storage," *Journal of Power Sources*, vol. 80, pp. 21–29, 1999.

[101] (2011, February) Vanadium (v) oxide. Wikipedia: The Free Encyclopedia. [Online]. Available: http://en.wikipedia.org/wiki/Vanadium(V)_oxide

[102] "Carbon dioxide emissions from the generation of electric power in the united states," Department of Energy, Environmental Protection Agency, Tech. Rep., July 2000. [Online]. Available: http://www.eia.gov/cneaf/electricity/page/co2_report/co2emiss.pdf